A translaminar cortical circuit driven by higher order thalamus initiates learning-related synaptic plasticity

Nick Audette
Department of Biological Sciences
Carnegie Mellon University
Pittsburgh, PA
August 2018

Abstract

The cortical column is an evolutionarily conserved and expanded processing unit that underlies mammalian perception, learning, and memory. A unifying trait of the cortical column across these functions is its capacity to undergo experience-dependent plasticity, and decades of research has used the somatosensory cortex as a model circuit to link this plasticity to specific cortical circuits. Patterns of local connectivity and primary thalamic input generated a model of sequential processing where computations are performed as information proceeds serially across cortical layers, with learning-dependent changes occurring at intracortical connections. While this model fits many features of the cortical circuit, a growing body of work suggests that the higher order posterior medial thalamic nucleus (POm) is also well-positioned to influence activity across multiple layers of the cortical column.

We set out to investigate the potential contribution of POm to cortical activity patterns under basal conditions and during sensory learning by measuring electrophysiological responses of cortical neurons following optogenetic activation of thalamic axons in vitro. We first used targeted whole-cell patch clamp recording in combination with transgenic mouse lines to determine the cell-type specific functional connectivity of POm afferents in control animals. In deep layers, POm provides strong, direct input to excitatory neurons synchronized by fast, feedforward inhibition from parvalbumin-expressing neurons. Alternatively, POm provides weaker direct input to excitatory neurons in superficial layers, but can facilitate over the course of stimulation due to weaker, delayed feedforward inhibition from 5HT3a neurons. In both layers, tonically active somatostatin-expressing inhibitory neurons were silenced by 5HT3a neurons.

To determine if this thalamocortical circuit is a locus of synaptic changes during learning, we developed a high throughput home-cage sensory association training assay that paired a multi-whisker stimulus with a water reward. We discovered that POm activation drove dramatically increased cortical activity in both deep and superficial layers after just 24 hours of training, when behavioral evidence for a learned association first emerged. This increase in activity did not occur in primary thalamocortical pathways and was caused by a learning-specific increase in synaptic strength at the POm to layer 5 synapse. Over longer durations of training, synaptic plasticity occurred at both thalamocortical (POm) and intracortical (layer 2) inputs onto layer 2 excitatory neurons. Together, our results show that the higher order thalamic nucleus POm drives characteristic patterns of activity in multiple cortical layers and is the initiator of cortical columnar rearrangements during sensory learning. This study provides a much-needed update to the long-held sequential view of cortical processing.

.

Acknowledgements

I would like to begin by giving my heartfelt thanks to Dr. Alison Barth. I am extremely fortunate to have had an advisor who cares so much about my scientific, professional, and personal growth. Ever since our first conversation at a recruiting visit in 2012, you helped me first cultivate a passion for neuroscience and then develop the skill and discipline to pursue it for many years to come. Your imprint will always be on me. It has been an incredible 5 years, characterized by mutual energy and passion, and I cannot thank you enough for believing in me, indulging me, and challenging me.

I would like to thank my committee members Sandy Kuhlman and Mac Hooks for their excellent feedback, guidance, and support throughout the years. It has been a pleasure getting to talk science with you, and I appreciate all your attention and time. I would also like to thank the members of the Barth lab past and present for helping to create such an engaging and enjoyable environment. A special thank you to Erika Fanselow who taught me to patch, to Megumi Matsushita whose friendship was as dependable as her genotyping, Dika Kuljis who has been with me the longest and helped make the lab such a bright and interesting place, to Ajit Ray for his kindness and comradery, and to Stephanie Myal who I've had the pleasure to watch grow over the past few years. I would also like to thank my classmates and the Great Hall of Brain Science community, especially DJ Brasier for all the thoughtful scientific insight throughout the years, and Amanda Willard who was a wonderful companion on a shared journey into neuroscience and through grad school.

I would also like to extend a huge thank you to my Pittsburgh family: Dire Wolf, Hot Metal, Alloy, the Taco Sunday Crew, the Rice Boys, and all the friends in between. A very special thank you to Carolyn Norwood and Kelly Gilmour, who stood by my side and supported me through the good times and bad. Finally, I would like to thank my family. Andre, Laura, and Dylan, you have been such a wonderful source of guidance, encouragement, and joy throughout my life and during this long academic journey. This thesis, which is the capstone of over two decades of education, is as much a product of your efforts as it is my own. Hope it doesn't suck!

To all: I have always been a person with many passions. Thank you for being understanding when my balance between family, friends, work, and personal pursuits tipped too far in one direction or the other, which it did for each in turn over the years. Your patience and acceptance has allowed me to do it all. It has made my time in Pittsburgh truly happy.

List of Figures

Table of Contents

1. Introduction

1.1 The cortical column: the processing unit of the neocortex

Over the course of mammalian evolution, the neocortex – which is critical to the complex behavioral patterns of mammals – has been evolutionarily expanded and conserved. The particular pattern of expansion suggests that there is a 'unit' of cortical processing which, over time, has been duplicated many fold and then adapted to serve different functions. Across these many functions, a unifying aspect of neocortical circuits is their capacity to undergo experience-dependent plasticity. Investigating how the specific circuitry of the neocortex enables this experience-dependent plasticity requires a model circuit that is both rich and tractable: the rodent vibrissal somatosensory cortex.

1.1.1 Humans, mammals, and brain size

The mammalian neocortex can be viewed as the pinnacle of millions of years of neural evolution and is widely believed to confer the cognitive power, behavioral diversity, and intelligence of mammals – especially primates – with respect to other animal species. The earliest version of the modern mammalian neocortex is believed to have emerged around 200 million years ago in the late Triassic period in small rodents (Rakic, 2009). In the time since, the neocortex has been evolutionarily conserved and expanded in a way that seems to trend both with the general size and intelligence of an organism. In humans, the neocortex makes up 75-80% of the mass of the brain. Primates and other large mammals are not far behind with the neocortex accounting for roughly 70-75% of brain mass (Herculano-Houzel, 2012). Smaller mammals, however,

have a notably smaller neocortex ranging from 40-60% of brain mass (Herculano-Houzel, 2009). While humans have the largest cortex in terms of relative mass, the small separation between humans and other large mammals does not correspond with the apparent difference in cognitive and behavioral complexity between them. Similarly, when comparing the ratio of the number of cortical neurons to total neuron count, the major difference occurs not between humans and other primates, but rather between primates in general and other mammals. The primate neocortex has greater neuronal density due to a downscaling of individual neuron size relative to brain size (Herculano-Houzel, 2009). Humans are the largest primates and thus have the greatest total number of cortical neurons of any measured animal. In terms of size and neuron count, the human neocortex can best be characterized as a linearly scaled up primate neocortex (Herculano-Houzel, 2009).

These primitive metrics of human cortical size do not substantially separate the human neocortex from that of other mammals and are insufficient to explain the behavioral differences between humans and other mammals. Even when focusing simply on numbers, the expansion the neocortex should not be the only focus, as the mammalian cerebellum scales directly with cortical size across species (Herculano-Houzel, 2012). There are many other types of changes that can occur within a set number of neocortical neurons to allow different cognitive capabilities ranging from gene expression variation to entirely new uses of cortical space. Finally, on a fundamental level, it is important to acknowledge that the full extent of modern human intelligence is not proximally caused by the biology of our brains. Humans are undoubtedly more intelligent than other organisms, especially when measured by the richness and

complexity of our behavioral patterns. Neuroscience researchers, for example, spend their entire lives consuming obscure bits of knowledge generated by other humans and using extremely complicated instruments in order to add a handful of facts about the inner workings of human biology to books and records that will only ever be actively read by an infinitesimally small percentage of our species. Chimpanzees, which may be the most intelligent non-human species, require years of training to be taught simple versions of sign language (Jensvold and Gardner, 2000). But the level of sophistication evident in human behavior is culturally evolved as much as it is neurologically generated (MacLean, 2016). As stated by Tomasello and Rakoczy (Tomasello and Rakoczy, 2003), “If we imagine a human child born onto a desert island, somehow magically kept alive by itself until adulthood, it is possible that this adult’s cognitive skills would not differ very much – perhaps a little, but not very much – from those of other great apes.” There are surely neurological adaptations specific to humans that enabled us to form the societies and institutions within which we all reside. However, the neurological changes that underlie the drastic behavioral differences between humans and other organisms are likely to be orders of magnitude more subtle than the observed behavioral differences.

When considering the whole range of existing life, mammals, as a collective, are truly remarkable. The biological and behavioral differences between a single celled organism, a plant, an insect, and a mouse are all considerably greater than the difference between a mouse, a chimpanzee, and a human. Mammals across all species have a substantial capacity for memory, decision-making, motor learning, communication, and planning. The purpose of this thesis, therefore, is not to seek to

understand the differences between mammalian species, but rather the general properties of the neocortex that enable these important cognitive functions across all mammals.

1.1.2 The evolutionary expansion of the neocortex

The most remarkable feature of neocortical evolutionary expansion is the geometrical pattern it has followed. The neocortex is a relatively thin sheet of neurons on the exterior of the brain that contains a generally consistent laminar structure throughout. Over millions of years, the neocortex has expanded only in two dimensions, rather than in three dimensions. Across a large number of mammalian species, the thickness of the cortical sheet varies 10-fold while the surface area varies 10,000 fold (Hofman, 1989). This horizontal expansion, along with general structural similarity across brain region and species, suggests that there is a conserved cortical processing unit that has been multiplied in number over the course of evolution. This processing unit is referred to as the cortical column, and consists of a local cluster of vertically arranged neurons spanning six cytoarchticturally defined layers. Cortical columns are characterized by dense vertical connections across layers, but relatively sparse and short-range horizontal connections within layers (Douglas et al., 1989; Jiang et al., 2015; Lefort et al., 2009; Thomson and Lamy, 2007; Yu et al., 2009). Neurons within a column also typically share similar receptive field centers and functional properties across layers, supprting the idea that a cortical column might be a generally functional, reproducible unit (Buxhoeveden and Casanova, 2002; Kaas, 2012; Woolsey and Van der Loos, 1970).

The developmental of the embryonic cerebral cortex sheds light both on the nature of this structure and on a mechanism that might explain its evolutionary expansion. During embryonic neurogenesis, neurons that are generated by progenitors in the ventral proliferation zone migrate radially outward from layer 6 (L6), guided by the shaft of radial glial cells which exist transiently during development (Rakic, 1995). The number of progenitor cells that are formed, as well as the duration of neurogenesis are tightly regulated as neurons fill in the cortical volume. This developmental process gave rise to the radial unit hypothesis (Rakic, 1995, 2009), which proposed an increase in the number of neural progenitors and a subsequent increase in cortical units and surface area. Because the number of progenitors is determined by multiple rounds of symmetrical neural stem cell division early in embryogenesis, a few extra rounds of division can lead to exponential increases in the number of progenitor cells and cortical units. Consistent with this theory, manipulations of neural stem cell division rates and the length of the division period in rodents have succeeded in expanding cortical surface area and even generating cortical convolutions (Chenn, 2011; Haydar et al., 1999). This theory provides a plausible explanation for the origin of expanded cortical surface area over time.

But how different are these cortical units across areas and species? The idea of a ‘canonical’ cortical circuit has been controversial and thoroughly reviewed (Douglas et al., 1989; Harris and Mrsic-Flogel, 2013; Harris and Shepherd, 2015; Herculano-Houzel et al., 2008; Miller, 2016; Rakic, 2008; Thomson and Lamy, 2007), but the debate is largely semantic. There are few who would deny the many qualitative similarities across modalities or the presence of many individual exceptions and quantitative variances.

Across species and across functional areas within a species, cortical columns have adapted to fit their function (Harris and Shepherd, 2015). The relative size of cortical layers are different across brain areas, an extreme example of which is the apparent absence of a granular L4 in the motor cortex (M1) (Hooks et al., 2011; Kaneko, 2013). Along with changes in laminar sizes, cortical columns can also have different functional subdivisions within layers, though standardizing nomenclature and agreeing on the appropriate degree of separation is not straightforward. At a functional level, the organization of neural representations can vary greatly, even for relatively straightforward features like sensory representations. This is showcased by visual system organization, where receptive field clustering is different for rodents, cats, and primates (Harris and Mrsic-Flogel, 2013; Kaas, 2012). While methodological difference across species and modalities can make comparing fine-grain circuit structure difficult (Jiang et al., 2013a; Ko et al., 2011; Lefort et al., 2009; Stepanyants et al., 2009), studies that have assessed connections using consistent methodologies have found reproducible differences across cortical areas within the same species (Hooks et al., 2011). Understanding the range of differences that exist between cortical columns is a monumental task, but there is certainly enough evidence to confirm the principle that the cortical column has been adapted over time to suit its local function. Importantly, many of these differences do appear to occur in a developmentally and genetically prescribed fashion, rather than deriving entirely from unique input identity and differences in inherited activity patterns. A study of global gene expression from the human fetal brain found widespread variability in transcription levels across different neocortical regions as well as numerous co-expression networks of groups of genes that typically function

together (Johnson et al., 2009). This differential gene expression, achieved through enhancers, promotors, and other regulatory motifs, can tightly control patterning and local and long-range interconnectivity of cortical neurons (Greig et al., 2013; Kwan et al., 2008; Prabhakar et al., 2008).

Despite this, the neuronal composition of most cortical areas closely follows a set of common principles. Both excitatory and inhibitory cortical neurons can be grouped into general classes based on their developmental origin, morphology, gene expression, and electrophysiological properties. For most cell types, these features co-vary and have allowed the scientific community to generate largely agreed-upon categories of neuronal identity. For excitatory neurons, the most easily identifiable features are laminar location and long-range projection target. These properties reflect developmental origin, predict local connectivity and in many cases align with known genetic markers (Brown and Hestrin, 2009; Harris and Shepherd, 2015; Hooks et al., 2013; Jiang et al., 2015; Kiritani et al., 2012; Thomson and Lamy, 2007). Inhibitory neurons are highly heterogeneous and easily separable based on morphology, local connections, developmental origin, and electrophysiological properties. Studying these properties has lead to the consensus that inhibitory neurons can be meaningfully grouped into three genetically identified non-overlapping populations (Lee et al., 2010). These systems of neural classification, which will be described in greater detail for relevant populations, is the product of decades of widespread effort across many brain regions and species. Comparing results across these studies has demonstrated a clear consistency in the number of cell types, the intrinsic properties of these cell typeps, and their local and long-range connection patterns (Jiang et al., 2015; Lee et al., 2010;

Pfeffer et al., 2013; Pi et al., 2013; Porter et al., 2001). This consistency in neuronal makeup and wiring leads to some shared functional properties as well. For example, excitatory neurons in L4 throughout the brain are a primary point of entry for ascending information, as neurons in L4 receive the bulk of their input from the thalamus and/or lower order cortical areas (Cruikshank et al., 2010; Delevich et al., 2015; Kloc and Maffei, 2014; Schiff and Reyes, 2012; Viaene et al., 2011a). Inhibitory neuron connectivity also generates common functional properties, including feedforward inhibition accompanying long-range inputs, feedback inhibition following local excitation, and specifically regulated inhibition of inhibition (Berger et al., 2010; Cruikshank et al., 2007; Kloc and Maffei, 2014; Lee et al., 2010, 2013; Pfeffer et al., 2013; Pi et al., 2013; Xu et al., 2013). These common principles of neuronal composition and cortical wiring suggest that they are inherently beneficial to many different types of information processing.

1.1.3 Plasticity is the hallmark of the cortical column

What is it about cortical circuit structure that confers this ability to perform useful computations when adapted to so many different purposes? In the most simplistic sense, it is possible that the general fixed structure of this circuit is such that its inherent computation is universally applicable. While this idea is enticing, it is difficult to imagine that a single mathematical operation could underlie the variety of functions it underlies. A slight variation on this idea is even more compelling: that the cortical circuit is universally applicable not because it performs a perfect static operation, but rather that its structure facilitates a massive capacity for change and adaptation within the lifetime of a single organism.

Cortical experience-dependent plasticity was first described in the visual system, when Hubel and Weissel were exploring its fundamental properties in cats (Wiesel and Hubel, 1963). Brief monocular eye-closure during development dramatically altered the tuning of visual cortex neurons, impairments which endured into adulthood. Since that time, decades have been spent studying the phenomenon of developmental critical periods, and similar processes have been observed across sensory systems (Berardi et al., 2000; Fox, 2002). In fact, experience dependent plasticity may even play a role in shaping correct cortical connectivity before an animal is even experiencing or interpreting information about the outside world. In the visual system, spontaneous traveling waves of excitation in the retina are transmitted to cortex via the thalamus and are believed to play an important role in establishing correct cortical connectivity (Ackman et al., 2012). A particularly powerful demonstration of the activity-dependent nature of cortical development was provided in a series of experiments lead by Mriganka Sur where a manipulation in early postnatal ferrets resulted in the ectopic transmission of visual information to the auditory cortex during development. In adulthood, the auditory cortex of these animals contained a three dimensional map of visual space as well as a rough approximation of orientation modules (Roe et al., 1990; Sharma et al., 2000). This type of experience-dependent plasticity can help explain how the neocortical circuits achieved such broad success, as newly expanded cortical areas without a concrete function could make themselves useful by processing new types of information, or duplicating already existing cortical areas.

Experience-dependent plasticity is not just a developmental or evolutionary trait; it is fundamental to the functional role and computational power the cortex provides to

adult animals. The capacity for cortical plasticity in adulthood is most easily observed in sensory cortical areas during large-scale alterations of sensory experience, similar to the initial discovery of critical period plasticity (Feldman and Brecht, 2005; Gavornik and Bear, 2014; Gilbert and Li, 2012). However, experience-dependent plasticity is also instantiated on a much subtler basis to facilitate learning and memory across every level of neocortical processing. Perceptual learning, where an organism becomes more adept at distinguishing or discriminating a sensory percept, is accompanied by changes in both primary sensory cortical regions and higher order sensory areas (Caras and Sanes, 2017; Makino et al., 2016). Association learning, where a perceived stimulus is paired with a behavioral outcome, also induces plasticity in both primary and higher order sensory areas (Lesburguères et al., 2011; Mcgann, 2015; Sacco and Sacchetti, 2010). Task- and rule-learning drives the emergence of task-related ensembles in frontal cortical areas (Garvert et al., 2015; Johnson et al., 2016; Le Merre et al., 2018), while acquiring new motor skills requires motor and premotor cortex and is accompanied by changes in these areas (Biane et al., 2016; Cao et al., 2015; Chen et al., 2015c; Kawai et al., 2015). As plasticity is such an innate aspect of cortical function, it is likely that the conserved structure of the cortex contributes substantially to this critical feature. Understanding the functioning of the cortex therefore requires not only understanding its circuitry, but how the elements work together during behavior to enable experience-dependent plasticity.

1.1.4 The Barrel Cortex as a model system

Bridging the gap between neocortical circuit structure and macroscopic function is inherently challenging because it requires a highly detailed understanding of circuit

elements, their specific connections, and their dynamic activity in relation to behavior. For this reason, experiments towards this goal must be performed in an appropriate system that is complex enough to manifest elements of shared mammalian cortical function but tractable enough to perform thousands of precisely targeted, efficient, and interpretable experiments. The rodent vibrissal somatosensory cortex (barrel cortex) fits all of these criteria and has become an important model for understanding the general function of the neocortical circuit. Rodents, despite having orders of magnitude fewer neurons than many other mammals, have neocortical sensory regions that follow similar rules of structure, organization, and function. The somatosensory cortex in rodents, as for humans, is topographically organized with different body parts represented in distinct columns in proportion to the number of nerve endings they contain. In rodents, a disproportionally large fraction of the somatosensory cortex is designated for sensation related to the whiskers, which are used as one of their primary means of sensing their environment (Feldmeyer et al., 2013). This modality is quite sophisticated, allowing them to sense their environment with the acuity comparable to or greater than that of human fingertips (Carvell and Simons, 1990). Work in rodents is well-suited for investigations that seek to bridge detailed circuit structure and behavior for a number of reasons. First, they are cheap to store and have a fast generation time (10 weeks for mice). Despite their small size, they have adept whisker sensation, have the capacity for short- and long-term memory, and are capable of learning a diverse array of tasks (Adaikkan and Rosenblum, 2015; Biane et al., 2016; Cao et al., 2015; Caras and Sanes, 2017; Chen et al., 2015a, 2015c; Kuhlman et al., 2014; Rioult-Pedotti et al., 2000). Perhaps most importantly, these factors have made rodents a commonly studied

organism and scientists have developed an impressive toolbox of genetic, imaging, and electrophysiological methodologies. For these reasons, the barrel cortex is perhaps the most well understood cortical circuit of any brain area or organism (Feldmeyer et al., 2013; Petersen, 2007). While there are some known differences between the circuitry of mice and rats – for example the lack of a clear septal compartment in mice- the cellular populations, connections, and inputs of the region are overwhelmingly similar. For this reason, our experiments – which seek to integrate new structural details of the neocortex with its important roles in information processing and plasticity – will be performed in the mouse barrel cortex to take advantage of the impressive array of mouse-specific genetic tools. For brevity, discussion of barrel cortex circuitry will not be qualified by whether experiments were done in mice or rats except when necessitated by conflicting findings.

1.2 A snapshot of the barrel cortex function circa June 2013

The rodent barrel cortex is the first of many hierarchically stacked cortical regions to process sensory information about peripheral whisker movements. Relative to other cortical regions, the barrel cortex receives very raw sensory information which makes it an ideal system for understanding how specific neuronal subtypes interact to perform computations. By studying the connections and response properties of neurons in the whisker pathway, scientists have developed one of the most complete working models of cortical columnar processing. This model, which is constantly evolving as new results emerge, has some major shortcomings that are ripe for investigation.

1.2.1 From periphery to cortex

The journey from periphery to cortex begins in the skin near whisker follicles, where changes in whisker position are transduced into electrical signals by nerve fibers that contain a number of specialized endings. While there are many fibers with many types of nerve endings around a given whisker, a single fiber contains only one receptor type and transduces information about only one whisker (Ebara et al., 2002). The cell body of peripheral neurons that innervate the whiskers are located in the trigeminal ganglion at the base of the skull, outside of the central nervous system. These cell bodies carry electrical signals about the movement of a single whisker via axonal projections to the principal nucleus (PrV) of the brainstem trigeminal nuclei where form dense, organized clusters, though axons from an individual animal can span multiple clusters (Sakurai et al., 2013). These clusters, called barrelettes, are spatially organized in a way that matches the topography of whisker location on the snout. The large majority of PrV neurons (68%, Veinante, Deschenes 1999) are responsive to a single whisker determined by their location in a whisker-specific barrelette (Veinante and Deschênes, 1999). These neurons receive input from peripheral sensory neurons expressing numerous receptor types but that are consistent in the whisker they innervate (Sakurai et al., 2013). PrV single whisker neurons then project to similarly organized barreloids in the ventroposterior medial nucleus of the contralateral thalamus (VPM), the primary thalamic nucleus in the somatosensory system (Chiaia et al., 1991; Veinante et al., 2000a). The large majority of neurons, which reside in the core of a given barreloid receive input only from PrV neurons related to a single whisker and thus have single whisker receptive fields (Urbain and Deschenes, 2007). VPM neurons then, in turn,

send dense axonal arborizations to layer 4 of the whisker-related S1, forming the barrels for which the region is named (Koralek et al., 1988; Simons, 1978; Welker, 1976; Woolsey and Van der Loos, 1970). VPM also sends less dense projections to layer 6 of the cortex (Crandall et al., 2017; Wimmer et al., 2010a). Neurons at every level of this pathway respond not only to external stimulation of the whisker, but also to animal-generated movement that occurs during whisking and active sensation (Moore et al., 2015).

Together, the barrel cortex system forms one of the most pronounced examples of a labeled line system in the brain, and is referred to as the single-whisker or lemniscal pathway. This name derives from the receptive field properties observed and not from its actual use, as both active sensation and passive stimulation almost always engage multiple whisker simultaneously. Despite this, there is further complexity both to the wiring and response properties than is presented above. At the level of the brainstem and thalamus, there are populations of neurons that have broader, multi-whisker receptive fields that exist in parallel pathways or different sub-regions of the same nuclei (Pierret et al., 2000; Veinante and Deschênes, 1999). Even the core neurons in the VPM can be activated by one or more surrounding whiskers, though to a lesser degree than a primary whisker (Diamond et al., 1992). Additionally, processing of whisker information does occur even at the level of the brainstem and thalamus, as neuronal responses even to an identical stimulus will vary based on factors such as stimulus history or internal brain state (Minnery, 2003; Simons and Carvell, 1989). The surround receptive fields and response variability observed in subcortical regions are enabled by interconnections across nuclei of the same hierarchical level (Furuta et al., 2008;

Jacquin et al., 1990) and as a result of feedback from the cortex (Furuta et al., 2010). While subcortical processing is an important area of active investigation, the activity within the primary thalamic nucleus VPM is predominantly related to the movement of a single whisker and is reliably transmitted to the cortex. The simplicity and organization of this system has enabled decades of research about cortical processing of a consistent and tractable sensory input.

1.2.2 A working model of cortical function

While ascending sensory information follows a linear and generally straightforward set of relays to the cortex, the circuitry and the flow of information becomes more complicated in the barrel cortex. A cortical column, which is defined by extending the 300um diameter of VPM L4 axonal projections to the white matter and pial surface, is divided into six layers that contain characteristic patterns of cell types, inputs, and projections. Each column contains roughly 10^5 predominantly excitatory neurons (~80%) distributed across layers 2-6. Excitatory neurons in the cortex are primarily pyramidal neurons, named for their soma morphology, and have reasonably homogenous intrinsic electrophysiological properties such as resting membrane potential and current-evoked firing phenotype. The most separable pools of pyramidal neurons based on electrophysiological properties are thin-tufted, regular spiking Pyr neurons and thick-tufted, intrinsically bursting Pyr neurons that are concentrated in L5a and L5b respectively (Jacob et al., 2012; Meyer et al., 2010a). Pyr neurons, even those that are electrophysiologically indistinguishable, do have characteristic local and long-range projection targets, which sometimes align with unique genetic profiles (Brown and Hestrin, 2009; Chen et al., 2013; Greig et al., 2013; Kiritani et al., 2012; Morishima,

2006; Yamashita et al., 2013). The local connections between excitatory neurons in the barrel cortex have been extensively studied using simultaneous whole-cell patch clamp recording in acute brain slices in vitro. These studies found that the most prominent connections are recurrent between excitatory neurons in L3-L5, ascending projections from L4 to L2/3, and descending projections from L2/3 to L5 (Crandall et al., 2017; Hooks et al., 2011; Lefort et al., 2009). Most cortical Pyr neurons also have long-range projection targets that are organized by layer. Neurons in L2/3 and L5 project to one of multiple cortical regions, especially the secondary somatosensory cortex (S2) and M1. Different neuronal populations in L5 and L6 project out of the cortex to the thalamus or to the striatum.

Inhibitory neurons, which are interspersed with excitatory neurons in L2-L6 and make up all of the neurons in the cell-sparse L1, are particularly heterogeneous. Inhibitory neurons even within the same layer have vastly different soma morphology, intrinsic properties, evoked activity patterns, and neurite structure. Genetic markers exist that separate the diversity of inhibitory neurons into three virtually-comprehensive and non-overlapping groups (Rudy et al., 2011). Parvalbumin-expressing (PV) inhibitory neurons can fire at high frequencies and inhibit the soma and dendritic arbors of neighboring Pyr neurons as well as some other inhibitory neurons (Atallah et al., 2012; Packer and Yuste, 2011; Pfeffer et al., 2013). These neurons can be activated by local Pyr neurons or by long-range input to the cortex (Jiang et al., 2015; Wall et al., 2016). Somatostatin-expressing (SST) inhibitory neurons have a slower and adapting firing phenotype, and appear to specialize in local feedback inhibition between Pyr neurons (Berger et al., 2010; Silberberg and Markram, 2007; Urban-Ciecko et al., 2015) but see

(Hu and Agmon, 2016; Porter et al., 2001; Tan et al., 2008; Wall et al., 2016). Pyr neuron input to SST cells is initially weak but facilitates when an input fires rapidly or when they receive coincident inputs (Berger et al., 2010; Silberberg and Markram, 2007). SST cells target the dendritic arbors of Pyr neurons. Finally, 5HT3a-expressing inhibitory neurons – which are themselves a diverse class – receive substantial input from long-range inputs to the cortex (Staiger et al., 1996; Wall et al., 2016) and specialize in the inhibition of other inhibitory neuron populations (Jiang et al., 2013b, 2015; Lee et al., 2010; Letzkus et al., 2011; Pi et al., 2013).

L4 is universally viewed as the primary entryway through which ascending sensory information enters the barrel cortex. L4 excitatory neurons have dendritic arbors restricted to a single barrel and thus receive input almost exclusively from VPM neurons which respond to a single whisker (Meyer et al., 2010a; Thomson and Lamy, 2007). L4 receptive fields are therefore highly specific for the barrel's primary whisker. Additionally, L4 neurons are only a few synapses from the periphery, and thus their response times are very short, on the order of 10-15ms from whisker stimulation (de Kock et al., 2007). While stimulus-evoked spiking occurs at a lower rate and is less reliable than in barrelettes or barreloids, spiking in L4 is both high frequency and highly reliable relative to other cortical layers and other cortical regions (Armstrong-James et al., 1992a; de Kock et al., 2007; Welker et al., 1993). In contrast, neurons in nongranular layers have broader dendritic arbors (Oberlaender et al., 2012a; Thomson and Lamy, 2007). Neurons in L2/3 have particularly broad and heterogenous receptive fields that are dynamically altered by context and brain state (Brecht et al., 2003; Clancy et al., 2015).

From this detailed understanding of columnar circuitry and response properties a sequential model of cortical function was derived. In this model, relatively raw sensory information from the thalamus is faithfully transmitted to L4 of the cortex and then traverses the cortical layers serially with computations occurring across and within layers. The pattern of connectivity suggested that information from L4 is first transmitted to L2/3, and then to deep layers of the cortex. Neurons in L2/3 send a copy of the partially processed information to higher cortical areas like S2, while the deep layers, which project to subcortical layers like the thalamus and striatum, were viewed as the main output of the cortex. The broad receptive fields of neurons in supragranular layers are explained by their broad dendritic arbors which allow them to sample input from multiple barrels. This view of sequential cortical processing was a powerful idea, and predominated for many years (Armstrong-James et al., 1992b; Douglas and Martin, 2007; Feldman and Brecht, 2005).

1.2.3. A working model of cortical plasticity

As described previously, experience-dependent plasticity is a prominent feature of neocortical circuits, and the unique topographical organization of the barrel cortex also makes it an ideal system for investigating patterns and mechanisms of cortical rearrangement. In its simplest sense, this involves altering the level of stimulation experienced by one or more whiskers and measuring the change in organization at the cortical level. This phenomenon, known as map plasticity, was first observed during development, where the whisker-mapping of stimulus-evoked activity levels in L4 neurons would change following the trimming of one or more whiskers. For example, when all but one whisker is trimmed from birth throughout development, L4 neurons in

neighboring barrels have unusually large responses to stimulation of the spared whisker that last into adulthood (Fox, 1992). While this manipulation has an early critical period around postnatal day 7 (P7), similar rearrangements of receptive fields in L2/3 are observed throughout adulthood (Fox, 1992; Glazewski and Fox, 1996). Deprivation also has an effect on cortical representations, as L2/3 neurons in deprived columns are less active than control animals following stimulation of their original primary whisker (Glazewski and Fox, 1996). Decades of experiments have followed, investigating the many ways in which altered sensory experience through strategic whisker-trimming can affect neuronal responses in the cortex (Feldman and Brecht, 2005; Fox, 2002). A first major takeaway is that the specific style of sensory alteration can greatly influence the changes observed at the level of the cortex. For example, while single-whisker experience will cause the spared representation to expand, mice with two adjacent spared whiskers will undergo a merging, but not expansion into other columns, of cortical receptive field (Diamond et al., 1994). In contrast, mice that are completely deprived of whisker experience after a second critical period specific to L2/3 at P12-14 will undergo no map plasticity (Stern et al., 2001). On the other extreme, prolonged environmental enrichment will cause retraction and sharpening of receptive fields for all whiskers (Polley et al., 2004). A second major takeaway is that this plasticity can be very rapid. In non-granular layers, receptive field changes in response to single-whisker experience (Diamond et al., 1994) or single-row deprivation (Jacob et al., 2012) can occur in 1-3 days, even in adult animals. A final observation from these studies is that, in the adult animal, neurons in L2/3 and L5 have a greater capacity for rapid experience-dependent changes than for neurons in L4 (Diamond et al., 1994; Jacob et

al., 2012; Polley et al., 2004). It is important to note that some experiments have observed experience-evoked anatomical changes in L4 by electron microscopy (Knott et al., 2002; Landers et al., 2011), by reconstruction of VPM thalamocortical axons (Oberlaender et al., 2012b; Wimmer et al., 2010b), or through cytochrome oxidase staining (Polley et al., 2004). However, only one of these studies found evidence of anatomical plasticity over a time period comparable to neurons in nongranular layers (Knott et al., 2002). This study used electron microscopy and actually found an increase of both excitatory and inhibitory synapses, and found only a modest decrease in L4 neuronal spiking at a delayed time point relative to stimulus presentation. The receptive fields of L4 neurons were not investigated. Together, studies of gross alterations in whisker activity tell us that experience dependent plasticity in the adult barrel cortex causes diverse outcomes, but that neurons in L2/3 and L5 have a particular capacity for undergoing rapid map plasticity.

Recently, experimental manipulations have become more sophisticated and behaviorally relevant. Monitoring the activity of superficial excitatory neurons via Ca++ imaging during the learning of a texture discrimination task shows sub-type specific alterations of response properties that progress over the course of a few days (Chen et al., 2015a). Similarly, longitudinal fluorescent imaging of dendritic spines in the somatosensory cortex during a whisker-mediated object localization task revealed major changes in spine turnover on the dendrites of L2/3 neurons throughout learning (Kuhlman et al., 2014). In addition to these active sensation tasks, whisker stimulation has been paired with positive and negative outcomes in association learning tasks. The most common paradigm is known as trace-eyeblink conditioning, where a whisker

stimulus is delivered followed by an aversive puff of air to the mouse's eye after a short delay. This, and other similar paradigms (Siucinska and Kossut, 1996), observed rapid expansion of the affected barrels when measuring by cytochrome oxidase staining or imaging of 2-deoxyglucose (2-DG, performed in rabbits)(Galvez et al., 2007). Recording from neurons in deep layers found enhanced responses to the conditioned whisker stimulus that correlated with behavioral learning in L5 and L6 (Ward et al., 2012). An appetitive conditioning task that follows a similar paradigm but pairs whisker stimulus to reward (sweetened water) found rapid alterations in 2-DG signal in L2/3 and L5 after just 3 days of training, and only observed changes in L4 2-DG signal after two months of training (Siucinska and Kossut, 2004). These findings show that the rapid plasticity observed in L2/3 and L5 neurons is not a result of aberrant deprivation protocols and extends to whisker related behavioral learning.

Altered cortical firing rates do not necessarily have to come from local synaptic changes, but the ability to track dendritic spines longitudinally has confirmed that cortical synaptic plasticity does occur in both L2 neurons and the apical dendrites of L5 neurons of the barrel cortex during sensory learning and deprivation paradigms (Holtmaat et al., 2006; Joachimsthaler et al., 2015; Kuhlman et al., 2014). Other studies have found alterations of neurite patterns and synaptic connections following adult sensory experience (Cheetham et al., 2008, 2014; Jacob et al., 2012; Kätzel et al., 2011). These studies, much like functional response properties, show that changes are happening in a subset of post-synaptic cortical excitatory neurons. However, it does not identify which inputs onto these neurons are strengthened, a critically important piece of information for understanding how the structure of the cortical circuit enables its

function. Given the standing model of cortical function, alterations in cortical activity level are largely believed to occur at intracortical synapses within and between layers. The first major reason for this, which has already been touched upon, is that thalamocortical inputs to L4 of the cortex appear largely stable in adulthood. Indeed, NMDA-dependent strengthening of VPM to L4 synapses has an early critical period that coincides with the critical period for map plasticity in L4 (Crair and Malenka, 1995). Second, synaptic plasticity at numerous intracortical sites can be readily evoked by artificial stimulation protocols in vitro and can even be observed in acute brain slices of animals that have undergone in vivo sensory experience (Allen et al., 2003; Banerjee et al., 2009; Brasier and Feldman, 2008; Cheetham et al., 2007; D'amour and Froemke, 2015; Feldman, 2000; Sjöström and Häusser, 2006; Sjöström et al., 2001; Takahashi, 2010; Wen and Barth, 2011; Zilberter et al., 2009). It is also clear that cholinergic signaling plays an important role in generating cortical synaptic plasticity. It was first discovered that activation of the basal forebrain or application of ACh in concert with auditory stimulation can shift receptive fields in a frequency-specific manner (Bakin and Weinberger, 1996; Froemke et al., 2007; Shulz et al., 2003). A similar result has been observed for whisker stimuli in the barrel cortex (Shulz et al., 2003).

Together, these data suggest a model where thalamocortical inputs to the cortex are stable in adulthood, and the changes in cortical response properties observed in nongranular layers are generated by activity-dependent plasticity at intracortical synapses, altering the sequential flow of information through the cortical circuit.

1.2.4 Shortcomings of cortical models

The model of sequential processing across layers, with learning-dependent changes at intracortical synapses, fits many features of cortical circuit architecture and dynamics. Despite this, it has some important limitations that were beginning to be acknowledged at the time this line of investigation was conceived. The first major issue is that it does not fit the timing and response properties of all cortical neurons. While early studies correctly determined that response latency was longer in superficial layers than in L4, response times in deep layers have been found to occur at similar latencies, indicating that their initial source of drive is not inherited serially from L4 via superficial layers (Constantinople and Bruno, 2013). Further, receptive fields in deep layers are tighter than in L2 (Armstrong-James et al., 1992b), which does not align with the putative input source of broadly tuned L2/3 neurons. Finally, cortical neurons, especially in L2/3, typically fire at low frequencies in the range of 0.01 to 0.5 Hz following a whisker stimulus (Barth and Poulet, 2012). Without an extremely high rate of neuronal convergence, individual cortical layers are unlikely to generate sufficient action potentials to provide the dominant source of drive to another cortical layer. Even for neurons within the same barrel, connection rates around 10-20% represent the upper threshold for local connectivity (Jiang et al., 2015; Lefort et al., 2009). The low firing rates observed in the barrel cortex are, in part, a product of strong, PV-mediated, feedforward inhibition that accompanies thalamic input and strong feedback inhibition from multiple inhibitory neuron types that follow cortical activity (Atallah et al., 2012; Packer and Yuste, 2011; Silberberg and Markram, 2007). Together, these findings make it unlikely that sequential intracortical connections are providing the dominant input to most cortical layers. This is particularly true for deep layer neurons which

receive intracortical input from sparsely active L2/3 and have potential access to primary thalamic input. This theory was tested directly by silencing superficial cortical neurons while recording whisker-evoked activity in deep cortical layers (Constantinople and Bruno, 2013). The finding that activity levels in deep layers were largely unperturbed by silencing superficial cortical layers was surprising to many and emphasized the need for an updated model of cortical processing. Finally, the sequential model of cortical processing deems deep cortical layers the endpoint of cortical processing. While it is true that only deep layers project to non-cortical targets like the striatum and thalamus, L2/3 neurons project to higher cortical areas like M1 and S2. Since the primary somatosensory cortex is handling relatively raw sensory information, its output to higher sensory areas and M1 intuitively seem more likely to eventually contribute to behavioral output than subcortical projections to the sensory thalamus.

In many ways, our understanding of cortical plasticity was based on the sequential idea of cortical processing and the proposed intracortical basis for response plasticity faces similar challenges. The generally accepted mechanisms of synaptic plasticity are activity-dependent (Malenka and Bear, 2004), guided by either high rates of post-synaptic activity, or precisely timed coincident action potentials between pre- and post-synaptic partners. The low firing frequency of cortical neurons and prominent cortical inhibition seem to provide few opportunities for activity dependent long term potential of excitatory synapses. Cortical firing rates in non-granular layers – especially in L2/3 – are particularly unreliable, displaying variable response latencies even for identical stimuli (Armstrong-James et al., 1992b; Welker et al., 1993). With firing rates

below 1 Hz in both pre and post-synaptic partners, it is difficult to understand how STDP or activity-dependent plasticity could reasonably occur. Disinhibition mediated by acetylcholine is a possible mitigating factor, but even in behaving mice instantaneous firing rates in superficial cortex rarely eclipse 5 Hz (Crochet et al., 2011; O'Connor et al., 2010). Improving our understanding of cortical circuit function will require addressing these issues by identifying additional circuit elements and mechanisms that explain both parallel information flow through the cortex and the generation of synaptic plasticity in sparsely active neuronal populations.

1.3 The potential contribution of the posterior medial thalamic nucleus

The long-standing model of cortical processing described above has focused entirely on a single, linear pathway from the periphery to cortex that obeys a single-whisker labeled line organization. However, it has long been known that there are additional subcortical pathways that activate the cortex. The most prominent of these, referred to as the paralemniscal pathway, proceeds through the posterior medial thalamic nucleus (POm). While it is often characterized as carrying ascending sensory information to the cortex in parallel to the lemniscal system, it has fundamentally different inputs and outputs that elevate its role in the functional hierarchy of the brain. The functional contributions of POm have been far less studied, but known properties of POm suggest that its role in cortical function has been underestimated. This study was designed and carried out to extend our understanding of the POm thalamocortical circuit in the hope of updating our model of cortical processing and plasticity.

1.3.1. Properties of the POm higher order thalamic nucleus

Similar to the VPM thalamic nucleus, ascending sensory information reaches the POm via peripheral sensory neurons and the brainstem. However, POm receives the bulk of its brainstem input from the trigeminal nucleus interpolaris (SpVi) and only a minority of its input from PrV (Chiaia et al., 1991; Veinante and Deschênes, 1999; Veinante et al., 2000a). Both neuronal populations that target POm, unlike the lemniscal pathway, have broad receptive fields (Jacquin et al., 1989; Veinante and Deschênes, 1999). These broad receptive field properties are reflected in POm neurons (Ahissar et al., 2000; Diamond et al., 1992), though major POm input also arises from an additional source. Unlike neurons in VPM, POm neurons receive strong driving input from both ascending trigeminal inputs and from the cortex (Groh et al., 2014a; Lavallee, 2005; Liao et al., 2010). This input originates from deep cortical layers of the whisker SI (Alloway et al., 2003; Deschênes et al., 1998; Landisman and Connors, 2007; Sumser et al., 2017) as well as S2 and M1 (Alloway et al., 2003; Hooks et al., 2013; Urbain and Deschenes, 2007). Interestingly, POm does not contain an apparent topographic organization at the level of ascending sensory inputs (Chiaia et al., 1991; Veinante et al., 2000b), but cortical feedback patterns to POm are topographically organized (Alloway et al., 2003; Sumser et al., 2017). Broadly tuned ascending sensory inputs combined with highly processed information from multiple cortical regions confers complicated patterns of activity in POm that are not well understood.

Early recordings, which were almost always performed under anesthesia, found that whisker deflections generated minimal spiking in broadly tuned POm neurons (Ahissar et al., 2000; Diamond et al., 1992; Lavallee, 2005). This sparse coding was

used as the basis for a theory that POm specializes in transferring whisker stimuli into rate codes (Ahissar et al., 2000). The same investigator later hypothesized that POm specializes in sensory reafference during whisking (Yu et al., 2006), and then again proposed POm as an important site of object localization (Yu et al., 2015). More recent studies in awake animals have found that stimulation of one or more whiskers does drive substantial activity in both the SpVi and POm, but that firing rates do not relate to specific kinematic features of whisker stimulus (Masri et al., 2008; Sosnik et al., 2001). Further, animal-generated whisker movements did not dramatically increase firing or position encoding in POm (Masri et al., 2008; Moore et al., 2015; Urbain et al., 2015). It has also been observed that arousal and cholinergic signaling can alter the flow of information through POm (Masri et al., 2006a; Sobolewski et al., 2015; Trageser, 2006). Clearly, the information content received and transmitted by POm is not well understood, and is not likely to have a simple answer. What is clear, however, is that the functional role of POm is not purely, or even primarily, related to the raw movements of whiskers. Due to the hub-like nature of POm, sitting at the interface of raw sensory information, processed sensory feedback, motor systems, and saliency systems, POm may participate in complex and context-dependent behavioral processes.

POm neurons themselves send axonal projections to S1, S2, and M1 (Hooks et al., 2013; Viaene et al., 2011b; Wimmer et al., 2010a). Single-cell tracing shows that an individual neuron makes broad axonal arborizations in both L1 and L5a of the barrel cortex (Ohno et al., 2012), a complementary pattern to that of VPM (Wimmer et al., 2010a). Computational analysis of reconstructed thalamocortical axons and cortical neurons suggests that neurons in almost every layer have axon-dendrite overlap with

both POm and VPM axons (Meyer et al., 2010b). Despite this, our understanding of how POm could impact or drive cortical activity was virtually nonexistent when this study was initiated in 2013. Laser scanning photo-stimulation and electrical stimulation in thalamocortical slice preparations revealed that POm could drive activity in excitatory neurons, especially in deep cortical layers (Bureau et al., 2006; Viaene et al., 2011b), and channel-rhodopsin-mediated activation of POm inputs revealed that POm could provide monosynaptic input to at least some cortical neurons (Petreanu et al., 2009). However, due to methodological or sampling limitations, it was unclear how many neurons, in which layers, and of what types actually did receive input.

1.3.2. The potential role of POm in cortical function

While many details of the POm thalamocortical circuit were – and still are – unknown, it is well positioned to contribute to some elements of cortical function that are not well explained by the conventional, sequential model. First, POm is a potential source of input to neurons in multiple cortical layers. This input, if strong enough, could put POm in a position to substantially impact the firing of cortical neurons, especially in L2 and L5. This is important, since activity in L2 and L5 was believed to be inherited largely from other cortical layers. This has important implications for the origin and significance of receptive fields and, along with direct VPM input, could contribute to the early spikes observed in L5 and occasionally L2. Perhaps more importantly, POm input to L2 and L5 could play an important role in cortical experience-dependent plasticity. The rapid alterations in response properties in these layers has historically been attributed to altered intracortical connections. If, however, POm is a major source of drive for these neurons, than alterations in their firing properties could be attributed to

altered input from POm. In support of this idea, preliminary investigations of activity levels in POm suggest that they are substantially greater than in typical cortical neurons (Masri et al., 2008; Urbain et al., 2015), which makes it a more likely candidate to undergo rapid activity dependent plasticity. While intracortical connections are capable of LTP and LTD under numerous artificial protocols, there is very limited evidence that these synaptic sites actually undergo synaptic plasticity during behaviorally relevant experience. Meanwhile, POm is well positioned to integrate both raw and processed sensory and motor signals and is wired into cholinergic systems that we know are important for plasticity (Masri et al., 2006a; Shulz et al., 2003; Sobolewski et al., 2015). The potential impact of POm on cortical function is clear, important, and ripe for investigation.

1.3.4 Experimental approach and findings

We set out to investigate the potential contributions made by POm to cortical activity patterns under basal conditions and during sensory learning. In order to attain the requisite level of cell-type specificity and to allow for highly controlled precise testing of individual circuit elements, we investigated the electrophysiological responses of individual cortical neurons following optogenetic activation of thalamic axons in acute brain slices containing largely intact barrel columns. We first used targeted whole-cell patch clamp recording in combination with transgenic mouse lines to determine the cell-type specific functional connectivity of POm afferents in control animals. In deep layers, POm provides strong, direct input to excitatory neurons synchronized by fast, feedforward inhibition from parvalbumin-expressing neurons. Alternatively, POm provides weaker direct input to Pyr neurons in superficial layers, but can facilitate over

the course of stimulation due to weaker, delayed feedforward inhibition from 5HT3a neurons. In both, tonically active somatostatin-expressing inhibitory neurons were silenced by 5HT3a neurons.

These findings, in concert with the recent discovery that long-term potentiation could be artificially driven at POm cortical inputs in vitro, lead us to investigate the potential for plasticity in POm thalamocortical circuits during learning. To enable a detailed, cell-type specific analysis of synaptic changes during learning, we developed a high throughput home-cage sensory association training assay that paired a multiwhisker stimulus with a water reward. We discovered that POm activation drove dramatically increased cortical activity in both deep and superficial layers after just 24 hours of training, when behavioral evidence for a learned association first emerged. This increase in activity did not occur in VPM pathways and was caused by a learning-specific increase in synaptic strength at the POm to L5 synapse. Over longer durations of training, synaptic plasticity occurred at both thalamocortical (POm) and intracortical (L2) inputs onto L2 Pyr neurons. Together, our results show that the higher order thalamic nucleus POm is wired to drive distinct patterns of input to deep and superficial cortical layers. Further we for the first time identify POm inputs to the cortex as the initiator of cortical rearrangements, facilitating sequential synaptic plasticity within the cortex during sensory learning. This study provides a much-needed update to the long-held sequential view of cortical processing and identifies the POm thalamocortical circuit as a critical component of future investigations of thalamocortical function.

2 *POm thalamocortical input drives layer-specific microcircuits in somatosensory cortex*

Higher-order thalamic nuclei, such as the posterior-medial nucleus (POm) in the somatosensory system or the pulvinar in the visual system, densely innervate the cortex and can influence perception and plasticity. To systematically evaluate how higher-order thalamic nuclei can drive cortical circuits, we investigated cell-type selective responses to POm stimulation in mouse primary somatosensory (barrel) cortex, using genetically-targeted whole-cell recordings in acute brain slices. We find that ChR2-evoked thalamic input selectively targets specific cell types in the neocortex, revealing layer-specific modules for the summation and processing of POm input. Evoked activity in pyramidal neurons from deep layers is fast and synchronized by rapid feedforward inhibition from GABAergic parvalbumin-expressing neurons, and activity in superficial layers is weaker and prolonged, facilitated by slow inhibition from GABAergic neurons expressing the 5HT3a receptor. Somatostatin-expressing GABAergic neurons do not receive direct input in either layer and their spontaneous activity is suppressed during POm stimulation. This novel pattern of weak, delayed, thalamus-evoked inhibition in layer 2 suggests a longer integration window for incoming sensory information and may facilitate stimulus detection and plasticity in superficial pyramidal neurons.

2.1 Introduction

How does sensory neocortex convert input into output, to influence and drive activity in downstream brain areas? The algorithm by which neocortical circuits

transform incoming sensory information is determined by the stereotyped connectivity and firing properties of neuronal cell types within the cortical column. Thus, defining the conserved architecture of these circuits within and between different neocortical areas has been of great interest (Bock et al., 2011; Hangya et al., 2014; Harris and Mrsic-Flogel, 2013; Harris and Shepherd, 2015; Jiang et al., 2015; Lee et al., 2016; Lefort et al., 2009; Miller, 2016; Pi et al., 2013; Vélez-Fort et al., 2014; Yuste, 2015).

Accumulating evidence indicates that there are common principles that regulate thalamic connections within the cortical column, suggesting that this transformation might have essential similarities across different primary sensory areas. For example, thalamic input to layer 4 (L4) targets both excitatory neurons as well as fast-spiking, parvalbumin-expressing (PV) inhibitory interneurons in primary visual, auditory, and somatosensory cortex but shows weak or negligible input to somatostatin-expressing (SST) neurons (Porter et al. 2001; Cruikshank et al. 2007; Schiff and Reyes 2012; Kloc and Maffei 2014; but see Hu et al. 2016). These principles for sensory-related thalamic input may extend to other layers (Ji et al., 2016).

In somatosensory cortex, the thalamocortical afferents from the ventro-posterior medial nucleus (VPM) in L4 have commonly been viewed as the main source of sensory input to the neocortex. However, it has become increasingly clear that another important source of cortical input comes from the posterior-medial nucleus of the thalamus (POm), a higher-order sensory nucleus with dense axonal arborizations in L1 and L5a (Chmielowska et al., 1989; Cruikshank et al., 2007; Koralek et al., 1988; Meyer et al., 2010b; Petreanu et al., 2009; Wimmer et al., 2010a). Neurons residing in POm have complex receptive fields, are driven by both peripheral sensory input and cortical

feedback from motor and sensory areas, and are modulated by whisker movement (Ahissar et al., 2001; Diamond et al., 1992, 1992; Groh et al., 2014b; Urbain et al., 2015; Yu et al., 2006, 2015). This suggests that POm, like the pulvinar in the visual system, incorporates contextual information and brain state with sensory information (Purushothaman et al., 2012; Roth et al., 2016). However, the role of higher-order thalamic nuclei in sensory processing is a topic of substantial debate (Constantinople and Bruno, 2013; Mease et al., 2016; Roth et al., 2016; Sherman, 2016; Yu et al., 2015), and much less is known about the distribution of POm inputs across diverse cell types, or how they drive the cortical circuit.

While prior studies have characterized the presence and sub-cellular location of POm inputs onto pyramidal (Pyr) neurons in superficial and deep layers (Bureau et al., 2006; Gambino et al., 2014; Jouhanneau et al., 2014; Petreanu et al., 2009; Viaene et al., 2011a), a comprehensive analysis of inputs across multiple layers and cell types has not been accomplished. This is particularly important for developing schema by which POm can drive network activity, where inhibitory neurons can play a powerful and diverse role. Understanding the algorithm by which sensory information is transformed by neocortical circuits will be impossible without fine-grained mapping. Here we use the mouse somatosensory (barrel) cortex as a model system to define the process by which the neocortex receives and transmits incoming sensory information, with a focus on input from the higher-order thalamic nucleus POm. We perform a systematic evaluation of POm-mediated excitatory drive to barrel cortex using the experimental precision afforded by recordings in acute brain slices to target four defined cell types across the column.

Using channelrhodopsin (ChR2)-mediated excitation of POm fibers in the neocortex, we first determined which layers and specific cell types receive strong input. Next, we isolated layer-specific properties of disynaptic, feedforward inhibition. Finally, we investigated how these wiring motifs were manifested in recurrent activity generated by repetitive POm stimulation. Our analysis reveals thalamic wiring principles that are conserved between L4 and L5 as well as novel mechanisms for feedforward inhibition in L2. We find that direct POm input to PV cells is strong in L5a but absent in L2, where POm activity drives firing in 5HT3a-expressing (5HT3a) cells. In both layers, direct synaptic input to SST neurons was negligible. These wiring patterns generate layer-specific processing of POm thalamocortical inputs, with temporally precise spikes in L5 Pyr neurons and weak but summating responses in L2 Pyr neurons. Our results show, for the first time, that a higher-order thalamic nucleus can drive activity in multiple cell-types throughout the column, and supports the idea that sensory information processing is fundamentally different across cortical layers.

Our data also recapitulate some cell-type-specific features of sensory-evoked activity – SST neuron hyperpolarization, and the initiation of recurrent network activity – that have been observed *in vivo* (Gentet et al., 2012; Jouhanneau et al., 2014; Mease et al., 2016), indicating that POm activity is sufficient to generate these phenomenon in acute brain slices with only local connections preserved. The ability to employ a functional readout of summated network interactions between multiple cell types with precise input control provides new insight into how large groups of interconnected neurons in the neocortex might behave during sensation.

2.2 Results

2.2.1 POm provides direct, glutamatergic input onto cortical excitatory neurons

To understand how POm activity is transformed by somatosensory cortex, we first mapped this input onto excitatory neurons across the cortical column. Prior studies have suggested that POm stimulation both *in vivo* and *in vitro* can drive short latency, excitatory responses in some neocortical neurons (Bureau et al., 2006; Gambino et al., 2014; Jouhanneau et al., 2014; Petreanu et al., 2009; Viaene et al., 2011a), but how they are distributed across excitatory neurons throughout the cortical column and within different cell types in a given layer has not been comprehensively investigated. To determine how POm inputs engage excitatory neurons from L2 to L6, we used a ChR2-based strategy to selectively excite POm afferents in combination with pharmacological methods to evaluate whether these inputs directly activated target neurons.

POm-targeted stereotaxic injections of ChR2-expressing virus were carried out in young postnatal mice, and POm targeting in acute brain slices was confirmed by a characteristic pattern of afferent labeling concentrated in L5a and L1 of S1 barrel cortex (Koralek et al. 1988, Meyer et al. 2010b). In cases where the injection site overlapped slightly with the ventro-posterior medial nucleus (VPM) of the thalamus, we could observe terminal labeling both in L4 (the VPM target layer) and L5a/L1, and this tissue was not used for further analysis.

Broad-field illumination of ChR2 afferents with a 5 ms blue light pulse elicited a short latency EPSC in Pyr neurons (Figure 1). These responses were eliminated in the

presence of the AMPAR-antagonist NBQX, indicating that POm input was glutamatergic (Figure 1B). For both L2 and L5 neurons, paired-pulse optical stimulation showed that

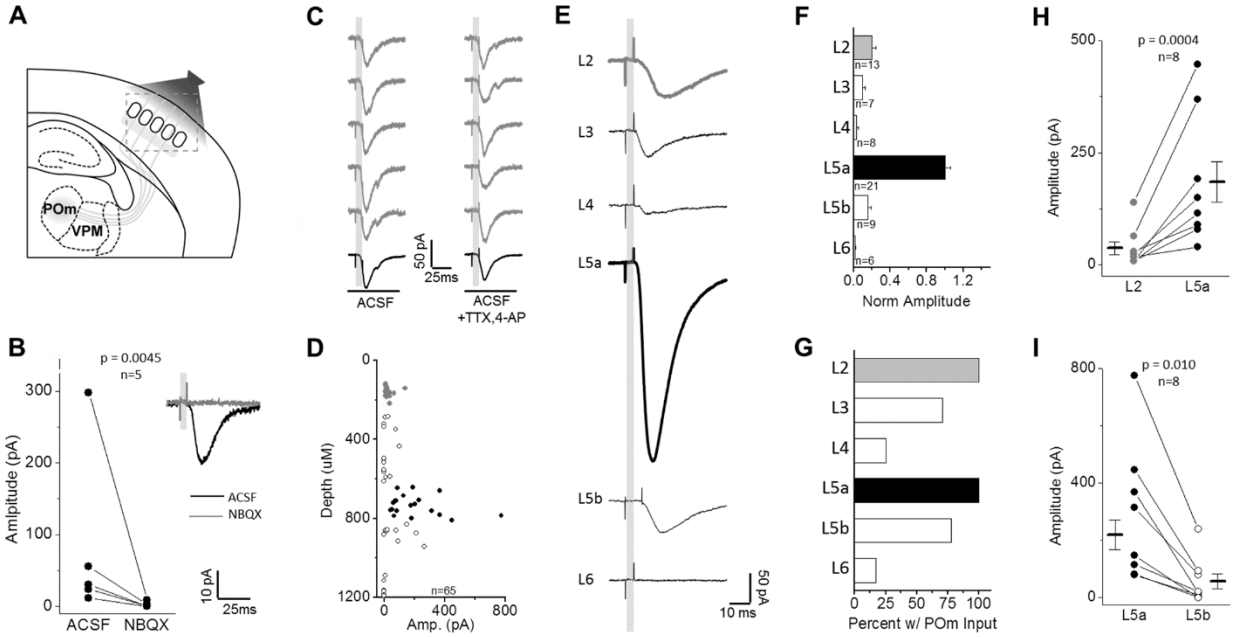

Figure 1. Excitatory neurons in all cortical layers receive direct synaptic input from POm. (A) Schematic of experimental design. POm-targeted ChR2 viral injection in POm neurons labeled axons in barrel cortex. (B) EPSCs evoked by POm light stim in L2 Pyr neurons, eliminated by addition of AMPAR antagonist NBQX. 5 consecutive trials (gray) followed by response average for 10 trials. (C) Short latency EPSCs in L2 Pyr neurons are direct from POm axons. EPSCs persist with addition of voltage-gated Na^+ channel antagonist TTX and K-channel antagonist 4-AP. (D) Direct POm-evoked EPSCs in cortical Pyr neurons in TTX and 4-AP plotted by depth from pia surface (gray: L2, black: L5a). (E) Average cell response (10 trials) for a representative cell in each cortical layer, defined by cytoarchitecture and depth. (F) Across-layer comparison of amplitude normalized to the average L5a response in each slice to account for across-preparation variance in ChR2 expression. (G) Percent of recorded cells in each layer that receive direct POm-evoked EPSCs. (H) L5a Pyr neurons receive larger direct input than in L2. Connected points represent a comparison of the average of all responses recorded in L2 or L5a neurons from a given animal. Data points and n value are animal averages and a paired t-test is used. (I) L5a Pyr neurons receive larger direct POm input than L5b neurons. Same as (H).

responses were depressing (Table 1), likely due to elevated initial release probability from ChR2-mediated depolarization.

To confirm that this excitation results from direct input from POm and not recurrent activation elsewhere in the neocortical circuit, tetrodotoxin (TTX) and 4-aminopyridine (4-AP) were bath applied to prevent network firing (Petreanu et al., 2009). Here, Ca^{++}-dependent synaptic release is thought to be mediated by ChR2-depolarization at the terminal that directly enables opening of voltage-gated Ca^{++} channels, and the addition of the K^+ channel blocker 4-AP increases the period of depolarization at the terminal to enhance release. In all cases, the EPSC persisted, although the onset latency and time to EPSC peak was increased slightly, most likely due to prolonged depolarization at the terminal (Figure 1C).

To systematically compare ChR2-mediated POm input strength across the entire column, excitatory neurons in each layer were targeted for voltage-clamp recordings. POm fiber activation generated the largest amplitude responses in L5a neurons (Figure 1D-F), consistent with the large density of fibers in this layer, and mean evoked EPSC amplitude for L5a neurons was nearly 5-fold greater in these neurons than for any other excitatory neurons in other layers (Figure 1F). To more accurately compare input strength across different preparations with varying levels of ChR2-expression, responses across the column were normalized to the mean strength of POm input to L5a neurons recorded in the same brain slice. Within the same slice, mean EPSC amplitude was always larger in L5a than L2 neurons (Figure 1E, F, H); a difference that was highly significant. Recordings from neurons whose cell bodies resided in L5b

		n	R_i (MΩ)	V_{rest} (mV)	*Depth (um)*	*EPSC Amp (pA)**	*EPSC Onset (ms)*[#]	*PPR*[$]	*EPSP Amp (mV)*[^]
L1	5HT	4	429 ± 81	-64.7 ± 2.1	59 ± 7	-74.7 ± 37	5.1 ± 0.6	0.63 ± 0.23	N/A
L2	Pyr	31	354 ± 22	-66.6 ± 1.4	157 ± 6	-45.0 ± 5.1	6.0 ± 0.3	0.68 ± 0.04	4.38 ± 0.53
	PV	7	228 ± 41	-62.0 ± 1.0	180 ± 15	-4.40 ± 1.1	7.2 ± 0.5	0.45 ± 0.19	0.310 ± 0.11
	SST	14	535 ± 71	-56.8 ± 2.1	162 ± 9	-4.20 ± 1.2	12 ± 1	0.60 ± 0.27	0.360 ± 0.26
	5HT	18	754 ± 99	-55.4 ± 1.8	132 ± 7	-16.7 ± 2.6	6.5 ± 0.3	0.67 ± 0.96	2.43 ± 0.67
L5a	Pyr	32	314 ± 22	-63.3 ± 0.8	749 ± 9	-196 ± 29	4.3 ± 0.1	0.68 ± 0.04	7.82 ± 0.88
	PV	9	286 ± 34	-59.1 ± 1.9	752 ± 19	-324 ± 52	3.9 ± 0.2	0.52 ± 0.05	N/A
	SST	9	235 ± 33	-56.1 ± 1.9	759 ± 20	-7.80 ± 3.9	5.6 ± 1	0.20 ± 0.13	-0.910 ± 0.87
	5HT	10	387 ± 59	-60.5 ± 2.1	644 ± 31	-56.8 ± 13	4.7 ± 0.2	1.06 ± 0.12	8.13 ± 1.5

Table 1: Intrinsic properties and POm-evoked responses of cortical neurons in rACSF

*Average maximum POm-evoked EPSC amplitude (from cell average responses, 10 consecutive sweeps, 5ms POm stim)

[#] Average POm-evoked EPSC onset latency from stimulus onset

[$] Paired pulse ratio, peak short onset-latency response for pulse 2/pulse 1 at 80 ms ISI

[^] Maximum EPSP amplitude following POm stimulation. Note that amplitude was not calculated for cells that fire action potentials

showed significantly weaker POm input, although >75% of these cells received some direct input (Figure 1G,I).

Although previous studies suggested POm inputs might be unevenly distributed across neurons in L2 and L5 (Bureau et al., 2006; Viaene et al., 2011a), our method revealed that 100% of L2 and L5a neurons received some POm input (Figure 1G). Relative input strengths for Pyr neurons in L2 and L5 are also generally consistent with prior studies using optogenetic activation , although we observed substantially larger relative excitation for L5b Pyr neurons compared to other reports (see Petreanu et al. 2009). Notably, at least a subset of excitatory neurons in all layers received synaptic POm input, although this input was more sparsely distributed and weakest in amplitude in L4 and L6, major targets for VPM afferents (Wimmer et al., 2010a). Overall, we find that neurons whose cell bodies reside in L2 and L5 are the primary targets for POm-mediated sensory input, with the strongest input found in L5a. These findings are consistent with the distribution of POm fibers in the cortical column (Meyer et al., 2010b) and suggest that POm-mediated information transfer to the neocortex will be initiated by circuit activity in these layers.

2.2.2 GABAergic neuron subtypes differentially receive direct POm input in L5

Cortical transformations of thalamic input will depend on the activity of both excitatory and inhibitory neurons. To identify principles of thalamic connectivity to specific subtypes of inhibitory neurons, we took advantage of three different Cre-driver lines of transgenic mice to identify the major subset of inhibitory neurons; SST-, PV-, and 5HT3a-expressing cells (Figure 2B-D) (Gong et al., 2007; Hippenmeyer et al.,

2005; Taniguchi et al., 2011). Together, these subtypes of inhibitory cells account for nearly 100% of all cortical GABAergic neurons (Rudy et al., 2011).

VPM thalamic input to L4 interneurons has been shown to mainly target PV cells (Cruikshank et al. 2007, but see Porter et al. 2001; Hu et al. 2016). To test whether this pattern of innervation was input- (both POm and VPM) and layer- (both L5 and L4) specific, PV neurons were genetically labeled using a PV-Cre driver line crossed to the Ai3 YFP reporter line, and double-transgenic mice were stereotaxically injected with ChR2 virus in POm.

PV cells in major POm recipient layers, L2 and L5, were targeted for whole-cell voltage clamp recordings (Figure 2B,E-F). In all experiments, Pyr cell responses were obtained in each slice to directly compared input strength between these cells and adjacent inhibitory neurons. Under conventional recording conditions (ACSF), POm-driven EPSCs were detected in all PV cells and the mean amplitude of this response was similar between PV and Pyr cells (Figure 2 E,K; 7/7 PV cells responding; all-cell mean PV -269±48 vs Pyr -325±44 pA). These responses persisted in the presence of TTX and 4-AP (Figure 2F, L; 6/6 PV cells responding; all-cell mean PV -87.6±24 vs Pyr -45.9±8.2 pA), indicating that they result from direct synaptic input from POm afferents to PV cells.

In contrast to strong input to PV neurons, light-evoked POm activation yielded no or a barely-detectable EPSC in SST neurons, despite a robust response in adjacent L5 Pyr cells (Figure 2C,E, K; 6/10 SST responding; all-cell mean, SST -8.3±4 vs Pyr -140±45 pA). Across different lines of transgenic mice, we found that the mean amplitude of SST responses was 30-fold lower than observed for PV cells in L5.

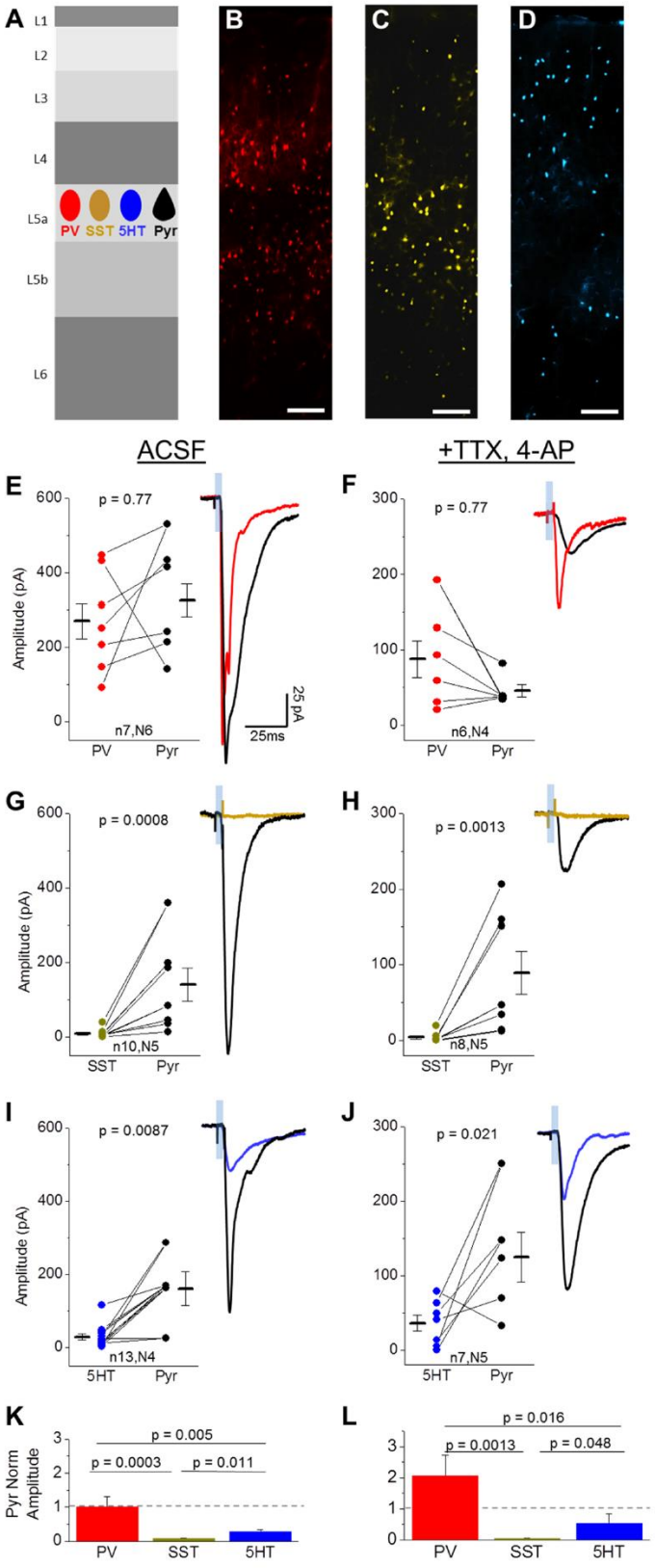

Figure 2. Direct synaptic inputs from POm onto three major interneuron classes in L5. (A) Schematic of experiment. Light-evoked EPSCs were recorded in labeled inhibitory neurons (PV-, SST-, 5HT3a-Cre X Ai3) and Pyr neurons in L5 of POm-ChR2 injected animals. (B-D) Laminar location of fluorescent PV (B), SST (C), and 5HT3a (D, abbreviated 5HT for brevity) inhibitory neurons, scale bar: 100 uM. (E,F) Comparison of peak (within 50ms of stim onset) POm-evoked EPSC amplitude (average, 10 trials) of a PV cell and nearby pyramidal neuron (<300um apart) in ACSF (E) and TTX, 4-AP (F). Sample trace shows PV (red) and Pyr (black) average response to 5ms light pulse in same slice. (G,H) POm-evoked responses of SST (yellow) and nearby Pyr (black) neurons in ACSF (G) and TTX, 4-AP (H). (I,J) POm-evoked responses of 5HT (blue) and nearby Pyr (black) neurons in ACSF (I) and TTX, 4-AP (J). (K,L) Average of inhibitory neuron response amplitudes normalized to nearby Pyr neurons in rACSF (K, ANOVA P-value: 0.0017) and TTX, 4-AP (L, ANOVA P-value: 0.011). N values correspond to values in E-J. Note that inhibitory neurons are compared to multiple Pyr neurons when more than one Pyr neuron was recorded in the same slice.

To determine whether these small responses resulted from direct thalamic input, POm stimulation was carried out with TTX and 4-AP in the bath. Under these conditions, short-latency EPSCs were virtually eliminated (Figure 2H, L; 2/8 cells SST responding; all-cell mean SST -4.1±2 vs Pyr -89.2±28 pA). These data indicate that, like in L4 (Cruikshank et al., 2007; but see Tan et al., 2008, Hu and Agmon 2016), thalamic input to L5 SST neurons is negligible to non-existent, and suggest that this might be a conserved wiring principle across layers.

Although PV and SST neurons make up >90% of the inhibitory neuron population in L5, 5HT3a-expressing cells are sparsely present (Figure 2D) (Lee et al., 2010; Rudy et al., 2011). POm-driven EPSC amplitudes in this population were on average larger than those observed in SST neurons but still 10-fold lower than adjacent L5a Pyr neurons (Figure 2I, K; 8/9 5HT3a cells responding; all-cell mean, 5HT3a -33.9±11 vs Pyr -166±2.0 pA). Input strength was heterogeneous in these cells, consistent with the diversity of cell types within this population (Lee et al., 2010; Miyoshi et al., 2010; Staiger et al., 1996).

POm-driven EPSCs onto 5HT3a-expressing neurons remained in the presence of TTX and 4-AP (Figure 2J, L; 4/5 5HT3a cells responding; all-cell mean, 5HT3a -31.9±11 vs Pyr -156±43 pA), indicating that this sparse cell population in L5 receives small but direct input from the thalamus. This connectivity motif has previously been observed for VPM inputs onto 5HT3a neurons in L4 (Lee et al., 2010; Staiger et al., 1996). POm input was significantly greater for PV cells compared to SST and 5HT3a neurons (Figure 2K,L).

Overall, the principles of thalamic connectivity to L5 appear similar to those described for VPM inputs to L4, with strong drive to PV neurons, weak and heterogeneous input to 5HT3a neurons (but see Ji et al. 2016), and virtually non-existent input to low-threshold spiking SST neurons (Chen et al., 2015a; Cruikshank et al., 2007; Hu and Agmon, 2016; Lee et al., 2010; Porter et al., 2001; Staiger et al., 1996; Swadlow and Gusev, 2002; Tan et al., 2008). Strong thalamic drive to PV neurons is observed for thalamocortical inputs to L4 in other primary sensory areas as well, suggesting that this may be a conserved motif for thalamocortical inputs throughout the brain (Delevich et al., 2015; Ji et al., 2016; Kloc and Maffei, 2014; Schiff and Reyes, 2012).

2.2.3 Thalamic input is differentially distributed across L2 inhibitory populations

To determine whether these principles of thalamic input were conserved for POm inputs in superficial layers, we investigated cell-type specific POm responses in the three broad classes of inhibitory neurons described above.

Surprisingly, PV cells in L2 showed negligible responses to POm afferent stimulation. Mean POm-evoked EPSC amplitude in L2 PV cells was nearly 10-fold lower (3/6 responding, all-cell mean -4.8±1 pA) than what was observed in adjacent Pyr neurons (-43.5±7.6 pA), a difference that was highly significant (Figure 3B, H). This small response was eliminated in TTX and 4-AP (Figure 3C, I; 1/8 PV cells responding; all-cell mean, PV -0.9±0.5 vs Pyr -24.0±5.4 pA). The lack of direct thalamic input to fast-spiking PV neurons suggested that neocortical transformations in this layer might be mediated through different principles than observed in deeper layers, either through a different population of interneurons or through reduced overall inhibition.

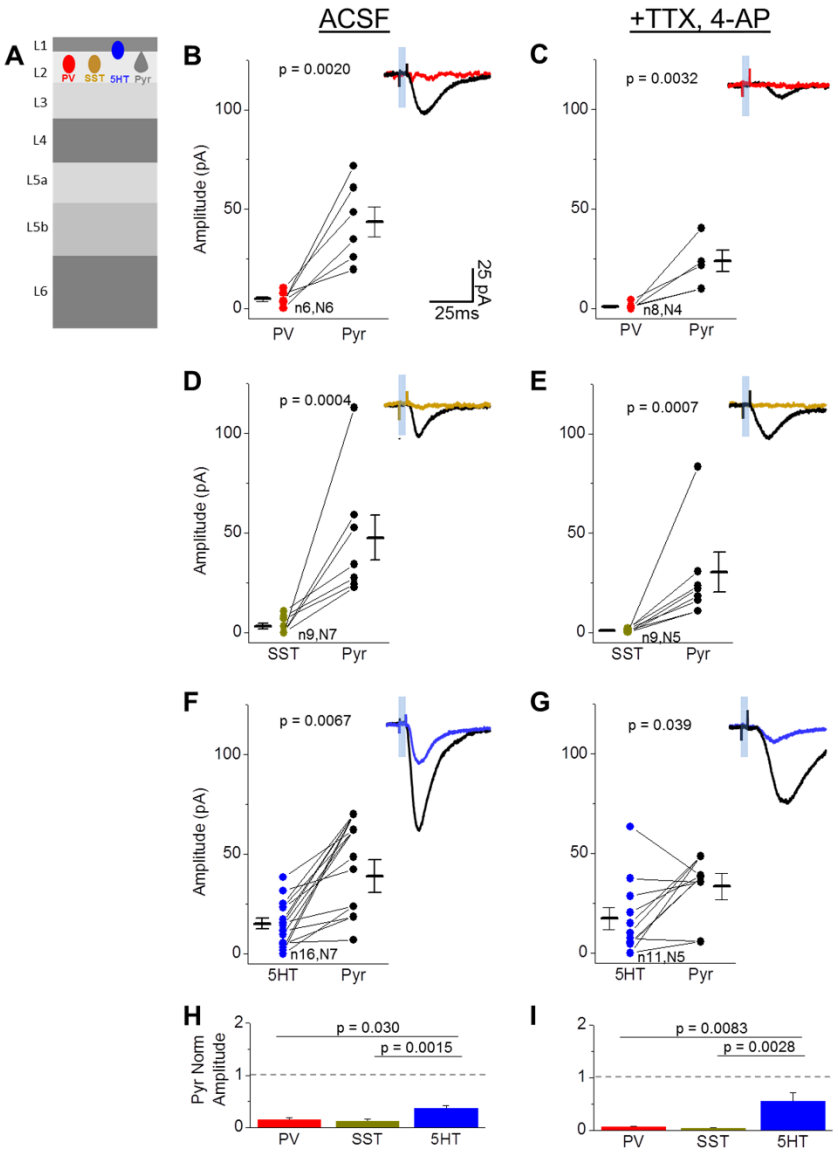

Figure 3. Direct synaptic input from POm onto three major interneuron classes in L2. (A) Schematic of experiment. Light-evoked EPSCs were recorded in labeled inhibitory neurons (PV-, SST-, 5HT-Cre X Ai3) and Pyr neurons in L2 of POm-ChR2 injected animals. (B,C) Comparison of peak (within 50ms stim onset) POm-evoked EPSC amplitude (average, 10 trials) of a PV cell and nearby pyramidal neuron (<300um apart) in control ACSF (B) and TTX, 4-AP (C). Sample trace shows PV (red) and Pyr (black) average response to 5ms light pulse in same slice. (D,E) POm-evoked responses of SST (yellow) and nearby Pyr (black) neurons in ACSF (D) and TTX, 4-AP (E). (F,G) POm-evoked responses of 5HT (blue) and nearby Pyr (black) neurons in ACSF (F) and TTX, 4-AP (G). (H,I) Average of inhibitory neuron response amplitude normalized to nearby Pyr neurons in rACSF (H, ANOVA P-value: 0.0053) and TTX, 4-AP (I, ANOVA P-value: 0.0049). N values correspond to values in B-G. Note that inhibitory neurons are compared to multiple Pyr neurons when more than one Pyr neuron was recorded in the same slice.

Targeted voltage-clamp recordings of SST neurons in L2 showed that, like L5, these cells receive little to no POm input compared to adjacent Pyr neurons (Figure 3D, H; 3/9 SST cells responding, all-cell mean -3.22±1.3 vs Pyr -47.6±11 pA). Indeed, in the presence of TTX and 4-AP, responses were eliminated (Figure 3E, I; 0/9 SST cells responding; all-cell mean SST -0.77±0.3 vs Pyr -30.3±10 pA).

Because excitatory inputs to SST neurons are strongly facilitating (Fanselow et al., 2008; Silberberg and Markram, 2007; Urban-Ciecko et al., 2015), we considered the possibility that release probability might be too low to detect a response after a single POm stimulus. To determine whether weak POm input might be revealed with repetitive POm stimulation as has been suggested in L4 (Hu and Agmon, 2016; Tan et al., 2008), a train of 10+ light pulses was delivered during SST-recordings in both L2 and L5 (Figure 4). In many cases POm drove a small, direct EPSC in an SST neuron (ACSF 4/5 cells; TTX, 4AP ¾ cells); notably, these responses were depressing, suggesting that ChR2-mediated release is highly efficient. In other SST cells (ACSF 1/5 cells; TTX 4AP ¼ cells), no synaptic response was observed even after a 10-pulse train (12.5 Hz), indicating that these neurons do not receive weak and facilitating inputs from the higher-order thalamic nucleus POm (Hu and Agmon, 2016; Tan et al., 2008).

5HT3a-expressing cells are abundant in L1 and 2 and account for half of all GABAergic neurons in superficial layers (Figure 2D) (Rudy et al., 2011). Whole-cell current clamp recordings confirmed that these cells are heterogeneous, composed of irregular spiking, late-spiking, fast-adapting and other cell types (Lee et al., 2010). Because 5HT3a cells do not show a clear distinction between L1 or L2 – and are

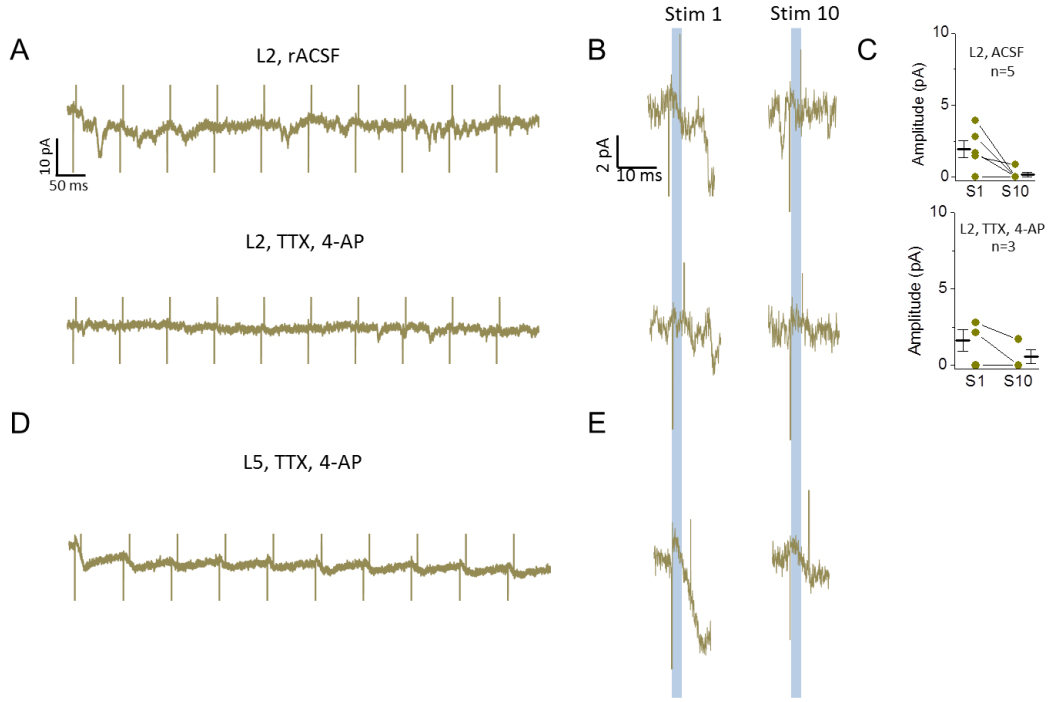

Figure 4. Cortical SST neurons do not receive facilitating input from POm (A) Cell average EPSC response (10 trials) to 10 5ms light pulses delivered at 80 ms inter-stimulus interval. Top: L2, rACSF; Bottom: L2 TTx, 4AP. (B) Close-up of SST response to POm stimulus 1 and 10 for sample cell shown in A. (C) EPSC amplitude of the first and tenth response. Top: L2, rACSF; Bottom: L2 TTx, 4AP. (D-E) Same as (A-B) in L5a.

frequently clustered at the border of these two layers making layer assignment difficult – these cells were grouped for further analysis.

Targeted recordings of 5HT3a-labeled cells showed that these neurons as a group are significantly more likely to receive POm input compared to SST or PV cells (13/16 cells), although input strength was heterogeneous across the group (Figure 3F-I). POm-evoked EPSC amplitudes appeared greater in adjacent Pyr cells (all-cell mean 5HT3a -15.1±2.7 vs Pyr -38.9±8.2 pA). Responses were maintained in TTX and 4-AP, indicating that most 5HT3a neurons receive direct POm input (Figure 3G, I; 9/11 5HT3a cells responding; all-cell mean -17.5±5.6 vs Pyr -33.4±6.5 pA), similar to inputs from primary thalamic nuclei in granular layers (Staiger et al. 1996; Lee et al. 2010; Wall et al. 2016; but see Ji et al. 2016).

Overall, these results predict that thalamocortical transformations in deep and superficial layers may be fundamentally different, where feedforward inhibition from PV cells in L5 may shape the flow of excitation in this layer but 5HT3a neurons assume this role in superficial layers.

2.2.4 POm-driven disynaptic inhibition differs between L2 and L5a Pyr neurons

Cell-type specific patterns of synaptic connectivity suggest characteristic sequences of neuronal activation induced by sensory input and constrain models of how thalamic information is transformed in the neocortex. Under our recording conditions, we found that POm stimulation elicited both excitatory and delayed inhibitory synaptic responses in Pyr cells (Figure 5 and Figure 6 C,D). Since POm input was exclusively excitatory (Figure 1B), we reasoned that this inhibition might be a property of the local

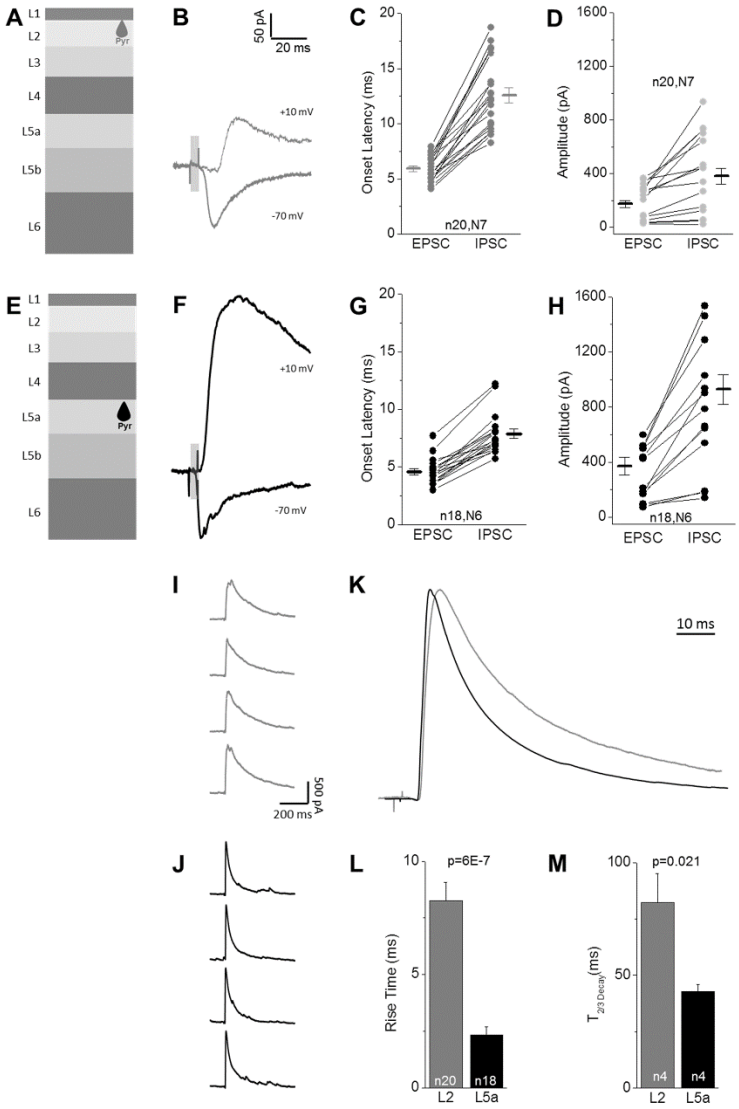

Figure 5. POm-evoked disynaptic inhibition is larger and faster in L5 pyramidal neurons. (A) Schematic of L2 targeted Pyr neurons. (B) Example traces of average POm-evoked EPSC (-70 mV) and IPSC (+10 mV) responses. (C) Onset latency of POm-evoked EPSCs and IPSCs for L2 Pyr cells. Connected values for same cell. (D) Peak amplitude (<50ms stim onset) of average EPSC and IPSC response for L2 Pyr neurons, connected values from same cell. (E-H) Example POm-evoked EPSC and IPSC (F), onset latency (G) and peak amplitude (H) for L5 Pyr neurons, same as A-D. (I,J) Consecutively recorded IPSCs in a L2 (I) and L5 (J) reveal kinetics and late-onset events. (K) Average of all L2 (gray) and L5 (black) IPSCs following minimal stimulation reveal differences in activation rate and duration of inhibition. Traces peak-scaled and aligned to rise. (L,M) Quantification of 10%-90% rise time (L) and decay time (M, Time to 2/3 decay) for POm-evoked IPSCs is L2 (gray) and L5 (black) Pyr neurons. Ns are different in (L) and (M) due to inability to calculate decay with multiple pulses in some experiments.

circuit. In addition, we predicted that the pattern of direct input identified across different populations of interneurons described in Figures 2-3 might help identify the cellular source(s) of this inhibition.

To investigate the properties of POm-driven inhibition in L2 and L5a, we carried out voltage-clamp recordings of Pyr cells at holding potentials designed to isolate excitatory (-70 mV) and inhibitory responses (+10 mV; Figure 5). Under conventional recordings conditions, mean EPSC onset was slightly faster in L5a than in L2 (Figure 5C, G). Within a given cell, IPSC latency was longer than observed for EPSCs in both layers (Figure 5B-G), consistent with disynaptic inhibition from an intermediate cortical inhibitory neuron.

Mean IPSC onset for L5a Pyr neurons was fast and regular across preparations, typically occurring <8 ms after light pulse initiation and approximately 3 ms after the EPSC onset (Figure 5F,G; range 5.7-12.2 ms). The very short latency between the POm-driven EPSC and the IPSC was consistent with only a single synapse between these events; i.e. that it did not result from recurrent excitation or feedback inhibition.

In L2 Pyr neurons, IPSC onset occurred at a significantly longer mean latency in aggregate, at 12.6 ms ($p<0.00001$), and the range of this latency across cells was greater than observed in L5a (Figure 5B,C; range 8.2-18.7 ms). Interestingly, this variable latency was also observed in consecutive sweeps within a single Pyr cell in L2, where onset latency could range as much as 4.5 ms, compared with only 1.5 ms for L5a. Because the latency of interneuron firing is influenced by the level of ChR2 expression across different preparations, it was useful to directly compare IPSC onset timing for cells within the same slice. Even when compared for cells collected from the

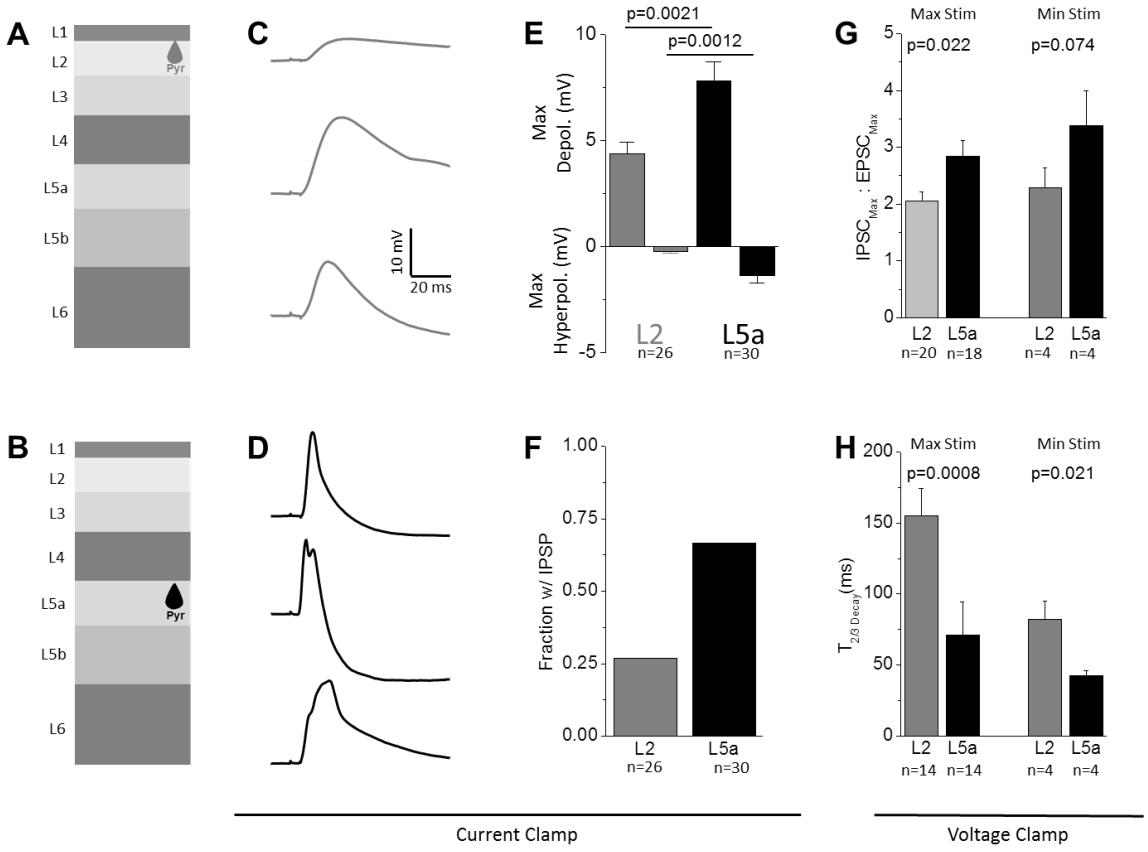

Figure 6. Laminar-specific differences in POm-evoked inhibition. (A,B) Schematic of targeted population. (C,D) Average POm-evoked EPSPs for L2 and L5a Pyr neurons. (E) Average maximum depolarization and hyperpolarization of L2 and L5a pyramidal neurons following POm stimulation. (F) Fraction of pyramidal neurons in each layer that displayed POm-evoked hyperpolarization following the early-onset EPSP. (G) Average of IPSC to EPSC amplitude ratio across all pyramidal neurons in L2 and L5a. Ratios are displayed for maximal light intensity and minimal response-evoking intensity. (H) Decay time (peak to 2/3 decay) of POm-evoked IPSCs in L2 and L5a pyramidal neurons. Decay times quantified for maximum stimulation and minimal stimulation.

same animal, IPSC onset latency was nearly 5ms longer in L2 than in L5a Pyr neurons (L2 11.7 ± 0.7ms vs L5a 7.1± 0.3ms; p= <0.0001;), indicating that inhibition in the two layers may originate from different sources.

Peak POm-evoked IPSC amplitudes were, on average, larger in L5 than L2 (Figure 5; L2 380±57 pA vs L5a 927±110 pA). Because L2 also showed a smaller amplitude of POm-mediated excitation, it was possible that the difference in IPSC amplitude might simply scale to overall input strength in this layer (Xue et al., 2014). However, calculating the ratio of excitation to inhibition from measured E- and IPSCs showed that inhibition was comparatively larger in L5a (p=0.022, Figure 6G). Thus, reduced and delayed inhibition in L2 is not a direct consequence of lower overall POm drive in this layer.

POm-evoked inhibition observed in L2 and L5a also had markedly different activation kinetics and duration, suggesting different sources of inhibition onto these two types of neurons. IPSCs in L5 showed a fast rise and decay time (Figure 5J, K-M), and inspection of individual evoked IPSCs indicated that the IPSC rise was smooth (Figure 5J), suggesting synchronized inhibition. In contrast, IPSCs in L2 Pyr neurons had a slower rise and a significantly longer decay (Figure 5I, K-M), suggesting that they might arise from a different cellular source with less synchronized activation. To determine whether the difference in decay might result from the smoothed average of delayed IPSCs in the post-stimulus window, we reduced the intensity of the light stimulus to improve IPSC isolation. Even under these conditions, the difference in duration of inhibition between L2 and L5a Pyr neurons persisted (Figure 6H). Thus, POm activity

drives both quantitatively and qualitatively different types of inhibition in deep versus superficial layers.

2.2.5 PV neurons provide fast disynaptic inhibition to L5a Pyr neurons

We first investigated the cellular source of disynaptic inhibition in L5a, since this layer received the strongest overall input. Our initial experiments indicated that fast feedforward inhibition likely originates in local PV- or 5HT3a-expressing interneurons in L5, since SST neurons did not receive direct synaptic input. The low input resistance of PV neurons (Table 1) likely increases the amount of current required to drive spiking in these cells. However, current-clamp recordings from PV-Cre neurons revealed that under our recording conditions, ChR2-mediated activation of POm afferents was sufficient to drive reliable, short-latency firing in this population (Figure 7D, F; 7/8 cells). Although ChR2-expression levels could differ from animal to animal, mean spike times in L5 PV cells were remarkably consistent between preparations (latency from light pulse onset 6.60±0.22 ms; n=7). Thus, PV neurons are strongly driven by POm input. Furthermore, these spikes were well-aligned to the mean IPSC onset recorded in Pyr neurons (Figure 7D, F; 7.25±0.3 ms; n=18), suggesting that these cells were the source of fast, disynaptic inhibition onto L5a Pyr neurons.

In contrast, mean POm-evoked spike times in L5 5HT3a-expressing neurons were significantly delayed compared to evoked spikes observed in PV cells (Figure 7D,F; 26.1±7 ms; n=2/7 cells spiking; $p<0.001$). Under our recording conditions, 5HT3a cells in L5 exhibited at most, a single spike within 80 ms of the light pulse onset (45% failure rate across trials for spiking neurons), and these spike times could vary substantially between trials even for the same neuron (Figure 7F). 5HT3a cells that did

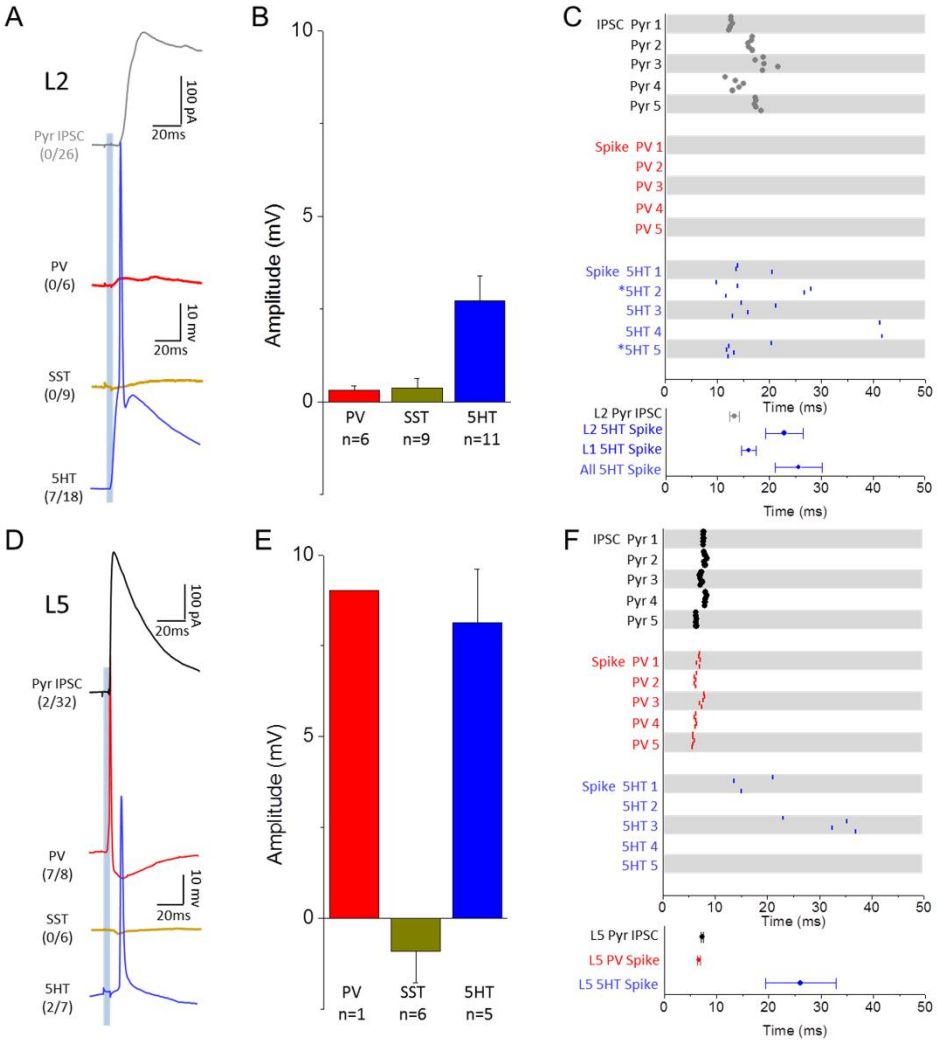

Figure 7. Feedforward inhibition is mediated by different inhibitory neuron populations in L2 and L5. (A) Example Pyr IPSC (black) compared to responses of PV (red), SST (yellow), and 5HT (blue) neuron populations in superficial layers following 5ms optical stimulation of POm axons (single cell average 10 trials). Parentheses quantify number of cells that fired APs out of the total number recorded for each group. (B) Average peak EPSP (<50ms post-stim) amplitude of non-spiking neurons for each inhibitory group. (C) Comparison of IPSC onset latency and spike timing for neuron populations in superficial layers. Raster (top) shows onset or spike peak time for 5 consecutive trials for 5 cells in each population. Asterisks (*) indicate 5HT neurons located in L1. Graph (bottom) quantifies average IPSC onset or spike peak latency across all neurons recorded in each population with 5HT neurons split by layer and in aggregate. (D-F) Same as (A-C) but for neurons in L5. Because all but one PV cell in L5 spiked in response to POm stimulation, the bar corresponding to L5 PV cell depolarization represents a single data point.

not fire an AP still experienced a strong membrane potential depolarization on average (Figure 7E; 8.13±1.5 mV). Although both PV cells and subsets of 5HT3a neurons are synaptically connected to neighboring Pyr neurons (Jiang et al., 2015; Pfeffer et al., 2013), the close apposition of the PV spike with the onset of the IPSC in L5a Pyr cells suggests that local PV cells are the source of fast feedforward inhibition during POm-evoked activation. In addition, the fast rise and decay kinetics of disynaptic IPSCs typically recorded in Pyr cells (Figure 5L,M) are consistent with their origin in PV cells, which have a preferred perisomatic location for inputs (Kawaguchi and Kubota, 1997). Although this does not rule out a contribution from 5HT3a neurons for disynaptic inhibition, it suggests that PV input is dominant.

As predicted from the pattern of direct synaptic input established in Figure 3, POm-evoked action potentials (APs) were never observed in SST-expressing neurons. In some cases, hyperpolarization of resting membrane potential was observed (Figure 7E; all-cell mean -0.91± 0.9 mV; 3/6 cells), even though cells were resting near the Cl- reversal potential and thus these effects may be underestimated.

2.2.6 Thalamocortical response transformations in L2 do not involve local PV interneurons

The lack of direct synaptic input to PV neurons in L2, and the delay in the disynaptic IPSC in L2 Pyr cells suggested that the thalamocortical response transformation might be qualitatively different in this layer. To determine whether POm stimulation could drive firing in any of the three interneuron populations in superficial layers, targeted current-clamp recordings were carried out. Evoked spikes were aligned to IPSC onset for L2 Pyr neurons (Figure 7A). POm stimulation never evoked an AP in

any L2 PV (0/6) or SST neuron (0/9), and elicited small or negligible membrane potential depolarizations (Figure 7A-C; PV-cell mean 0.31±0.1 mV; SST-cell mean 0.36±0.3 mV). In contrast, in 7/18 5HT3a neurons POm stimulation was sufficient to drive an AP, and the timing of these spikes was significantly delayed compared to evoked spikes in L5 PV neurons (spike latency L5 PV 6.6±0.2 ms vs L1/2 5HT3a 22.9±3.6 ms). Of note, spike times for a given 5HT3a neuron were heterogeneous across stimulus trials, varying by as much as 10 ms, consistent with the large variability of IPSC onset observed for L2 Pyr neurons.

Overall, mean IPSC onset in L2 Pyr neurons occurred substantially later than L5 PV cell activity (Figure 7C,F) and aligned with the earliest spikes in 5HT3a neurons (Figure 7A, C), suggesting that L2 inhibition arises from neurons within this population. Consistent with this, previous studies have confirmed that superficial neurogliaform cells and, to a lesser extent, VIP-expressing neurons in L2 are synaptically connected to nearby pyramidal neurons (Jiang et al., 2015; Pfeffer et al., 2013).

2.2.7 POm-driven recurrent activity is layer-specific

Our previous experiments employed recording conditions that isolated direct synaptic input from POm (in TTX and 4-AP), or in ACSF that enabled a single POm-driven spike in cortical neurons. To visualize a more complex sequence of recurrent network activity initiated by POm input and evaluate how different cell subtypes respond to this stimulus, we adjusted the bath solution to more closely mimic the composition of CSF *in vivo* (Table 2) (Sanchez-Vives and McCormick, 2000; Shruti et al., 2008; Urban-Ciecko et al., 2015; Yassin et al., 2010). Under these conditions, we observed occasional (<0.01 Hz) spontaneous membrane depolarizations similar to upstates,

		n	R_i (MΩ)	V_{rest} (mV)	*Depth (um)*	*Spont. (Hz)**	*Stim (Hz)#*	*Post (Hz)^*
L1	5HT	6	382 ± 57	-60.2 ± 2.3	60 ± 7	0.0 ± 0	1.2 ± 0.8	0 ± 0
L2	Pyr	9	236 ± 30	-66.3 ± 1.5	147 ± 6	0.0 ± 0	0 ± 0	0 ± 0
	PV	6	196 ± 16	-64.0 ± 1.4	150 ± 9	0.0 ± 0	0.4 ± 0.2	0.3 ± 0.2
	SST	6	418 ± 17	-52.0 ± 1.79	172 ± 11	6.0 ± 0.5	1.6 ± 1.2	8.0 ± 1.8
	5HT	5	539 ± 100	-61.8 ± 0.8	110 ± 7	0.1 ± 0.1	2.1 ± 0.9	1.6 ± 1.1
L5a	Pyr	13	250 ± 22	-66.3 ± 0.6	704 ± 13	0.0 ± 0	1.4 ± 0.6	0.04 ± 0.0
	PV	6	250 ± 22	-66.0 ± 0.6	710 ± 29	0.0 ± 0	24.3 ± 5.5	1.0 ± 0.8
	SST	7	518 ± 110	-52.8 ± 2.1	762 ± 17	4.9 ± 0.7	1.3 ± 1.0	7.3 ± 0.8
	5HT	6	281 ± 67	-61.0 ± 2.9	644 ± 31	0.0 ± 0	2.08 ± 1.8	0 ± 0

Table 2. Intrinsic properties and POm-evoked responses of cortical neurons in mACSF.

*Average spontaneous firing rate (for all: frequency in Hz, 10 consecutive trials) for 500ms immediately preceding stimulus onset.
#Average POm-evoked firing rate during 500 ms beginning at stimulus onset (5x, 5ms POm pulses, 12.5 Hz)
^ Average post-stimulus firing during 500 ms immediately following the stimulus train.

similar to those that have been described both *in vitro* and *in vivo* (Beltramo et al., 2013; Fanselow and Connors, 2010; Neske et al., 2015).

Current-clamp recordings were carried out to examine how repetitive ChR2-mediated POm activation might drive recurrent activity across different cell types in L2 and L5 of the cortical column. POm stimulation was carried out at 12.5 Hz (5 pulses), a frequency that has been observed in POm neurons in awake animals (Urbain et al., 2015).

Consistent with EPSC measurements, L2 Pyr neurons showed a small EPSP, but firing was never evoked in these cells (Figure 8B) even after long POm stimulus trains. These results are consistent with sparse activity that has been observed in L2 pyramidal neurons, especially in somatosensory cortex (Barth and Poulet, 2012; Jouhanneau et al., 2014; Yamashita et al., 2013). In some cases, repetitive POm stimulation was sufficient to drive prolonged depolarization that could last for several seconds (Figure 9).

L2 PV neurons exhibited either no response or a small EPSP, with markedly less summation (Figure 7C). On trials where very strong recurrent network activity was generated (Figure 8, Table 2) PV spiking was sometimes observed late in the stimulus train, and it could persist past the stimulation window (Figure 8C, F). APs in L2 PV cells were never observed after the first few POm stimuli.

Previous studies have shown that both *in vivo* and *in vitro*, SST neurons throughout the neocortex exhibit tonic firing activity independent of synaptic input (Fanselow et al., 2008; Gentet et al., 2012; Urban-Ciecko et al., 2015). Interestingly,

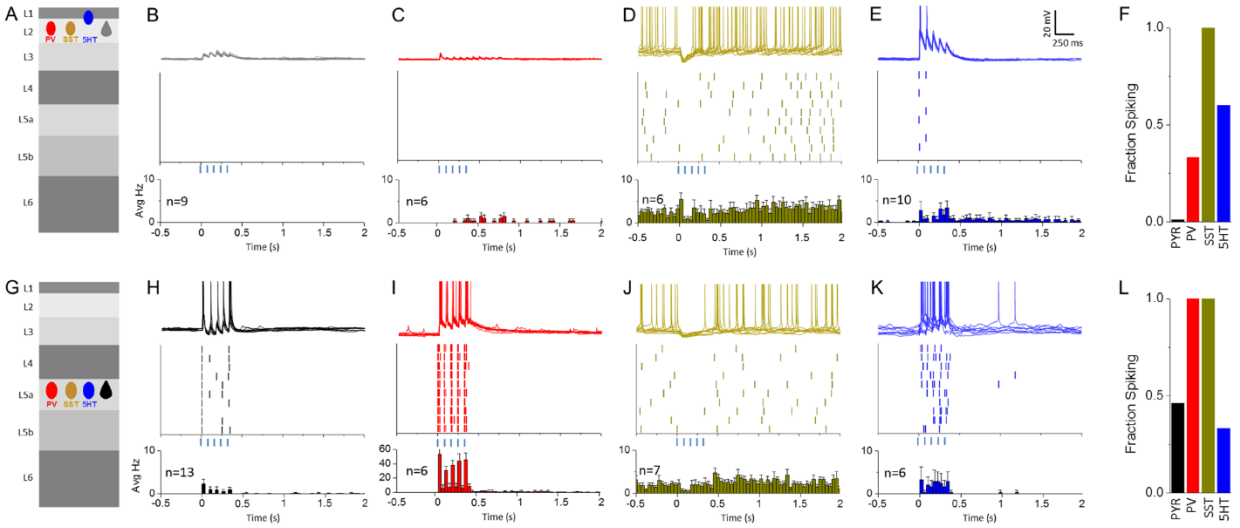

Figure 8. POm stimulation drives distinct patterns of recurrent activity in L2 and L5. (A) Schematic of cell-type and layer of recorded population. (B) Top: 10 consecutive sweeps overlaid of L2 Pyr neuron in response to optical activations of POm in mACSF (For all: 5 pulses, 80ms isi). Middle: Raster plot showing spike peak times for example L2 Pyr cell. Bottom: Average peri-stimulus firing histogram for all L2 Pyr neurons recorded (For all: bin size 40 ms). Histogram includes cells that generated no APs. (C-E) As described in (B) for L2 PV (C), L2 SST (D), and L1/2 5HT neurons (E). SST neurons, if required, were manually adjusted to 48 ± 3 mV to evoke spontaneous APs and mimic *in vivo* membrane potential. (F,L) Bar graphs representing the fraction of neurons for each cell type that fired at least one AP during the stimulus window for each layer. (G-K) As described for (A-E) but in L5.

POm input initiated a hyperpolarization of resting membrane potential in SST neurons (Figure 8D, J and Figure 9), remarkably consistent with sensory-evoked responses in this cell population in awake animals (Gentet et al., 2012). This hyperpolarization was sufficient to suppress spontaneous firing at the onset of the stimulation window. After an initial phase of firing suppression, mean SST firing frequency was modestly enhanced relative to baseline, though this increase was not significant (Figure 9, Table 2, baseline 6.0 ± 0.4 Hz, post-stim 8.0 ± 1.8 Hz, p=0.4 paired t-test).

In contrast to the inability of POm stimulation to drive firing in other L2 cell types even when recurrent activity in the slice was enabled, 5HT3a neurons in superficial layers showed evoked firing, although the pattern and timing of spikes differed across cells. The 5HT3a neurons that exhibited POm-evoked firing were predominantly found in L2 or at the border between L1 and 2. As in Figure 7, spike times were heterogeneous even within a cell but were typically aligned to the stimulus pulse (Figure 8E, F). In some cases, 5HT3a-cell firing persisted past the stimulus window, a phenomenon that was associated with strong recurrent activity as indicated by prolonged subthreshold depolarizations (Figure 9, Table 2).

VIP cells are a subset of 5HT3a-expressing GABAergic neurons (~38% of all 5HT3a neurons also show ed VIP immunoreactivity in this 5HT3a-Cre line, similar to previous reports; Lee et al. 2013) and have been shown to synaptically inhibit SST neurons, a motif that is conserved across multiple brain areas including S1 (Jiang et al., 2015; Lee et al., 2013; Pfeffer et al., 2013; Pi et al., 2013; Zhou et al., 2014). Thus, it is possible that POm-evoked firing suppresses SST spontaneous activity at least in part

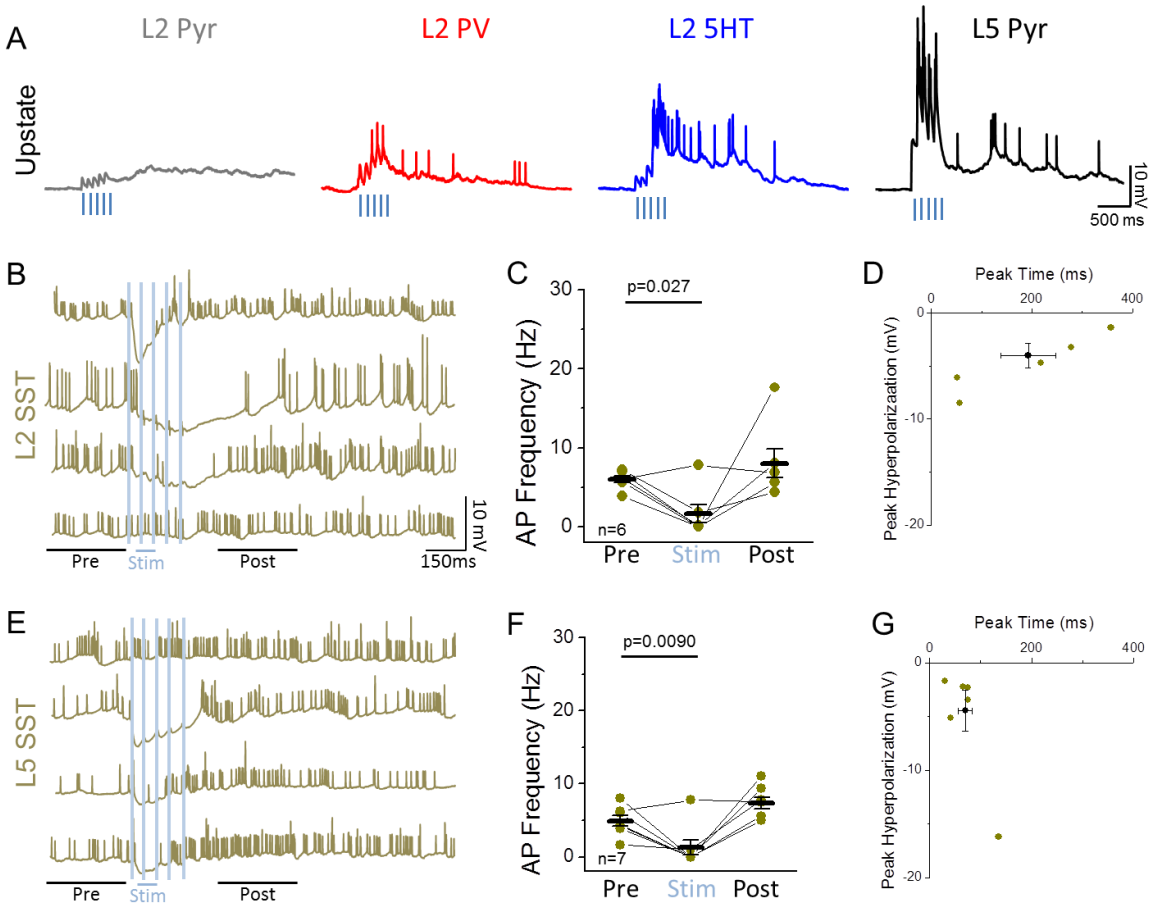

Figure 9. POm-stimulation can drive recurrent network activity and SST-interneuron hyperpolarization. (A) Example responses to repetitive POm stimulation for subsets of cells that displayed prolonged activity following stimulation (average of 10 consecutive traces, 5 light pulses, 80ms isi, max intensity). (B, E) Cell average responses to repetitive POm stimulation for 4 different SST-expressing neurons in L2 (B) and L5a (E). (C,F) Firing rate quantification for control (500ms before stim), early stimulus period (120 ms, beginning 40 ms after stimulus onset), and and post stimulus (500ms following stimulus offset. Time bins are diagramed in (B) and (E). (D,G) Mean peak hyperpolarization versus peak hyperpolarization time post-stim for the maximum amplitude of hyperpolarization observed for L2 (D) and L5a (G) SST neurons.

through this disynaptic connection, from POm to VIP cell, to SST cell. To test whether POm can drive VIP neuron firing, fluorescently-labeled L2 VIP neurons in S1 were targeted for recording in a VIP-Cre transgenic line (Taniguchi et al., 2011) with POm-targeted ChR2 expression. Optogenetic POm stimulation was carried out under recording conditions that enable recurrent activity (Figure 10). Half of recorded VIP neurons (5/10) were strongly driven by POm stimulation across the stimulus window (Figure 10B,C). Because VIP-inhibition of SST neurons has been well-documented, we conclude that this is a likely pathway by which POm-driven hyperpolarization of SST neurons can occur.

Are VIP neurons the only source of POm-driven SST inhibition? 5HT3a neurons that exhibited non-VIP characteristics (L1 location or neurogliaform-like firing pattern) also were driven by POm stimulation, and these cells also inhibit SST neurons (Chittajallu et al., 2013; Jiang et al., 2013a). Importantly, despite the reduction in inhibition from SST neurons during the stimulus period, POm activation was still insufficient to drive APs in L2 Pyr neurons under our recording conditions.

2.2.8 Recurrent activity in L5 neural subtypes is dominated by Pyr and PV neurons

POm stimulation was sufficient to drive firing in some L5a Pyr cells, where spikes occurred at short latency and with high fidelity. Although L5a Pyr neurons could fire after a single POm stimulus, this activity did not generate strong recurrent excitation in the circuit, and subsequent pulses were in fact less likely to trigger an AP.

These observations are consistent with POm-mediated, feed-forward inhibition in the circuit, most likely from PV neurons that synapse densely onto neighboring L5 Pyr

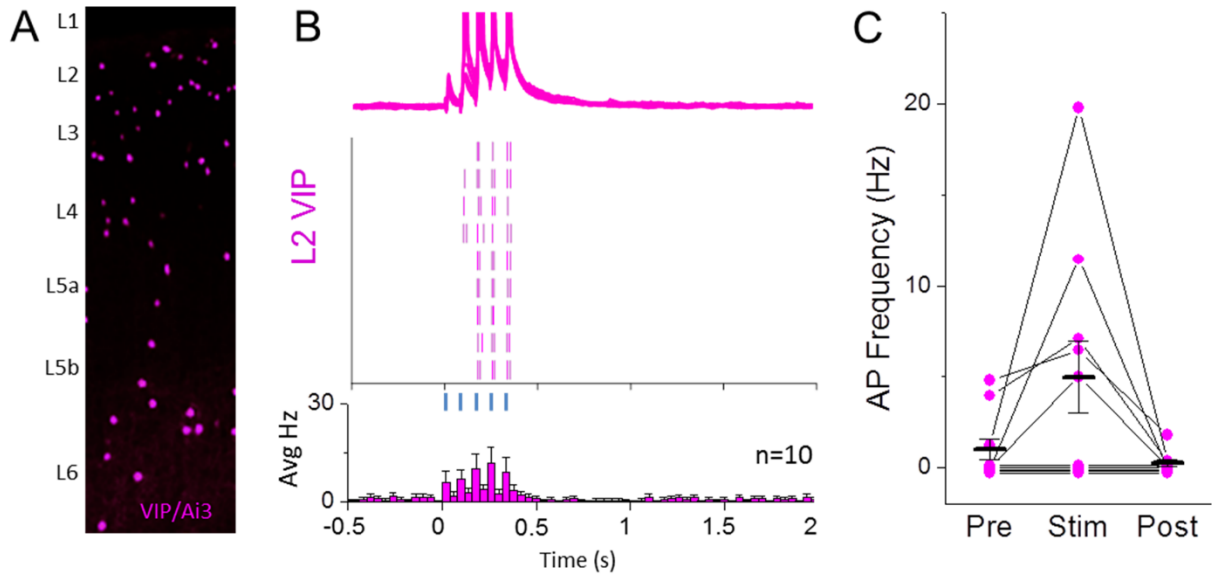

Figure 10. A subset of L2 VIP GABAergic neurons contribute to POm-evoked spiking pattern of L2 5HT neurons. (A) Schematic of VIP-expressing GABAergic neurons throughout a cortical column in S1 imaged with YFP fluorescence. (B) Top: Overlay of 10 consecutive POm-evoke responses in mACSF (5 light pulses, 80ms ISI, max intensity). Middle: Raster plot showing spike times for 10 consecutive traces shown for sample cell. Bottom: average peri-stimulus firing histogram for all L2 VIP neurons recorded. (C) Firing rate quantification for 500 ms bins before, during, and after POm stimulation for all VIP neurons recorded. Cells with no evoked spikes are slightly offset for visibility.

neurons (Avermann et al., 2012; Jiang et al., 2015; Packer and Yuste, 2011; Pala and Petersen, 2015). Indeed, ChR2-activation of POm afferents drove reliable and short-latency firing in L5 PV cells, and multiple spikes with very short inter-spike intervals (5-10ms) were frequently observed after each light pulse (Figure 8I,L). Prolonged activation after the stimulus window of L5 PV neurons was occasionally observed (2/6 cells).

L5 SST neurons showed similar behavior to those in L2: POm stimulation hyperpolarized these cells, suppressing spontaneous firing activity, especially during the early post-stimulus period (Figure 8J, Figure 9). Similarly to L2, a minority of SST neurons displayed increased spontaneous firing after the POm stimulus window (Figure 9, Table 2; all-cell means, baseline 4.9 ± 0.7 Hz, Post-stimulus 7.3 ± 0.8 Hz, p=0.740 paired t-test).

The number of 5HT3a-expressing neurons in L5 is an order of magnitude lower than PV and SST neurons (Figure 2D) (Lee et al., 2010), and it was often difficult to find more than one or two cells in a region with strong POm fiber labeling. However, as in L2, POm stimulation effectively drove firing in a subset (2/6) of 5HT3a neurons, and this firing was mainly restricted to the stimulus window although it was not tightly coupled to the stimulus itself (Figure 8F,L). The sparseness of this cell population, the speed and reliability of POm-evoked firing in L5 PV cells, and the rapid IPSC onset observed in L5a Pyr cells suggest that inhibition from PV cells is likely to be a more potent regulator of L5a Pyr cell output.

2.3 Discussion

Here we use a variety of electrophysiological methods to isolate, synapse by synapse and cell-type by cell-type, the earliest stages of thalamocortical response transformations. We show that a higher-order thalamic nucleus engages fundamentally distinct circuits in deep and superficial cortical layers, suggesting different modes of sensory processing in different lamina. Neurons in L5a are the main recipients of POm-driven activity, where Pyr neurons fire at short latency and with high precision maintained by fast, feedforward inhibition from local PV cells. In contrast, L2 Pyr neurons receive weak but direct POm input that summates over time due to delayed feedforward inhibition, likely from nearby 5HT3a cells. Remarkably, activation of POm inputs was sufficient to recapitulate dynamics of interneuron activity observed in awake animals *in vivo*, including weak excitation of L2 Pyr neurons, activation of putative 5HT3a neurons, and the sensory-evoked hyperpolarization of SST neurons (Gentet et al., 2012).

Anatomical versus functional connectivity of thalamic input

Our results both complement and constrain prior anatomical studies that attempt to define thalamocortical circuits (Agmon et al., 1993; Koralek et al., 1988; Meyer et al., 2010b; Oberlaender et al., 2012a; Wimmer et al., 2010a; Woolsey and Van der Loos, 1970). Dense reconstruction through electron microscopy images as well as rabies-virus mediated identification of presynaptic partners for a given cell type, seek to understand the function of thalamocortical inputs by defining the connection

probabilities of specific neural subtypes. Although anatomical data can constrain hypotheses about neural computation, experimental approaches that evaluate circuit properties through electrophysiological measurements will be required to determine how this architecture functions in real time.

For excitatory neurons, we found that direct synaptic input from POm onto excitatory neurons aligns with predictions based on axon-dendrite overlap and prior electrophysiological findings (Meyer et al., 2010b; Petreanu et al., 2009). In contrast, functional inputs onto cortical inhibitory neurons showed cell-type specificity. In deep layers, POm provided direct input to PV- and 5HT3a-expressing interneurons but was not observed for SST neurons. In superficial layers, substantial direct input was only observed for 5HT3a-expressing interneurons and was absent for both PV and SST neurons. This layer-specific pattern of synaptic connectivity is surprising, since individual neurons in POm send axons to the cortex that branch and arborize in both L5a and L1 with the potential for substantial axon-dendrite overlap with SST and PV neurons in both layers (Ohno et al., 2012).

Our data suggest that SST neurons receive either weak or no input from POm, a finding that is on face inconsistent with a recent anatomical study using rabies virus to identify cell-type specific presynaptic partners in somatosensory cortex (Wall et al., 2016). In this study, POm was identified as a presynaptic source of input to SST neurons from across the cortical column. How can this be reconciled with the current findings? First, our study focused on SST neurons in L2 and L5. In contrast, Wall et al examined inputs generally to SST neurons across the column. Because L4 SST neurons are molecularly and electrophysiologically distinct (McGarry et al., 2010) and

may receive thalamic input (Hu and Agmon, 2016; Tan et al., 2008), they may have been a major contributor driving apparent POm connectivity in rabies virus tracing studies.

In our assay, it is possible that POm synapses onto SST neurons were undercounted because they are strongly facilitating (Hu and Agmon, 2016; Tan et al., 2008). However, ChR2-mediated release is typically very effective, even at synapses where release probability is low, and in our experiments even long stimulus trains did not reveal functional connections. Distal POm inputs to SST neurons might be anatomically present but electrophysiologically hard to detect; however, in most cases we did not observe even small or kinetically slow inputs following POm stimulation. It remains possible that there is state-dependent enhancement of weak POm inputs that could not be detected in our assay. Overall, functional data provided by electrophysiological measurements will be critical for understanding the circuit computations of different anatomical motifs.

Common principles for thalamic input to granular and infragranular layers

POm input to L5 obeys wiring principles previously observed for VPM input to L4, with strong direct input to Pyr neurons, PV-expressing fast-spiking inhibitory neurons, and a sparse subpopulation of 5HT3a interneurons, and an absence of drive to SST neurons (Cruikshank et al., 2007; Staiger et al., 1996). Similar to VPM input to L4, POm activation can drive short-latency, temporally-precise APs in L5a Pyr neurons due to strong feedforward inhibition from PV interneurons. Parallel input to both excitatory and fast-spiking interneurons is believed to sharpen spatial and temporal resolution of sensory responses, and has been observed for thalamic input to L4 and non-granular

layers in different regions of sensory neocortex (Cruikshank et al., 2007, 2012; Delevich et al., 2015; Gabernet et al., 2005; Ji et al., 2016; Kloc and Maffei, 2014; Schiff and Reyes, 2012).

VPM and POm have comparable levels of firing during wakefulness and whisking (Urbain et al., 2015), indicating that these inputs are simultaneously active. Although we found that POm stimulation elicited the strongest depolarization in L2 and L5, excitatory neurons in all layers showed some response, similar to what has been inferred for VPM synapses (Meyer et al., 2010b; Oberlaender et al., 2012a). Thus, neocortical neurons, particularly those in L5, are in a position to receive direct convergent input from both thalamic nuclei (Mease et al., 2016; Meyer et al., 2010b). Because the thalamic wiring principles for different cell types are conserved between L4 and L5, we predict that simultaneous activation of VPM and POm will have qualitatively similar effects, i.e., forcing temporal fidelity of spikes in L5 Pyr neurons to a stimulus.

POm-activation drives progressive depolarization in L2 Pyr neurons

In striking contrast to L5a, we found that POm was insufficient to drive APs in L2 Pyr neurons, despite the absence of local PV inhibition and even with EPSP summation during repetitive POm stimulation. The lack of firing is particularly notable because ChR2-stimulation of POm afferents is synchronous, unlike what might occur during normal sensation, and provides an upper bound for how strong this input can be.

Our findings are consistent with observations that L2 neurons fire sparsely during whisker stimulation *in vivo* (Barth and Poulet, 2012; Chen et al., 2013; de Kock et al., 2007; Yamashita et al., 2013). What might be the right conditions to drive firing in L2

Pyr cells? *In vivo*, both POm and are simultaneously active (Urbain et al., 2015), and this combined input (direct from POm and indirect via L4 from VPM), especially with a more complex sensory stimulus, might be sufficient to drive spikes in some neurons. In addition, weak and delayed inhibition from 5HT3a neurons - in combination with the silencing of SST interneurons – might enable L2 Pyr neurons to be particularly sensitive to delayed and convergent input from other brain areas, such as M1 or S2, or ascending inputs within the column (Feldmeyer et al., 2013; Kinnischtzke et al., 2014; Urban-Ciecko et al., 2015). Indeed, L2 neurons show considerable experience-dependent plasticity *in vivo* (Benedetti et al., 2009; Clem and Barth, 2006; Fox, 1992; Gambino et al., 2014; Glazewski and Fox, 1996; Margolis et al., 2014; Wen and Barth, 2011), a property that might be related to their ability to associate inputs arriving from multiple sources.

Cell-type specific dynamics are similar to *in vivo* recordings

In vivo, targeted whole-cell recordings of identified neuronal subtypes have revealed characteristic sensory-evoked responses in superficial layers of barrel S1 and other cortical sensory areas (Gentet et al., 2012; Mesik et al., 2015). For example, whisker stimulation elicits depolarization but not spiking in L2 Pyr cells, hyperpolarization in SST cells, and delayed firing in subsets of 5HT3a cells. Remarkably, our data indicate that the essential circuitry to generate previously observed, cell-type specific patterns of activity can be retained in a reduced preparation and do not require input from other brain areas.

SST inhibition by VIP-expressing interneurons is a common connectivity motif that has been observed in multiple brain areas, including S1 (Fu et al., 2014; Jiang et

al., 2015; Lee et al., 2013; Pfeffer et al., 2013; Pi et al., 2013; Zhang et al., 2014). We found that POm activation could drive firing in 5HT3a neurons, a large and heterogeneous class of inhibitory neurons that includes VIP cells. Indeed, optogenetic POm stimulation evoked firing in VIP neurons, providing a mechanism by which POm-driven SST hyperpolarization might occur. However, POm stimulation also evoked firing in L1 5HT3a neurons, where VIP cells are not observed (Jiang et al., 2013b, 2015; Lee et al., 2013; Olàh et al., 2007). Thus, there may be multiple pathways by which thalamic input can suppress SST activity.

Even within defined subpopulations of 5HT3a neurons, such as L2 VIP neurons or L1 5HT3a neurons, synaptic and firing responses were still heterogeneous. These properties are consistent with the anatomical and electrophysiological diversity observed in this general cell class (Lee et al., 2010; Prönneke et al., 2015) and support the idea that there may be multiple functionally distinct subpopulations with unique roles in shaping cortical responses. Interestingly, the preliminary evidence for input from primary thalamic nuclei, such as VPM or the lateral geniculate nucleus, to VIP neurons is inconsistent across cortical regions (Ji et al., 2016; Staiger et al., 1996; Wall et al., 2016). It will be critical to determine how long-range and local circuits target specific anatomically and genetically defined sub-populations of 5HT3a neurons to understand the effect of this population on cortical processing.

POm-mediated SST silencing was observed in both superficial and deep layers, despite the scarcity of 5HT3a neurons in granular and infragranular layers. It is possible that translaminar inhibition from superficial VIP neurons or NGF neurons in L2 might contribute to POm-evoked SST silencing in deep layers (Lee et al., 2010; Prönneke et

al., 2015), and translaminar synaptic connections to SST cells have been documented (Jiang et al., 2015). A reduction in the tonic firing of SST neurons, observed *in vivo* and also in our experimental preparation, may be important for stimulus detection and circuit plasticity.

In vivo, POm neurons fire at 10-15 Hz during active touch, and optogenetic activation of these inputs trigger prolonged firing in the neocortex when paired with whisker stimulation (Mease et al., 2016; Urbain et al., 2015). In these experiments even transient optogenetic stimulation of POm alone was sufficient to drive prolonged firing in L5 neurons. Although repetitive POm fiber activation in acute brain slices cannot capture all properties of this corticothalamic loop (Crandall et al., 2015; Cruikshank et al., 2010; Groh et al., 2014b), the earliest sequence of synaptic input and spikes are likely to be conserved. POm stimulation at naturalistic frequencies was sufficient to drive prolonged network activity in both L2 and L5 which could last hundreds of milliseconds after the final stimulus. While additional long-range pathways may also contribute to the delayed activity observed *in vivo*, our results indicate that some of this activity must be generated by local circuit interactions.

Future Directions

Results presented here showcase the ability of *in vitro* methods to replicate complex, *in vivo* dynamics and attribute them to specific long-range inputs and cell populations. This detailed and dynamic analysis of individual long-range inputs will help build conceptual bridges between precise cell-type specific connectivity maps and the complex dynamics observed during active sensation and behavior *in vivo* (Fino and Yuste, 2011; Gentet et al., 2012; Jiang et al., 2015; Pala and Petersen, 2015; Pfeffer et

al., 2013; Pi et al., 2013). Further, these methods are modular and can be easily expanded to investigate the interplay of multiple, precisely controlled long-range inputs using multi-channel optogenetic strategies (Klapoetke et al., 2014).

Additionally, the activation of VIP interneurons, relief of SST inhibition, and the absence of strong PV inhibition in L2 with POm activation may have important implications for plasticity both of thalamocortical inputs and intracortical circuits (Fu et al., 2015). Understanding what information is conveyed by POm activity, dissecting how multiple thalamic and cortical pathways converge on individual neurons and probing the role of POm in plasticity and ensemble formation will be critical for advancing our understanding of the algorithm by which cortical circuitry transforms sensory input.

2.4 Materials & Methods

All experimental procedures were conducted in accordance with the NIH guidelines and were approved by the Institutional Animal Care and Use Committee at Carnegie Mellon University.

Viral Injections and Mouse Strains

ChR2 tagged with m-cherry (300-400 nl; AAV1.CAG.hChR2(H134R)-mCherry.WPRE.SV40, ID no. AV-1-20938m, PENN Vector Core, Philadelphia, PA) was stereotaxically injected into the POm following a small craniotomy (bregma -1.7, lateral 1.00, depth 3.25 mm) of isoflurane-anaesthetized mice aged postnatal day 10-15 (P10-15) using a Hamilton syringe (Hamilton; Reno, NV), Stoelting infusion pump (Stoelting; Wood Dale, IL, Model #53210), and custom injection cannulas (Plastics One; Phoenix,

AZ). To avoid injection spillover into VPM, injections were targeted toward the medial portion of POm. In some animals, areas of the parafasicular nucleus were labeled; however, since this nucleus does not have direct cortical projections (Allen Brain mouse connectivity atlas; http://connectivity.brain-map.org/) it is unlikely that it contributed to the responses observed in S1. After injection mice were treated once with ketoprofen (5 mg/kg, Sigma-Aldrich; St. Louis, MO) and additional doses were administered as necessary. Mice recovered in their home cage for 6-10 days prior to preparation of acute brain slices. Experiments targeting excitatory neurons were performed on C57Bl6 mice (Harlan). Specific inhibitory neuron populations were targeted using the following transgenic mice: *Sst-IRES-Cre* (Jackson Labs stock # 013044)(Taniguchi et al., 2011), *Pval*$^{tm1(cre)Arb}$ (Jackson Laboratory stock # 017320)(Hippenmeyer et al., 2005), *5HT3a-cre* (GENSAT 036680-University of California -Davis), and VIP-Cre (Jackson Labs stock # 010908) (Taniguchi et al., 2011), and some excitatory neurons were recorded from these lines as well. Mice were mated with Ai3 (Jackson Laboratory Stock # 007903) mice to create heterozygous transgenic mice with YFP-labeled SST, PV, 5HT3a, or VIP interneurons.

Slice Preparation and Injection Site Confirmation

Injected mice were sacrificed at age P16-25 by brief isoflurane anesthesia and decapitation. Coronal slices 350 µm thick were prepared in regular ice-cold artificial cerebrospinal fluid (ACSF) composed of (in mM): 119 NaCl, 3.5 KCl, 1 NaH_2PO_4, 26.2 $NaHCO_3$, 11 glucose, 1.3 $MgSO_4$, and 2.5 $CaCl_2$ equilibrated with 95%/5% O_2/CO_2. Slices were allowed to recover at room temperature for 45 minutes in the dark before recording.

The injection site was confirmed anatomically using the mCherry-tagged ChR2 fluorescence in cell bodies at the injection site and the characteristic pattern of fluorescent axonal labeling in the barrel cortex, concentrated in L1 and L5a (Wimmer et al., 2010a). Only slices that had fluorescently labeled axons in both L1 and L5 but not in L4 were used in our experiments. Retrogradely-labeled, $ChR2^{+}$ neurons in the somatosensory cortex were never observed.

General Electrophysiology

In slices with confirmed injections, cortical excitatory Pyr neurons and identified inhibitory neurons were targeted for whole-cell recording in the posteromedial barrel subfield using an Olympus light microscope (BX51WI) with a mercury lamp for fluorescence imaging and borosilicate glass electrodes resistance 4-8 MΩ. Electrode internal solution, except for a small subset of experiments described later, was composed of (in mM): 125 potassium gluconate, 10 HEPES, 2 KCl, 0.5 EGTA, 4 Mg-ATP, and 0.3 Na-GTP, pH 7.25-7.30, 280 mOsm. For some cells trace amounts of AlexaFluor 594 were added to the internal solution to confirm cell targeting. Electrophysiological data were acquired using a Multiclamp 700B amplifier (Axon Instruments, Foster City, CA) and a National Instruments acquisition interface (National Instruments; Austin, TX). The data were filtered at 3 kHz, digitized at 10 kHz and collected using custom macros in Igor Pro 6.0 (Wavemetrics, Lake Oswego, Oregon).

Cell Identification

The morphology and basic electrophysiological properties of all recorded cells were evaluated to aid in cell identification: resting membrane potential (V_{Rest}), input

resistance (R_i), series resistance (R_s), and firing phenotype using brief depolarizing currents in current clamp (Table 1, Table 2). Cells were allowed to equilibrate for 5 minutes before data collection. Following recording, cells were imaged to determine neurite morphology if fluorescently filled and to measure their laminar location based on depth from pial surface and relevant cytoarchitectural features. L2 neurons were defined as neurons up to 100 um below the cell-sparse area of L1, typically 50-150 um below the pial surface. L3 neurons were selected 100 um above the L4 barrel, visually identifiable under bright field illumination. These criterion necessarily excluded cells at the margin of L2 and L3, since they could not be unambiguously assigned. L4 neurons are defined as inside the upper and lower limit of the L4 barrel, but were selected from both “barrel” and “septal” regions, since segregated barrel and septal circuits in mouse L4 are absent (Feldmeyer et al., 2013). L5a neurons made up the visually identifiable area ~150-200 um below the L4 barrels corresponding to the location of fluorescent POm axons. L5b was defined as the area up to 150 um below L5a, and L6 was defined as the 150 um above the white matter. Cre-dependent YFP fluorescence within a cell population reflected well-defined electrophysiological properties and firing phenotype (Agmon and Connors, 1992; Kawaguchi and Kubota, 1997; Lee et al., 2010; Neske et al., 2015; Xu et al., 2013). SST cells had a medium to large input resistance (536 ± 71 MΩ) with a low-threshold-spiking firing phenotype that showed rate and amplitude accommodation. A small number of SST cells identified by reporter expression exhibited a FS firing phenotype (Tan et al., 2008) and were excluded from further analysis. Notably, their POm responses obeyed their firing phenotype classification rather than their SST marker gene expression. PV neurons had a very low R_i (286 ± 34 MΩ) and a

fast-spiking firing phenotype. 5HT3a cells, which are known to be a heterogeneous population, displayed diverse electrophysiology properties and firing phenotypes (Lee et al., 2010). Excitatory neurons were characterized by a pyramidal soma morphology, a regular spiking firing phenotype, intermediate R_i, (354 ± 23 MΩ) and presence of dendritic spines when fills were available. R_s and R_i were monitored for the duration of experiments and cells with R_i below 100 MΩ, R_s greater than 45 MΩ, or where R_s changed by more than 30% over the course of data collection were excluded from further analysis.

POm Synaptic Input

To assess excitatory synaptic input to cell populations, POm axons were stimulated optically while holding cells at -70 mV, the calculated E_{Cl}. Single or paired 5ms light pulses (12.5 Hz, 479 nm) were delivered through a 40x water-immersion objective (Olympus) at the recording site using a white LED (Prizmatix; Israel) in combination with an 40 nm excitation filter centered at 480nm (Chroma; Bellows Falls, VT). Light intensity at 470 nm was measured at 2.13 mW, distributed over a beam area ~1 mm diameter, in line with parameters employed in similar slice experiments (Cruikshank et al., 2010; Kinnischtzke et al., 2014; Petreanu et al., 2007). Timing of optogenetic simulation was controlled by a Master-8 (A.M.P.I; Jerusalem, Israel). All experiments were performed at a maximum light intensity to allow for better comparison of currents and timing across experiments. Stimulus trials were carried out at low frequency (0.05 Hz). For all cells and conditions, responses following stimulation were averaged across 10 trials and the amplitude of POm-evoked EPSCs was taken as the peak amplitude in the 50 ms following stimulus onset for events with an onset latency of

less than 10ms post-stimulus. Responses below 3pA could not be resolved from noise and were given a value of 0. Paired-pulse ratio for POm-evoked responses was calculated by measuring EPSC amplitude for two responses at an 80ms inter-stimulus interval. To confirm that the observed input was glutamatergic, the AMPA receptor antagonist NBQX (10 µM, Sigma-Aldrich; St. Louis, MO) was applied in a subset of experiments.

To isolate direct POm-evoked responses in excitatory and inhibitory neurons, the voltage-gated sodium channel antagonist TTX (0.25-0.5 µM, Sigma-Aldrich; St. Louis, MO) was applied to prevent polysynaptic activity along with 100 µM 4-AP (Sigma-Aldrich; St. Louis, MO) to assist in axonal depolarization and neurotransmitter release (Petreanu et al., 2009). As a positive control, a light-triggered POm response had to be recorded in a Pyr neuron in each slice for each condition to be included in analysis to insure that the absence of a light-evoked response was not caused by low levels of viral transduction.

Laminar Input to Excitatory and Inhibitory Neurons

The amplitude of direct POm input was recorded in TTX and 4-AP for excitatory Pyr neurons across multiple cortical layers within a single slice; at least one L5a Pyr neuron was recorded from in every slice.

POm input onto SST, PV, and 5HT3a neuron populations were recorded in separate experiments using different transgenic mice. In a subset of animals, immunohistochemistry was performed against YFP to visualize the distribution of each inhibitory neuron population across cortical layer. In each slice, interneurons and Pyr

neurons (<200 µm apart) were recorded in pairs or sequentially to account for across-animal differences in viral expression. POm-evoked EPSCs in inhibitory neurons, and their corresponding Pyr neurons, were recorded as described above in ACSF and in the presence of TTX and 4AP to reveal all input and direct input respectively. For a subset of L2 and L5 SST neurons we delivered long stimulus trains (10+ pulses, 80ms ISI) to identify any facilitating responses with and without TTX and 4-AP.

Polysynaptic Inhibition and AP Generation

In a subset of experiments we characterized POm-evoked polysynaptic inhibition onto L2 and L5a excitatory neurons by recording in current clamp. Here, the EPSP and IPSP amplitude was calculated as the maximum depolarization or hyperpolarization following POm-stim.

For isolating IPSCs in voltage clamp, L2 and L5a Pyr neurons were held at +10 mV using a Cs-based internal solution containing (in mM): 130 cesium gluconate, 10 HEPES, 0.5 EGTA, 8 NaCl, 10 Tetraethylammonium chloride (TEA-Cl), 4 Mg-ATP and 0.4 Na-GTP, pH 7.25-7.30, 280-290 mOsm. POm-evoked EPSCs and IPSCs following 5ms optogenetic stimulation of POm fibers (same as above) were averaged across 10 trials and the magnitude was taken as the maximum amplitude within 50ms following stimulus onset. Rise and decay times for each cell were measured from the cell average IPSC (10 sweeps). Rise time was measured from 10-90% and decay time was measured as the time from response peak to return to 1/3 of the max amplitude. Decay time and inhibitory to excitatory current ratio was calculated for both maximum stimulation and a minimal stimulation where light intensity was decreased until single, smooth IPSCs were elicited.

To determine which inhibitory neuron populations mediate the polysynaptic inhibition observed in L2 and L5a Pyr neurons, AP generation and timing was assessed for all cell-types in ACSF. Cell responses to a single 5 ms light pulse were recorded in current clump at resting membrane potential for each neuron. Cells that fired APs on any of 5 consecutive sweeps were designated as firing APs. For each cell, the average spike time was determined by taking the mean average of the spike-peak latency following stimulus onset for 5 consecutive sweeps. The amplitude of POm-evoked EPSPs and IPSPs was also recorded for each cell population, but could not be calculated for neurons that fired APs on every trial.

Ongoing POm Stimulation and Recurrent Activity

To determine the effect of ongoing POm activity on cortical network dynamics we delivered trains of light pulses while recording in a modified ACSF solution (mACSF, in mM: 119 NaCl, 2.5 KCl, 1 NaH_2PO_4, 26.2 $NaHCO_3$, 11 glucose, 0.5 $MgSO_4$, and 1 $CaCl_2$) which simulates the neuronal activity levels observed *in vivo* (Urban-Ciecko et al., 2015) and allows for recurrent network activity. We recorded from L2 and L5 Pyr, SST, PV, 5HT3a, and VIP neurons in current clamp while delivering trains of 5 ms light pulses at 12.5 Hz at an inter-trial interval of 0.05 Hz. This frequency is physiologically relevant and matches the firing rates observed for POm cells in awake, behaving animals (Urbain et al., 2015). For each cell, 10 consecutive trials were recorded and displayed as overlays of all trials and as a raster plots that show AP peak time for each trial. Spike data was binned at 40 ms intervals and averaged across all cells of a given population to generate an average PSTH. Some cells displayed prolonged epochs of depolarization and AP generation similar to an upstate following POm activation, and

were included in analysis. *In vivo*, SST cells rest depolarized and fire spontaneously (Gentet et al., 2012) so SST cells when necessary were given a depolarizing holding current to adjust V_m to -48 mV ± 2mV, allowing us to measure POm-evoked hyperpolarization and modulation of firing frequency.

For each cell type, the average firing rate was calculated for 500 ms pre-stim (i.e. spontaneous activity), during stim, and post-stim, displayed in Table 2. In SST neurons, the length of hyperpolarization was different across cells therefore the during-stimulus bin is calculated for 40-160 ms post-stim to capture the consistent early hyperpolarization observed.

Statistical analysis

For each analysis as described throughout, values were measured from average responses of 10 consecutive sweeps unless otherwise noted. Unless indicated, calculations and statistics were performed on cells and all statistical tests are non-parametric Wilcoxon rank sum tests. Standard error of the mean is reported with all averages and as error bars unless otherwise reported. Cell (n) and animal values (N) are reported in each figure.

3 ***POm plasticity initiates learning-related reorganization of the cortical column***

Neocortical circuits are sensitive to experience, showing both anatomical and electrophysiological changes in response to altered sensory input. We examined input- and cell-type specific changes in thalamo- and intracortical pathways during learning using an automated, home-cage sensory association training (SAT) paradigm that couples multi-whisker stimulation to a water reward. We found that POm, but not VPM, drives increased cortical activity after 24 hours of SAT, when behavioral evidence of learning first emerges. Synaptic strengthening within the POm thalamocortical pathway was initiated at thalamic inputs to L5 and was not generated by sensory stimulation alone. Synaptic changes in L2 were delayed relative to L5, requiring 48 hours of SAT to drive synaptic plasticity at thalamic and intracortical inputs onto L2 Pyr neurons. These data identify the POm thalamocortical circuit as site of rapid synaptic plasticity during learning and indicate a temporal sequence to learning-evoked synaptic changes in the sensory cortex.

3.1 Introduction

Experience-dependent plasticity is a cardinal feature of the neocortex. Abundant evidence indicates that motor or perceptual learning drives changes in neocortical circuits, with changes observed in fMRI signals (Shibata et al., 2016; Summerfield et al., 2006), altered topographic organization (retino-, tono- or somatotopy; (Harris et al., 2001; Kilgard, 1998; Schwartz et al., 2002)), enhanced feature-selective responses and increased spike output to previously undetectable stimuli (Glazewski and Barth, 2015;

Karni and Sagi, 1991), and increased synaptic strength (Cheetham et al., 2008; Clem, 2010; Rioult-Pedotti et al., 2000).

How is learning associated with plasticity in specific neocortical circuits? In rodent somatosensory cortex, experience-dependent changes are concentrated in infra- and supra-granular layers, rather than layer 4 (L4 (Chandrasekaran et al., 2015; Diamond et al., 1994; Glazewski and Barth, 2015; Glazewski and Fox, 1996; Jacob et al., 2012; Oberlaender et al., 2012b). This dissociation could be a product of post-synaptic differences, but also aligns with the laminar targets of the two thalamic input streams that drive the barrel cortex. The primary, ventral posterior-medial (VPM) thalamic nucleus provides the dominant glutamatergic input to L4 (Feldmeyer et al., 2013), while neurons in L2 and L5 receive strong glutamatergic input from the higher-order posterior-medial (POm) thalamic nucleus (Audette et al., 2017; Bureau et al., 2006; Petreanu et al., 2009), raising the possibility that the two thalamocortical circuits might be related to differences in plasticity induction across different cortical layers.

VPM neurons receive ascending sensory information directly from the trigeminal brain stem nucleus and respond robustly to the deflection of a single whisker (Feldmeyer et al., 2013). VPM faithfully relays these signals to L4 of the cortex, where excitatory neurons fire short-latency action potentials time-locked by fast, feedforward inhibition (Cruikshank et al., 2010; Feldmeyer et al., 2013). While VPM input plasticity has been observed in early development, electrophysiological and anatomical changes in L4 of the adult mouse are typically only detectable after prolonged periods of drastically altered sensory input levels (Crair and Malenka, 1995; Diamond et al., 1994; Fox, 1992; Glazewski and Fox, 1996; Oberlaender et al., 2012b).

The higher-order thalamic nucleus POm also receives sensory signals from the brainstem, but integrates this information with strong cortical feedback from reciprocal connections to S1, S2, and M1 (Alloway et al., 2003; Groh et al., 2014b; Urbain and Deschenes, 2007). Like other higher-order thalamic nuclei such as the pulvinar, POm neurons are well positioned to provide contextual information to the cortex and are strongly modulated by arousal and cholinergic activity (Masri et al., 2006a; Purushothaman et al., 2012; Roth et al., 2016; Sobolewski et al., 2015). POm axon terminals, concentrated in L1 and L5, provide direct synaptic input to excitatory neurons in L2 and L5 (Audette et al., 2017; Bureau et al., 2006), and POm activation can prolong and enhance sensory responses in S1 (Mease et al., 2016). Plasticity of POm afferents onto L2 excitatory neurons can be elicited over short timescales by artificial whisker stimulation in anaesthetized mice, indicating that these synapses possess the machinery for long-term potentiation (Gambino et al., 2014).

Since POm inputs can undergo activity-dependent synaptic strengthening, convey contextual and brain state information to the cortex, and drive activity in highly plastic cortical neuron populations, we hypothesized that POm-related pathways would undergo experience-dependent modifications during whisker-dependent learning. To test this, we developed a high-throughput, home-cage system for automated sensory association training that couples a multi-whisker stimulus to a water reward in freely-moving mice. Animals exhibit behavioral evidence of learning within the first 24 hours (hrs) of training, and performance increases with longer training intervals.

Using acute brain slices for pathway-specific activation and precise targeting of postsynaptic neurons across different cortical layers, we identified changes in excitatory

synapses during early learning and then later, as behavioral performance improved. Neocortical responses to optogenetic activation of thalamic inputs were changed at the earliest stages of learning, where POm, but not VPM, drove significantly greater evoked firing in neocortical neurons in both deep and superficial layers after just 24 hrs of training. Synaptic strengthening of direct POm inputs to L5 neurons was linked to increased spiking during early training, but was not manifested in L2 neurons until 48 hrs of training. Synaptic strengthening of intracortical pathways, primarily at L2-L2 excitatory inputs, was delayed with respect to plasticity at POm synapses in L5. Importantly, these synaptic changes were not observed with unrewarded sensory stimulation. Together, our results indicate that plasticity at thalamic inputs from POm initiate cortical rewiring during sensory learning, revealing a temporal sequence of synaptic changes that begin in L5 and then progress to L2.

3.2 Results

3.2.1 Automated, home-cage sensory association training

Time-intensive animal training paradigms are not well-suited to a comprehensive electrophysiological analysis of cell-type and input-specific excitatory synaptic changes during learning. Thus, we designed an automated home-cage training system for freely-moving animals where a multi-whisker stimulus was predictively coupled to the cage water source (Figure 11A,B). We developed a mouse-initiated training paradigm adapted from classical trace conditioning, where a conditioned sensory stimulus (CS)

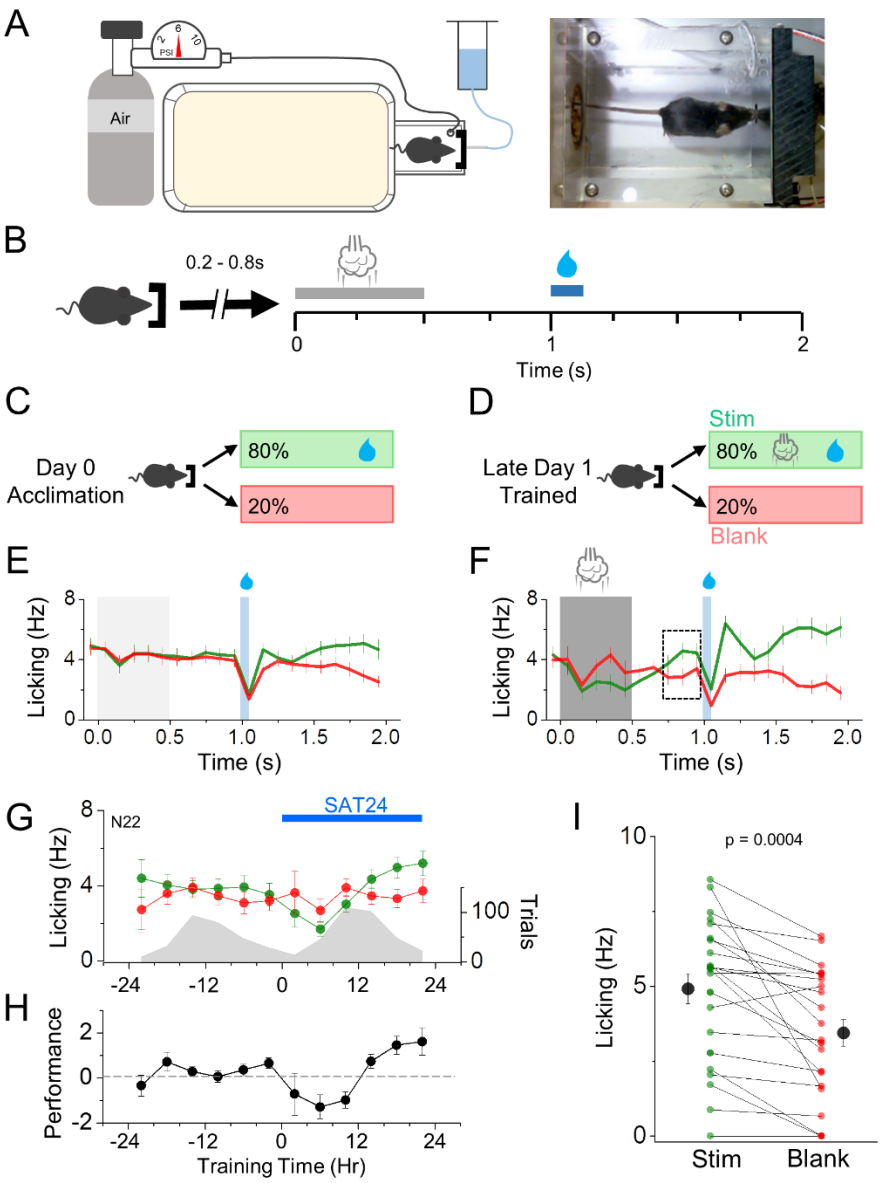

Figure 11. Automated home-cage training enables rapid acquisition of multi-whisker sensory association. (A) Schematic of home-cage sensory association training cage (left) and image of mouse initiating a training trial (right). (B) Sensory association training paradigm. Upon IR beam-break measured nose poke, a random delay (200-800ms) occurs prior to trial initiation. Air puff delivery period (CS, 500ms duration, 6PSI) occurs at t=0 following random delay with water delivery (US, 75ms, ~50uL) occurring at t=1s, leaving a 500ms delay in between the CS and US. A new trial could not be initiated until t=2s. (C,D) Identical trial structure during acclimation and SAT, with 80% of initiated trials providing water and air puff (no air puff during acclimation), and 20% of trials delivering neither air puff or water. (E,F) Average global lick rates

was followed by an unconditioned stimulus (US) at a fixed delay (Galvez, 2006). We elected to use a gentle airpuff as the CS, since it is a naturalistic stimulus and can activate multiple whiskers without precise animal positioning, well-suited for training freely-moving mice. On training trials, snout entry into the water port triggered a short random delay (200-800ms) followed by a gentle airpuff (CS, 6 psi, 500 ms), a fixed delay (500ms), and then water delivery (US, Figure 11B,D, green).

Blank trials, where no CS or US was delivered, were randomly interleaved on 20% of trials (Figure 11C,D, red). Prior to training, mice received one day of acclimation to the home-cage drinking setup where they experienced an identical trial structure but without presentation of the CS (Figure 11C). Mice readily learned to drink from the lick port and behavior data, including nose-poke times and licking, was recorded throughout the acclimation and training period.

In trace conditioning, the CS consistently predicts the US and becomes sufficient to evoke an unconditioned behavioral response, in this case licking (Cohen et al., 2012; Galvez, 2006). CS-US association was monitored by comparing the lick frequency prior to the time of potential water delivery, i.e. anticipatory licking (referred to as “licking”), between training and blank trials. Before sensory association training (SAT), licking was identical for both trial types (Figure 11E), as expected since no cue differentiated water-reward versus blank trials. A transient suppression of lick rates at the onset of SAT recovered rapidly, and the total trials/day were comparable between acclimation and training days (Figure 11G). By the end of the first day of training (24 hrs), mice increased their lick rate following the airpuff but not on blank trials, evidence of a predictive CS-US association (Figure 11F-H)(Cohen et al., 2012).

Behavioral evidence of learning after 24 hrs of training was monitored by assessing the difference in licking for airpuff-water paired versus blank trials (performance: $L_w - L_b$) over time (Figure 11H). An increase in lick frequency for paired trials was visible between 12 and 24 hrs and became significantly different from blank trials by 24 hrs. More than 90% of animals showed increased licking by the end of the first training day (Figure 11I). These data show that home-cage trace conditioning can drive the acquisition of a multi-whisker sensory association that is observable after just 24 hrs, which enabled electrophysiological investigation of circuitry changes at the earliest stages of sensory learning.

3.2.2 Increase in POm-evoked cortical activity after 24 hrs of SAT

A broad comparison of cortical responses to POm stimulation before and after SAT could reveal sites of synaptic change that are related to learning. To examine how POm-evoked firing was changed by SAT, we recorded from pyramidal neurons (Pyr) in the major POm-recipient layers, L2 and L5a (referred to as “L5” for brevity) (Audette et al., 2017; Bureau et al., 2006; Viaene et al., 2011a) following activation of thalamic axons. Experiments were performed in acute brain slices cut to preserve columnar interactions from control and SAT mice. To isolate cortical responses specific to this pathway, ChR2 was expressed in POm (Figure 12). Although virally-expressed ChR2 expression can vary across animals, strict criteria were used to ensure a minimum level of ChR2 viral transduction monitored by fluorescence signal in cortical POm afferents. Light intensity for stimulation was kept constant over all experiments, and a large number of animals were used for each experimental group (>9 animals per group). In addition, animals were

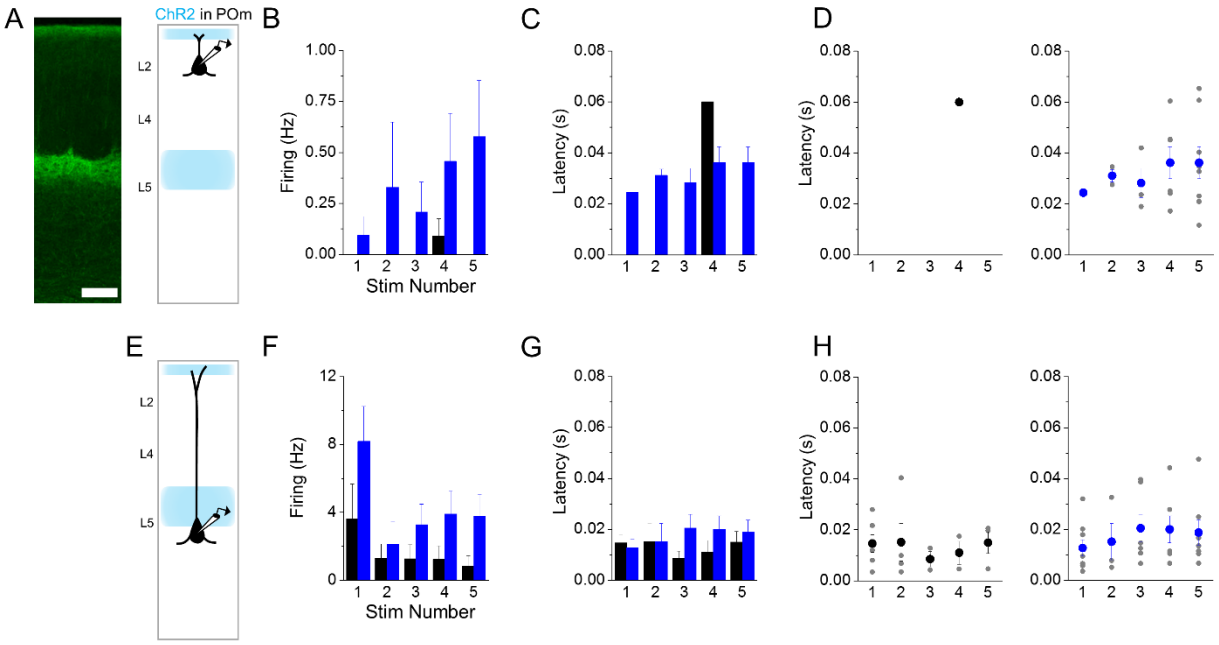

Figure 12. POm-evoked action potential latency changes after SAT. (A) Fluorescent image of POm ChR2-expressing axons in vS1, (Scale bar 250 um) and schematic of experimental setup. (B) Quantification of L2 Pyr spike rate in 80ms following each stim in a train for CTL (black) and SAT24 (blue) animals. (C) Latency of first spike occurring in the 80ms following each stim in a train for CTL (black) and SAT24 (blue) animals. Number of values for each stim is variable since not all cells fired action potentials. (D) First spike latency reported in (C) showing the average for each cell in CTL (black, left) and SAT24 (blue, right) animals. (E-H) Same as (A-D) but for L5 Pyr neurons.

assigned to control or SAT groups without prior knowledge of ChR2 expression levels and average fluorescent labeling was comparable across groups.

In tissue from control animals (acclimation but no whisker stimuli), optogenetic stimulation of POm axons (5 pulses, 80ms ISI) drove short latency spiking in L5 Pyr (14.6±3.4 ms; Figure 12) and subthreshold EPSPs in L2 Pyr, consistent with prior work (Figure 13C, H)(Audette et al., 2017). POm stimulation occasionally caused prolonged, recurrent sub- and suprathreshold activity in the post-stimulus period that lasted for several seconds, although action potentials were only rarely observed in L2. Both spike probability and EPSP amplitude depressed with subsequent stimuli in L5 Pyr (Figure 13H,K; Figure S2)(Audette et al., 2017).

After 24 hrs of SAT, POm-evoked cortical firing was dramatically increased (Figure 13D,I). The fraction of neurons spiking during the stimulus and/or the post-stimulus period increased from 60% to 92% in L5, and 14% to 63% in L2. In both L2 and L5, neurons from SAT mice POm stimulation evoked a marked increase in recurrent activity during the post-stimulus period (Figure 13D,E,I,J).

In L5, the SAT-associated change in POm spiking was most notable in response to the first light pulse, where mean firing frequency in the first 10ms after POm stimulation increased 4-fold (control 1.65±1.00Hz; SAT 24 4.25±1.25Hz), and the latency to spike was slightly reduced (control 15±3ms; SAT 24 13±3ms; Figure 12). L2 Pyr spiking during the 500 ms stimulus window increased nearly 20-fold, where the increase in spike output after 24 hrs SAT was most pronounced for later light pulses in the train. Spikes in L2 Pyr neurons typically occurred 10-40 ms after an individual light pulse stimulus and showed high trial-to-trial variability (Figure 12).

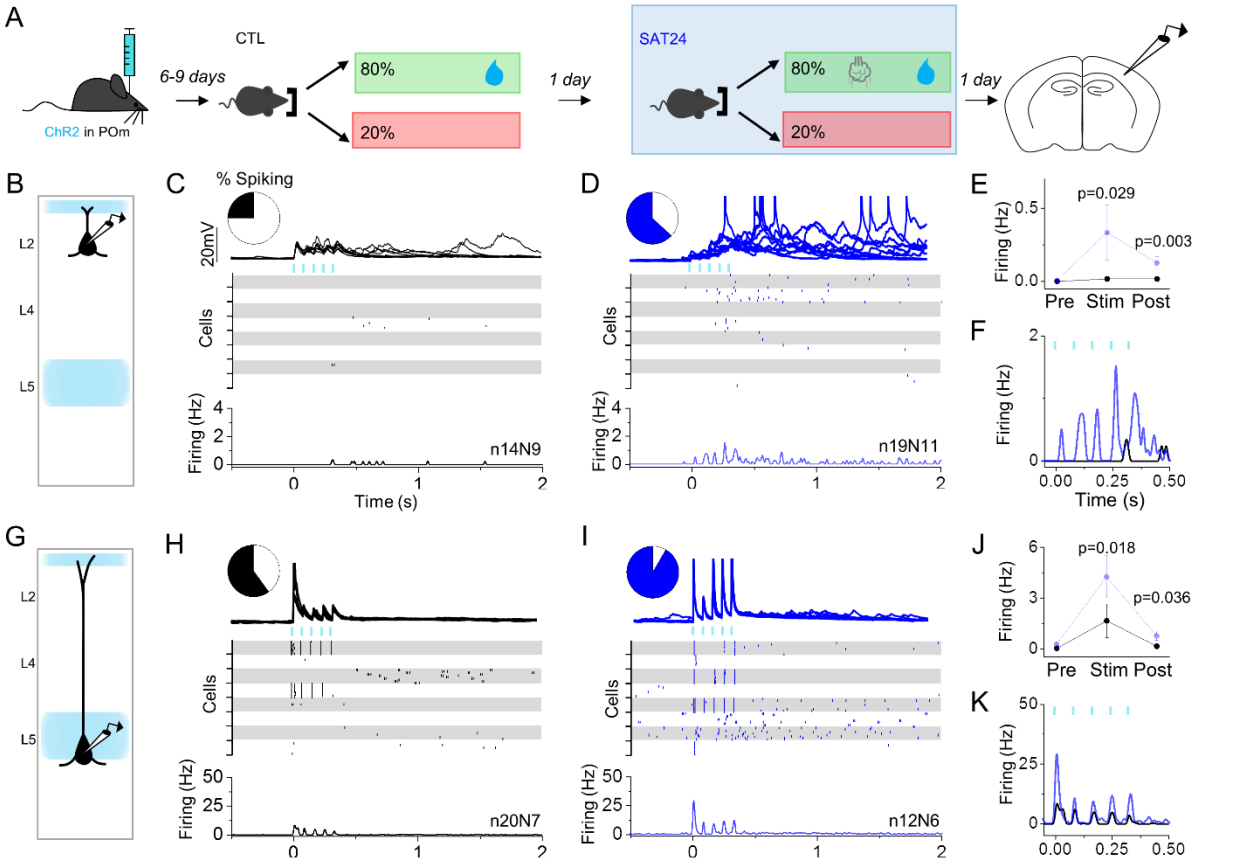

Figure 13. Increase in POm-evoked cortical activity after 24 hrs of SAT. (A) Schematic of experiment with recordings performed in ChR2-injected mice after 24 hrs of acclimation and 24 hrs of SAT. (B) Schematic of POm axonal labeling and laminar pyramidal neuron recording site in L2. (C,D) POm-evoked activity (blue bars, 5 pulses, 5ms, 80 ms ISI) in L2 Pyr neurons of control animals that received 24 hrs of acclimation (left, black) and 24 hrs SAT (blue, right). Pie chart shows fraction of neurons that generated any action potentials following stimulation. Example cell response (top) shows 10 consecutive trials for an individual neuron. Raster (middle) shows spiking activity on 10 consecutive trials for 8 example cells. Global peri-stimulus time histogram (PSTH, bottom, 10ms bins) shows average firing frequency across all cells in group. (E) Average firing frequency across all cells during the 500ms preceding POm stimulation (Pre), during stimulation (Stim) and directly following stimulation (Post). (F) Overlay of POm-evoked spiking activity (10ms bins) for CTL (black) and SAT24 (blue) animals. (G-K) Same as C-F, but for L5 Pyr neurons.

These results indicate that 24 hrs of SAT drives a major increase in Pyr responses to POm stimulation that are manifested across the cortical column.

3.2.3 VPM-evoked responses are unchanged

Although plasticity at VPM inputs is generally restricted to early development in L4, VPM axon remodeling in L4 has been observed in adult animals (Oberlaender et al., 2012b), and VPM-related plasticity in other cortical layers has not been well-investigated. We used optogenetic activation of ChR2-expressing VPM afferents to screen for changes in evoked firing of regular spiking (L4) or Pyr neurons in L2 and L5, which receive both direct and indirect VPM input (Bureau et al., 2006).

We first investigated SAT-induced changes in L4, the main VPM-recipient layer (Bureau et al., 2006; Cruikshank et al., 2010; Meyer et al., 2010b). In control animals, optogenetic stimulation of VPM axons drove precisely timed, short-latency (10.1 ± 1.5ms) action potentials in the majority (55%) of L4 neurons that were restricted to the stimulus window (Figure 14H,I) (Cruikshank et al., 2010). After SAT, a slightly smaller fraction of L4 neurons fired with VPM stimulation (43%), and spike latencies were unchanged (Figure 15G,H). The mean firing frequency across the entire stimulus period was indistinguishable between control and SAT (control 2.89±0.98Hz; SAT 24 2.58±0.86Hz, Fig 14J). Unlike POm-evoked activity in L2 and L5, VPM stimulation never drove recurrent firing in the post-stimulus period, consistent with strong feed-forward inhibition in this layer (Cruikshank et al., 2010; Porter et al., 2001).

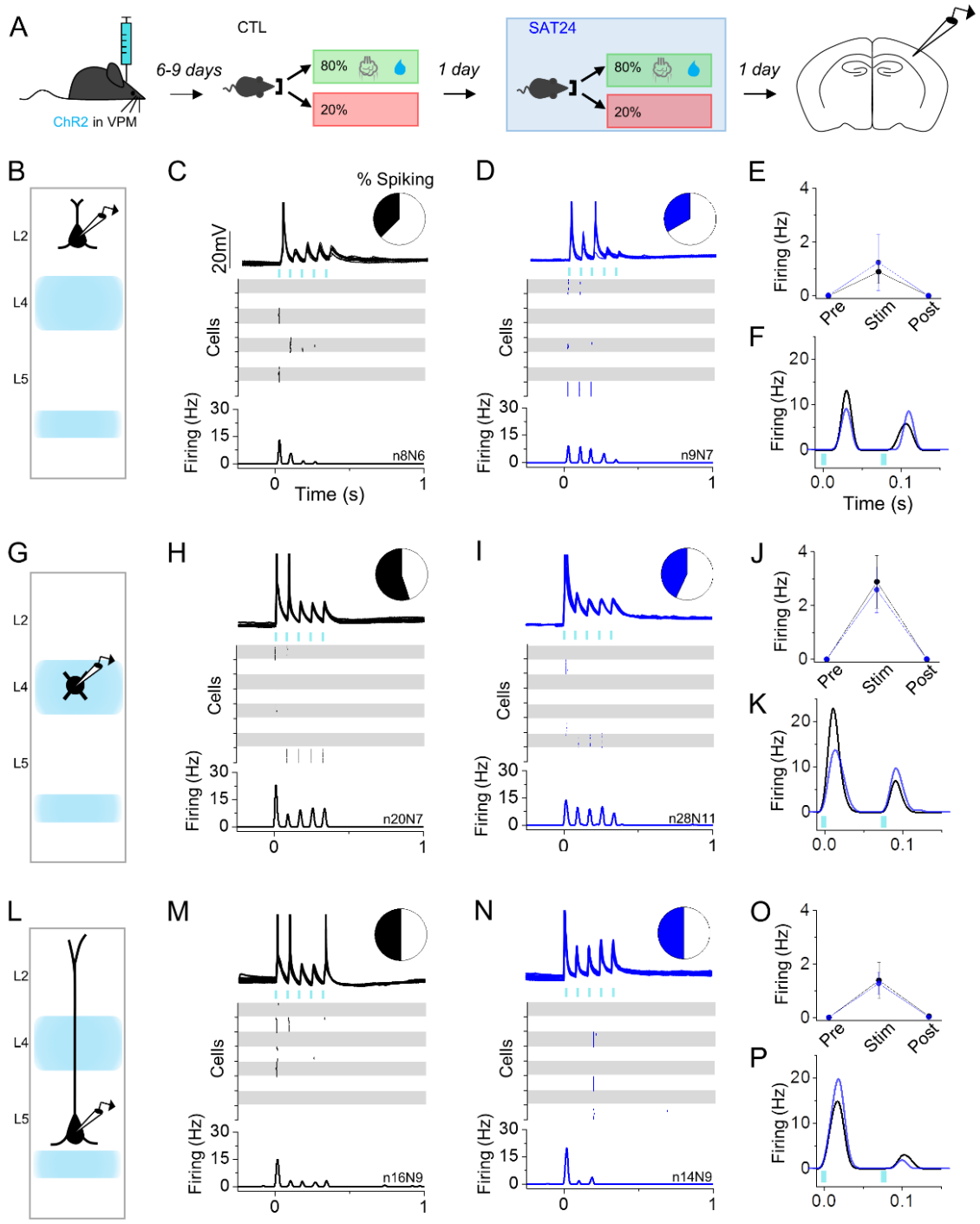

Figure 14. No change in VPM-evoked cortical activity after 24 hrs of SAT. (A) Schematic of experiment with recordings performed in ChR2-injected mice after 24 hrs of acclimation and 24 hrs of SAT. (B) Schematic of VPM axonal labeling and laminar pyramidal neuron recording site in L2. (C,D) VPM-evoked activity (blue bars, 5 pulses, 5ms, 80 ms ISI) in L2 Pyr neurons of control animals that received 24 hrs of acclimation (left, black) and 24 hrs SAT (blue, right). Pie

chart shows fraction of neurons that generated any action potentials following stimulation. Example cell response (top) shows 10 consecutive trials for an individual neuron. Raster (middle) shows spiking activity on 10 consecutive trials for 8 example cells. Global PSTH (bottom, 10ms bins) shows average firing frequency across all cells in a population. (E) Average firing frequency across all cells during the 500ms preceding VPM stimulation (Pre), during stimulation (Stim) and directly following stimulation (Post). (F) Overlay of VPM-evoked spiking activity for CTL (black) and SAT24 (blue) animals. (G-K) Same as C-F, but for L4 excitatory neurons. (L-P) Same as C-F but for L5 Pyr neurons.

VPM provides direct synaptic input to L5 (Bureau et al., 2006; Meyer et al., 2010b), and SAT could conceivably drive changes at this connection. Indeed, experience-dependent changes in L5 firing have been observed in some studies (Diamond et al., 1994; Jacob et al., 2012; Ward et al., 2012), and the change in POm-evoked firing in L5 we observed might reflect a special capacity for plasticity of neurons in this layer. However, optogenetic activation of VPM afferents revealed that SAT did not change the fraction of L5 spiking neurons (50% for both conditions) or their mean evoked firing frequency during or after the stimulus window (Figure 14L-P). Thus, the pathway-specific activation of thalamic afferents in acute brain slices reveals an input-dependent, SAT-induced change in L5 response properties, something that would not have been easy to decipher from sensory stimulation *in vivo*.

L2 Pyr neurons receive minimal direct input from VPM, but do receive strong ascending input from L4. Consistent with this circuitry, optogenetic activation of VPM afferents in control samples was sufficient to drive firing in a fraction of L2 Pyr neurons (38%) that were delayed compared to spikes generated in deeper layers (L2: 24.3±0.5ms; L4: 10.1±1.5ms; L5 14.0±1.7ms; Figure 15). SAT did not change the fraction of spiking neurons (33%) or the mean evoked firing response during the stimulus period. As in L4, VPM stimulation did not elicit recurrent activity in the post-stimulus window for either L2 or L5 (Figure 14E,O).

Lack of changes in VPM-evoked firing could result from a homeostatic reduction in intrinsic excitability (Lambo and Turrigiano, 2013; Mrsic-Flogel et al., 2007). However, input-output curves and resting membrane potential for L2, L4, and L5

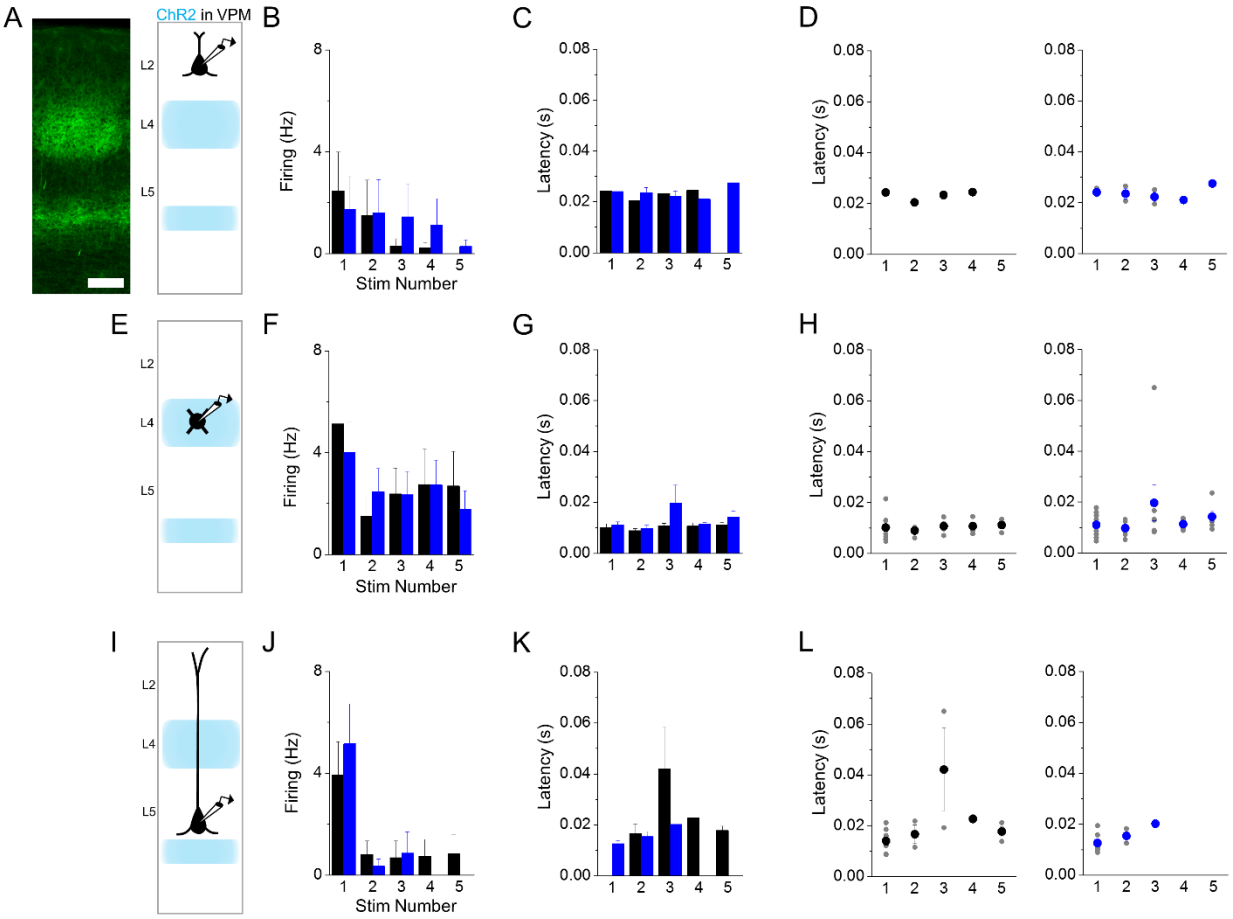

Figure 15. VPM-evoked action potential latency after SAT. (A) Fluorescent image of VPM ChR2-expressing axons in vS1, (Scale bar 200um) and schematic of experimental setup. (B) Quantification of L2 Pyr spike rate in 80ms following each stim in a train for CTL (black) and SAT24 (blue) animals. (C) Latency of first spike occurring in the 80ms following each stim in a train for CTL (black) and SAT24 (blue) animals. Number of values for each stim is variable since not all cells fired action potentials. (D) First spike latency reported in (C) showing the average for each cell in CTL (black, left) and SAT24 (blue, right) animals. (E-H) Same as (A-D) but for L4 excitatory neurons. (I-L) Same as (A-D) but for L5 Pyr neurons.

excitatory neurons showed no significant increase in either property between control and SAT neurons (Figure 16).

Our assay indicates that VPM-associated cortical pathways do not become potentiated during learning. Although L4 to L2/3 synapses can undergo spike-timing dependent plasticity (STDP) *in vitro* (Banerjee et al., 2009), the conditions engaged by SAT *in vivo* may not be sufficient to activate these well-described mechanisms. These results point to a special role for POm in driving learning-related changes in cortical response properties.

3.2.4 Target-specific potentiation of POm inputs

The increase in POm-evoked firing in both supra- and infragranular layers following 24 hrs of SAT, despite unchanged intrinsic firing properties, suggested that POm inputs to Pyr neurons might be strengthened after SAT. To isolate POm inputs and compare the amplitude of quantal excitatory postsynaptic currents (qEPSCs), we carried out voltage-clamp recordings from Pyr neurons during ChR2-activation of POm afferents in the presence of Sr^{++} to desynchronize neurotransmitter release (Biane et al., 2016). This method enables detection of EPSCs from single-vesicle release events to provide evidence for postsynaptic plasticity (Clem and Barth, 2006).

The short latency of POm-evoked spikes in L5 Pyr, both in control and SAT neurons, suggested that these L5 neurons were firing as a direct result of POm input. Thus, we hypothesized that POm inputs to L5 Pyr might be potentiated. After 24 hrs of SAT, the mean amplitude of POm-mediated qEPSCs was significantly increased

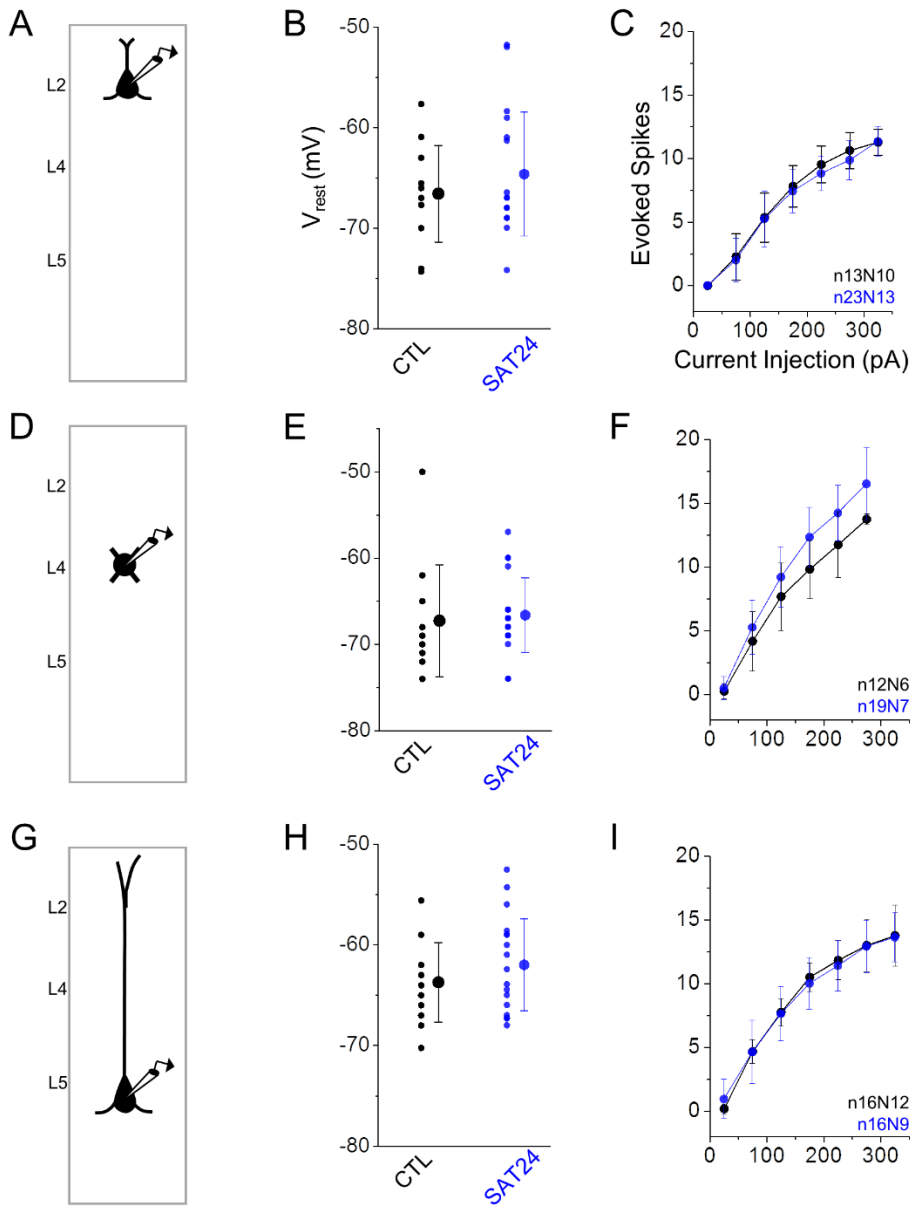

Figure 16. No change in intrinsic properties of cortical excitatory neurons after SAT. (A) Schematic of experimental setup. (B) Average resting membrane potential of L2 Pyr neurons form CTL (black) and SAT24 (blue) animals. (C) Average spike count during 500ms current injections (25pA steps) for L2 Pyr neurons from CTL (black) and SAT24 (blue) animals. (D-F) Same as (A-C) but for L4 excitatory neurons. (G-I) Same as (A-C) but for L5 Pyr neurons.

(control 15.7±0.5pA; SAT 24 20.4±1.0pA; Figure 17F-H). This difference was also observed as a rightward shift in the cumulative distribution of qEPSCs amplitudes (Figure 17H).

Although POm recipient L2 Pyr neurons also exhibited an increase in evoked firing after 24 hrs SAT, mean POm-qEPSC amplitudes were unchanged between control and SAT neurons (control 17.8±0.8pA; SAT 24 18.8±1.2pA; Figure 17B-D). Significant differences were not observed even in the cumulative distribution of qEPSCs, suggesting that this pathway is unaltered at this time point in learning (Figure 17D).

Synaptic strengthening at POm to L5 synapses may be well positioned to initiate further changes in neocortical circuitry, since these neurons show short spike latencies in response to POm stimulation and increase their POm-evoked firing after SAT (Figure 12, Figure 13). The lack of even modest potentiation at POm to L2 synapses at this time point suggests that the conditions for the induction of synaptic plasticity are different between L2 and L5 Pyr neurons, in the behaving animal.

3.2.5 Elevated POm-evoked activity is driven by ascending input from infragranular layers

SAT increases POm-evoked firing of L2 Pyr neurons both during and after the optogenetic stimulus window. If POm inputs to L2 are not potentiated after 24 hrs of SAT, we hypothesized that this increased activity may be inherited from spiking in other cortical layers. For example, POm-evoked spikes in L5 occur within 15 ms of the

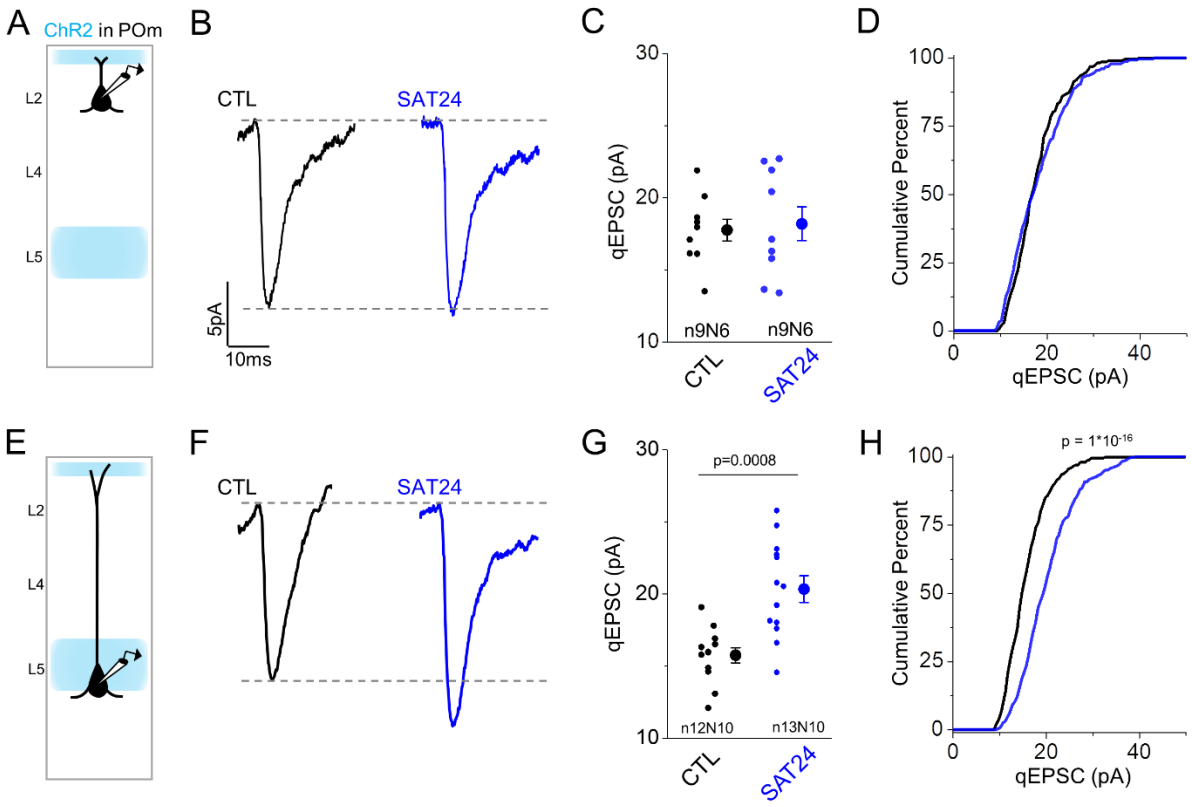

Figure 17. 24 hrs of SAT strengthens POm synaptic inputs onto L5 Pyr neurons. (A) Schematic of experimental setup in L2 Pyr neurons. (B) Global average qEPSC in control animals (black, left) or in animals that received 24 hrs of SAT (blue, right). All well-isolated light-evoked qEPSCs in a cell (≥25 for inclusion) were aligned to rise time and averaged to generate an average cellular POm qEPSC. Cell averages were aligned to rise and averaged to generate global average qEPSC for each condition. (C) Quantification of mean qEPSC amplitude for each cell, measured as the mean of individual qEPSC peak amplitudes within a cell. (D) Cumulative distribution histogram of POm qEPSC amplitudes for CTL (black) and SAT24 (blue) animals. Distributions comprise 25 randomly selected events from each cell, compared using a K-S test. (E-H) Same as (A-D) but for L5 Pyr neurons.

optogenetic pulse, and ascending input from L5 Pyr to L2 could summate with direct POm EPSPs in L2 neurons to drive firing in these neurons. Indeed, POm-evoked EPSPs in L2 Pyr neurons were often complex, where individual trials showed multiple inflection points during the EPSP rise time that correspond to asynchronous synaptic inputs (Figure 18).

Thus, we hypothesized that POm-initiated, delayed synaptic input from L5 could contribute to the polysynaptic EPSPs and spiking activity observed in L2 Pyr. To test this, we compared the POm-evoked response properties of L2 Pyr neurons, before and after mechanical separation of supra- and infragranular layers, in acute brain slices from mice trained for 24 hrs (Figure 18A-D). Neurons were paired from the same region of the same slice prior before and after transection to ensure the initial presence of POm-evoked activity. The incision through L4 should not affect light-evoked neurotransmitter release, since channelrhodopsin is believed to drive vesicle fusion through local cation entry in the synaptic terminal (Petreanu et al., 2009).

Slice transection completely abolished POm-evoked action potentials in L2 Pyr neurons (Figure 18D,G), without changing resting membrane potential (control -66.7±1.9mV; SAT 24 -69.0±1.9mV). EPSP onset latency and slope were not altered (onset latency: control 4.6 ± 0.3 ms; SAT 24 5.0±0.6 ms; slope: control 0.37±0.06; SAT 24 0.35±0.09), but EPSP peak latency was significantly shorter (control 38.3±3.8ms; SAT 24 26.9±1.5ms), consistent with the inheritance of polysynaptic input originating in infragranular layers. After slice transection, POm stimulation no longer initiated recurrent activity in L2, indicating that POm-initiated activity from infragranular layers is also important in maintaining activity in the post-stimulus window. These data indicate

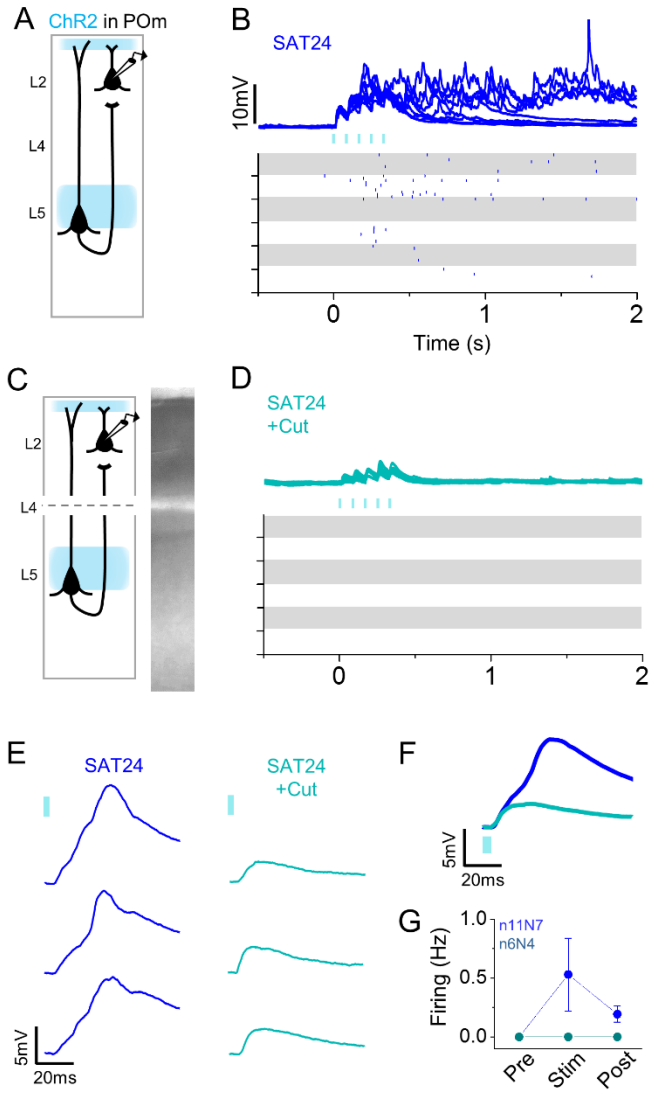

Figure 18. Elevated POm-evoked activity in trained animals is driven by ascending input from infragranular layers. (A) Schematic of experimental setup for ChR2-evoked firing of Pre-Cut L2 Pyr neurons in SAT24 animals. (B) Light-evoked activity (blue bars, 5 pulses, 5m, 80ms ISI) on 10 consecutive trials in an example L2Pyr cell (top) and for 10 example cells (bottom) in SAT24 animals. (C-D) Same as (A-B) but for L2 Pyr neurons after a mechanical incision through cortical L4. Each collected post-cut cell had at least one recorded L2 Pyr recording in the same slice prior to cut, and example cells in (B,D) were recorded in the same slice. (E) Comparison of subthreshold responses on 3 consecutive sweeps following the first light pulse for example cells in (B,D). (F) Average response (10 consecutive sweeps) to first light pulse for SAT24 (dark blue), and SAT24+Cut (light blue) example cells in (B,D). (G) Average firing frequency across all cells during the 500ms preceding VPM stimulation (Pre), during stimulation (Stim) and directly following stimulation (Post).

that the increase in POm-evoked L2 firing relies upon convergent excitation from both POm and infragranular layers.

3.2.6 Intracortical changes are not present at 24 hrs of training

The increase in L2 POm-evoked firing after 24 hrs of SAT could result solely from the increase in synaptic drive from POm to L5 that is inherited by L2 Pyr, or could occur concurrently with excitatory synaptic potentiation within L5 or at L5 inputs to L2 Pyr. We examined both pathways using Sr^{++}-replaced ACSF to isolate pathway-specific quantal EPSCs.

To examine SAT-associated changes within the L5 local excitatory circuit, we used an extracellular stimulating electrode placed in L5 and recorded quantal EPSCs in L5 Pyr neurons (Figure 19). Optogenetically-evoked intralaminar L5 qEPSCs showed no difference between control and trained animals (control 19.6±0.4pA; SAT 24 19.85±0.5pA, Figure 19A-D).

To test whether L5 to L2 qEPSCs were increased after 24 hrs SAT, we expressed ChR2 specifically in L5 neurons using the Etv1-Cre driver line for ChR2 expression. A comparison of optogenetically-evoked L5 qEPSC amplitudes in L2 Pyr neurons showed no difference between control and trained animals (control 20.1±1.1; SAT 24 19.6±1.4pA; Figure 19E-H). These results suggest that the training-induced increase in POm-initiated spiking activity in L2 Pyr cannot be attributed to synaptic strengthening of intralaminar L5-L5 or translaminar L5 to L2 excitatory inputs, and that

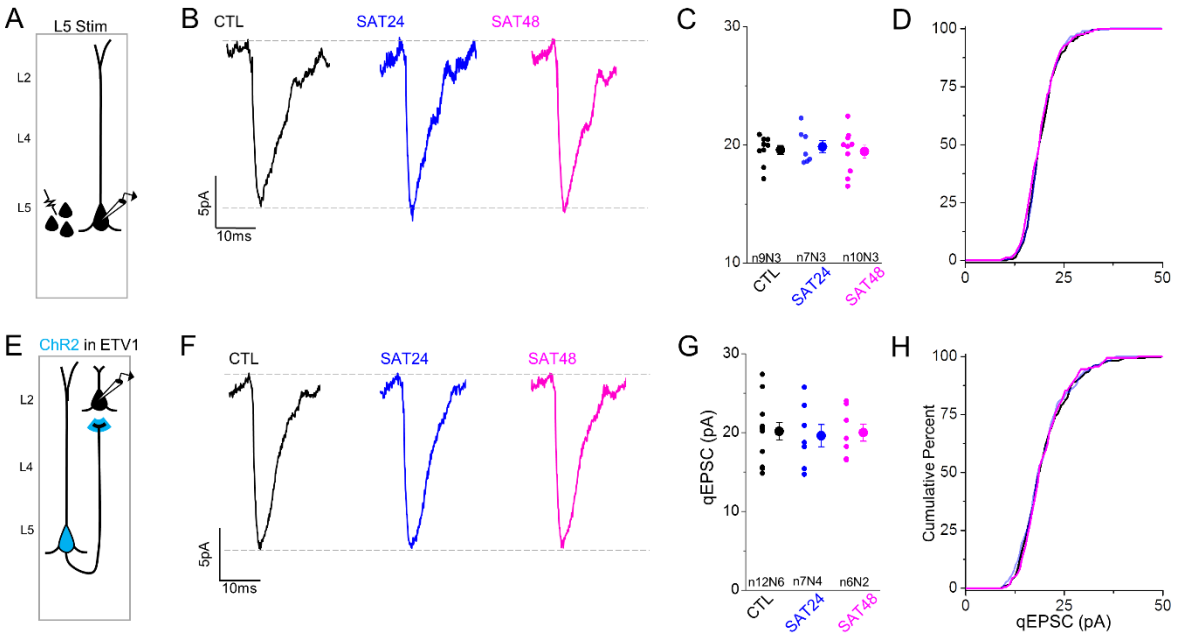

Figure 19. Average quantal amplitude of L5-L5 excitatory connections is unchanged following SAT. (A) Schematic of experimental setup for assessing L5-L5 connection strength using local placement of an electrical stimulation electrode. (B) Global average qEPSC in CTL (black, left), SAT24 (blue, middle), or SAT48 (magenta, right) animals. All well-isolated light-evoked qEPSCs in a cell (≥25 for inclusion) were aligned to rise time and averaged to generate an average cellular qEPSC. Cell averages were aligned to rise and averaged to generate global average qEPSC for each condition. (C) Quantification of mean qEPSC amplitude for each cell, measured as the mean of individual qEPSC peak amplitudes within a cell. (D) Cumulative distribution histogram of qEPSC amplitudes for CTL (black), SAT24 (blue), and SAT48 (magenta) animals. Distributions comprise 25 randomly selected events from each cell, compared using a K-S test. (E-H) Same as (A-D) but for L5 to L2 connections using transgenic expression of ChR2 in L5 under the control of the ETV1 promotor.

this activity is driven by increased L5 Pyr firing associated with potentiation of POm to L5 excitatory inputs.

3.2.7 Sensory stimulation alone does not drive POm plasticity

To determine whether POm to L5 synaptic changes were linked to learning, or more generally to stimulus exposure during the training period, we created a pseudotraining paradigm with identical trial and stimulus structure but with altered reward contingency such that the whisker stimulus no longer predicted reward (Figure 20A). Similarly to SAT, we observed a transient dip in anticipatory lick rates following stimulation presentation early in training that rapidly recovered, indicating that the animals perceived the stimulus and rapidly habituated to it.

After 24 hrs of pseudotraining, animals displayed no difference in anticipatory licking behavior between stimulus trials and non-stimulus trials, as both trial types had a 50% chance of water delivery (Figure 20B,C). Importantly, the number of airpuff-exposed trials for pseudotrained animals was greater than the mean trial number for SAT animals (Figure 20C). We attributed this increase to the fact that water was only provided on 50% of trials, versus 80% of trials during SAT, requiring greater trial numbers to achieve the same volume of water delivery.

To determine if synaptic strengthening of POm inputs in L5 Pyr neurons was specific to sensory learning or was a more general response to passive sensory stimulation, POm qEPSC input strength was recorded in pseudotrained animals. After 24 hrs, mean POm synaptic strength onto L5 neurons was unchanged from control

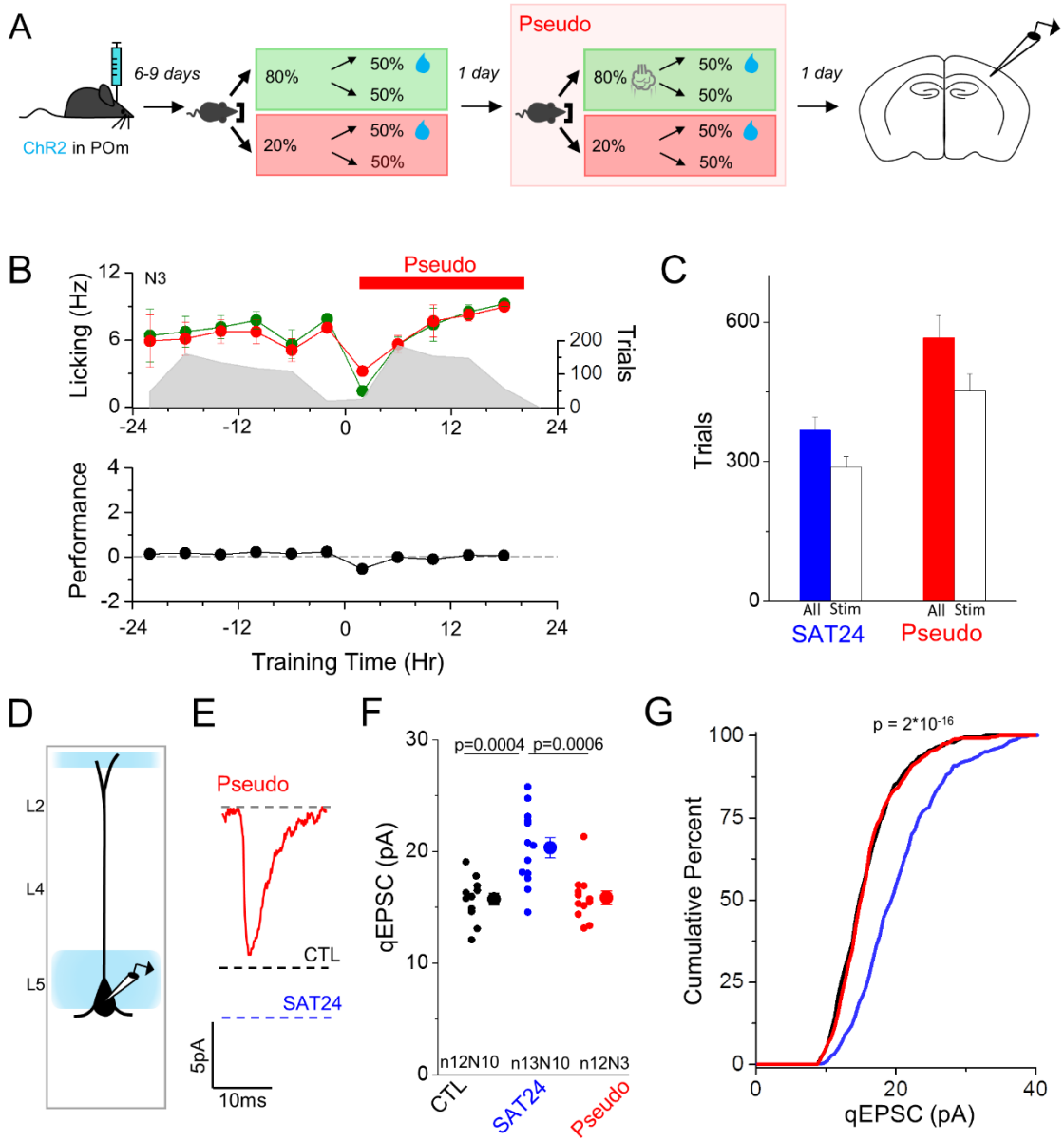

Figure 20. Sensory stimulation alone does not drive POm plasticity. (A) Schematic of experimental setup and pseudo-training behavioral paradigm. Cages, training structure, stimulus, and timing were identical to SAT but water delivery (US) was uncoupled from (CS) and randomly delivered on 50% of trials regardless of CS presentation. (B) Time course of anticipatory lick rates (left axis, 300ms prior to water delivery, 4 hr bins) over the course of training for blank (20%, red) and stim trials (80%, green) averaged across all animals. Trial initiation counts (right axis) are shown in grey for the same time bins, red bar denotes pseudo-training period. (C) Comparison of animal-initiated trial counts during 24 hrs of SAT (blue) and Pseudotrained (red). Solid bars indicate total trials received while white bars show the number of stimulus (CS) trials received. (D) Schematic of experimental setup. (E) Global average qEPSC in Pseudotrained animals. All well-isolated light-evoked qEPSCs in a cell (≥25) were aligned to rise time and averaged to generate an average cellular POm qEPSC. Cell averages

values and significantly smaller than POm qEPSCs in animals that had undergone SAT (control 15.8±0.53; pseudotrained 15.8±0.59pA; Figure 20E-H). These results indicate that sensory stimulation decoupled from reward is not sufficient to drive POm thalamocortical plasticity at L5 Pyr neurons.

3.2.8 Pathway-specific changes in L2 Pyr neurons after SAT

The absence of plasticity at POm inputs to L2 Pyr neurons after 24 hrs SAT might suggest that the conditions required for synaptic potentiation have not yet been met, or it could mean that L2 neurons do not possess the machinery for learning-dependent synaptic plasticity. To test whether longer periods of SAT might be sufficient to change POm input strength in L2 Pyr neurons, we examined ChR2-evoked POm-mediated qESPC amplitudes at a later time point. After 48 hrs of SAT, task performance was further enhanced, driven primarily by an increase in stimulus-associated licking and not a depression of licking in blank trials (Figure 21B,C).

After 48 hrs SAT, qEPSC amplitude of POm to L2 Pyr neurons was significantly increased (control 17.8+0.77; SAT 48 22.0+0.49pA; Figure 21D-G). The increase in POm input to L2 Pyr was not matched by a further enhancement of POm input strength onto L5 Pyr (Figure 21H-K). Taken together, these data indicate that the absence of POm thalamocortical plasticity in L2 Pyr at 24 hrs SAT is not dependent on postsynaptic cell identity but rather training duration, and that 48 hrs of training is sufficient to increase POm input strength onto L2 Pyr neurons.

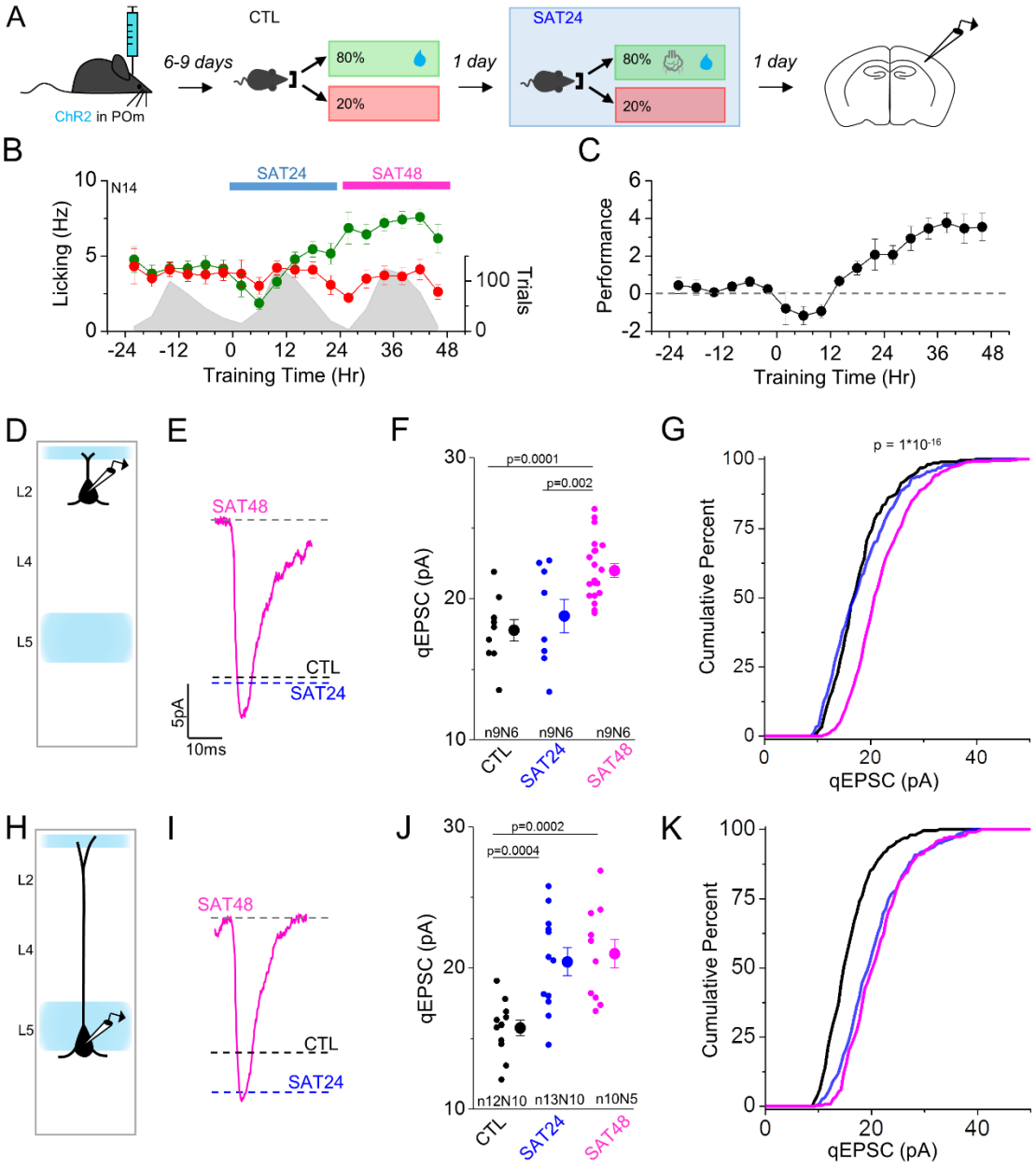

Figure 21. SAT drives sequential thalamocortical plasticity in L5 then L2 Pyramidal neurons. (A) Schematic of experiment with recordings performed in ChR2-injected mice after 24 hrs of acclimation and 48 hrs of SAT. (B) Time course of anticipatory lick frequency (left axis, 300ms prior to water delivery, 4 hr bins) over the course of acclimation and training for blank (red) and stim/water trials (green) averaged across all animals. Trial initiation counts (right axis) are shown in grey for the same time bins. (C) Quantification of performance defined as the difference in anticipatory lick rates between stim/water trials and blank trials during learning for the 4 hour bins shown in (B). (D) Schematic of experimental setup for recording POm qEPSCs

in L2 Pyr neurons. (E) Global average qEPSC in SAT48 animals. All well-isolated light-evoked qEPSCs in a cell (≥25) were aligned to rise time and averaged to generate an average cellular POm qEPSC. Cell averages were aligned to rise and averaged to generate global average qEPSC. Global average POm qEPSC amplitudes in control (black) and SAT24 (blue) animals for comparison (F) Quantification of average qEPSC amplitude for each cell, measured as the average of individual qEPSC peak amplitudes within a cell for control (black), SAT24 (blue), and SAT48 (magenta) animals. (G) Cumulative distribution histogram of POm qEPSC amplitudes for CTL (black) and SAT24 (blue) animals and SAT48 animals (magenta). Distributions comprise 25 randomly selected events from each cell, K-S test compares Pseudo and 24 hrs. (H-K) Same as D-G but for L5 Pyr neurons.

Synaptic plasticity between L2 Pyr neurons in barrel cortex has been well-documented, both in acute brain slices and after *in vivo* sensory experience (Albieri et al., 2015; Cheetham et al., 2008; Rodríguez-Moreno and Paulsen, 2008; Wen and Barth, 2011); however, rewiring of this local network has not been linked to sensory learning. To determine whether POm thalamocortical plasticity during SAT occured concurrent with changes in the L2 excitatory network, we examined changes in qEPSC amplitudes measured from local afferent stimulation, using an extracellular electrode placed in L2.

After 24 hrs of SAT, mean qEPSC amplitudes under these conditions were indistinguishable from control values (control 19.5+0.64; SAT 24 19.7+0.63pA; Figure 22A-D). Indeed, cumulative distribution histograms showed that EPSC values were completely overlapping (Figure 22). Thus, despite the increase in POm-evoked firing in L2, potentiation of intralaminar inputs cannot be detected during the initial stages of SAT.

Are longer periods of SAT sufficient to drive changes in local L2 Pyr neuron connection strength? We used the same assay to examine local input strength after 48 hrs of SAT. At this stage, qEPSC amplitudes were significantly increased in L2 Pyr neurons from both control and 24 hr values (SAT 48 21.7+0.28pA; Figure 22).

We also examined whether L5 to L2 or L5 to L5 qEPSC input strength might also increase after 48 hrs of SAT, since this pathway is important for the intralaminar transfer of excitation. This was not the case (Figure 22A-H). Thus, although L2 Pyr neurons are

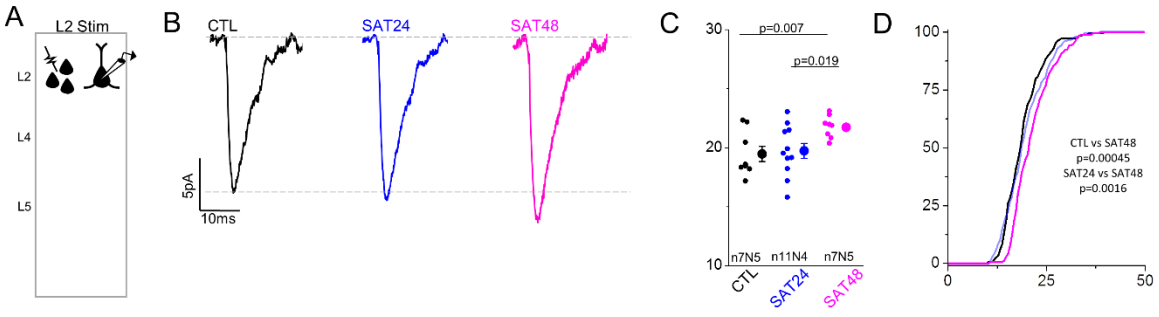

Figure 22. Average quantal amplitude of L2 intralaminar connections following SAT. (A) Schematic of experimental setup for assessing L2 to L2 connection strength using local placement of an electrical stimulation electrode. (B) Global average qEPSC in CTL (black, left), SAT24 (blue, middle), or SAT48 (magenta, right) animals. All well-isolated light-evoked qEPSCs in a cell (≥25 for inclusion) were aligned to rise time and averaged to generate an average cellular qEPSC. Cell averages were aligned to rise and averaged to generate global average qEPSC for each condition. (C) Quantification of mean qEPSC amplitude for each cell, measured as the mean of individual qEPSC peak amplitudes within a cell. (D) Cumulative distribution histogram of qEPSC amplitudes for CTL (black), SAT24 (blue), and SAT48 (magenta) animals. Distributions comprise 25 randomly selected events from each cell, compared using a K-S test. Control vs 48 hr p=0.00045, 24 hr vs 48 hr p=0.0016.

more responsive to POm-stimulation after 24 hrs SAT and excitatory activity from infragranular layers is important to drive POm-evoked spiking in L2, these synaptic inputs do not readily show evidence of postsynaptic plasticity, even after 2 days of training. Overall, these data show that SAT-initiated increases in L2 excitatory strength are delayed with respect to L5, and that L2 synaptic potentiation can be pathway-specific, occurring at thalamocortical and intralaminar but not at L5 to L2 excitatory synapses after 48 hrs of SAT.

3.3 Discussion

We aimed to develop a comprehensive account of how a learned sensory-association task alters synaptic function in neocortical circuits, with isolation of specific input pathways and targeted recordings from specific cell types across different layers of the cortex. High-throughput, home-cage sensory-association learning revealed that thalamocortical synapses are the site of the earliest change in primary somatosensory cortex, with selectivity for POm but not VPM-related pathways. Synaptic potentiation at POm inputs onto L5 Pyr neurons was then followed by POm input potentiation to L2 Pyr neurons and within the L2 excitatory circuit over subsequent days of training. Importantly, changes were not observed with pseudo-conditioning, indicating that they were not driven by repeated exposure to the sensory stimulus. These data show that sensory association training drives sequential changes in excitatory synaptic strength in an input- and layer specific manner, and lay a foundation for understanding how learning alters that flow of information across the cortical column.

Thalamocortical plasticity during learning

Thalamocortical connections, particularly from VPM to L4, have been considered the major source of cortical input to somatosensory cortex, although there is an increasing awareness that POm inputs also provide significant drive (Audette et al., 2017; Gambino et al., 2014; Jouhanneau et al., 2014; Mease et al., 2016). Abundant experimental evidence supports the notion that after a short window early in development VPM inputs are resistant to experience-dependent alterations (Feldman and Brecht, 2005). However, prior studies have largely ignored the potential role of POm in neocortical response plasticity. We used pathway-specific activation of VPM and POm thalamic inputs and targeted recordings in the cortex as a screen for learning-related changes across the cortical column. We observed remarkable stability in VPM-evoked cortical firing after early sensory association training in thalamorecipient L4 and L5, as well as in the downstream target L2/3. In contrast, POm-evoked firing was dramatically increased. Although we cannot rule out target-specific changes in VPM input strength – for example, opposite changes in VPM drive to excitatory and inhibitory neurons that result in no net change in firing output – our assay clearly revealed an increase in response output in POm-recipient layers. POm thalamocortical synaptic plasticity may contribute to the rapid change in stimulus-evoked activity observed in L5 Pyr neurons following sensory experience (Diamond et al., 1994; Jacob et al., 2012; Ward et al., 2012).

What might explain the difference in plasticity between VPM and POm pathways? L4 neurons may be particularly resistant to post-critical period plasticity (Crair and Malenka, 1995; Fox, 1992), but we did not observe enhanced firing

elsewhere in the VPM pathway, for Pyr neurons in L2/3 and L5. Also, because L5 Pyr neurons are post-synaptic targets of both VPM and POm, it is difficult to attribute the lack of change in VPM-evoked activity solely to identity of the postsynaptic cell. Differences in plasticity induction could be attributed to the pattern or duration of sensory-evoked activity in VPM and POm during sensory stimulation in our task. For example, sensory-evoked responses are enhanced in both VPM and POm during alert states, but POm responses may be more significantly increased (Sobolewski et al., 2015). Because POm is more strongly influenced by descending cortical drive than VPM, it is possible that recurrent corticothalamic circuitry may prime POm circuits for learning-dependent plasticity. Finally, our assay revealed differences between VPM and POm-evoked intracortical dynamics. Optogenetic activation of VPM inputs never evoked recurrent activity in any cortical layers, whereas POm activation frequently did. This recurrent activity may be permissive to plasticity induction that is specific to POm-recipient circuitry. Future experiments will differentiate the relative contribution of thalamic and cortical activity for plasticity in primary sensory cortex.

The capacity for learning-induced strengthening of thalamic inputs, while unexpected in the sensory cortex, has been previously described in the M1 (Biane et al., 2016). Our results suggest that the properties of first-order sensory thalamic nuclei may not generalize to other thalamocortical circuits in the brain (Acsády, 2017). Therefore, it is possible that rapid learning-related thalamic input plasticity may be an important feature of analogous higher-order sensory thalamic nuclei, such as the pulvinar (Arcaro et al., 2015; Purushothaman et al., 2012; Roth et al., 2016).

<u>Sequence for cortical rewiring during sensory learning</u>

Behavioral evidence for learning emerged early during SAT and performance increased with longer training periods. The slow trajectory of learning provided a good platform to evaluate progressive synaptic changes in the neocortex. Increased POm-evoked firing in both deep and superficial layers occurred at the same time as synaptic strengthening of POm inputs to L5 Pyr neurons, after only 24 hrs of training. Because POm-evoked spikes in L5 Pyr occurred at short latencies after stimulation and intrinsic membrane properties of these neurons were not changed after 24 hrs of SAT, we conclude that synaptic strengthening at POm inputs to L5 Pyr drove the increase in spiking. Although L2 Pyr neurons also showed an increase in POm-evoked firing after 24 hrs of SAT, we did not observe synaptic changes at thalamic or intracortical inputs to L2 at this time point and slice transection data indicate that this increased drive was indirect, arising from ascending input from infragranular layers. However, 48 hrs of SAT was sufficient to drive both POm to L2 Pyr synaptic strengthening as well as intralaminar plasticity in local L2 excitatory circuits.

Why was synaptic plasticity in L2 delayed relative to POm plasticity in L5? One possibility is that activity levels in superficial layers of the sensory cortex, which are notoriously sparse (Barth and Poulet, 2012), are too low initially to engage activity dependent plasticity mechanisms. It is therefore notable that the increase in POm-evoked activity in L2 is evident prior to any observable change in synaptic strength in these neurons. It is tempting to speculate that early synaptic strengthening in the more robustly active L5 could play a role in enhancing stimulus-evoked activity in L2 and thus enable activity-dependent synaptic plasticity in these neurons. Our results identify POm thalamic inputs to L5 as the cortical ‘first responder’ for training-evoked cortical

plasticity. It will be of great interest to identify the dependent processes that underlie the sequential pattern of cortical changes revealed in this study.

Notably, we did not find evidence for synaptic potentiation at translaminar L5 to L2 synapses, nor within the L5 excitatory circuit, despite well-documented anatomical pathways and prior experimental evidence that these connections can be plastic under some circumstances (Sjöström and Häusser, 2006). Our assays may have been too coarse to detect subtle changes between specific subtypes of L5 Pyr neurons, or opposing changes within the same pathway. Our recordings also did not evaluate learning-dependent changes in inhibitory synapses (Chen et al., 2015c; Kaplan et al., 2016), which will be an important direction of future investigations. In addition, longer periods of training may reveal additional sites of delayed learning-dependent changes. Nonetheless, our data suggest that associating a salient sensory stimulus with reward drives a stereotyped sequence of synaptic changes that cascade across the cortical column and may contribute to altered neural response properties.

Learning-related changes in neocortical circuits

POm-related synaptic changes, despite proceeding at the same timescale as behavioral learning, could have been generated by repeated sensory stimulation rather than learning. We examined this possibility using a pseudotraining procedure that provided the same or even a greater number of airpuff stimuli to animals, decoupled from a water reward. Although the airpuff stimulus is likely to be particularly salient and thus a good activator of POm circuits (Jouhanneau et al., 2014; Sosnik et al., 2001), it is notable that pseudoconditioning did not generate any change in POm input strength in

L5 Pyr. These findings indicate that synaptic plasticity in primary sensory cortex is strongly influenced by contingent reward, not just stimulus exposure.

Do cortical synaptic changes relate to sensory perception and task performance? POm input strength and task performance were modestly correlated (data not shown), a finding that cannot attribute the direction of potential causality. We did not directly address whether perceptual learning (improvement in stimulus detection, often at lower thresholds) occurred in our assay, although it is likely to have occurred. Association learning (connecting a percept to an action or another percept) is thought to be discrete from perceptual learning, but it has been difficult to separate these two types of learning, both behaviorally and with regard to specific neural circuits (Makino et al., 2016; Mcgann, 2015).

Wide-ranging approaches suggest varied, and often contradictory, locations and mechanisms underlying perceptual and associative learning, but perceptual learning has been more closely linked to changes in primary sensory cortex (Caras and Sanes, 2017; Makino et al., 2016; Mcgann, 2015). POm and analogous higher-order thalamic nuclei interface between primary sensory cortex, association cortex, M1, and the striatum, making them well-positioned to integrate and transmit diverse information that may be important both for learning and initiation of cortical plasticity. It will be of great interest to determine how different types of learning, with different task requirements and sensory stimuli, engage and alter specific neocortical circuits.

<u>High-throughput, home-cage behavioral training</u>

Analysis of learning-dependent reorganization of excitatory circuits across the cortical column with layer- and input-specific resolution was facilitated by a high-throughput home-cage training system, optimized for training large numbers of animals with minimal handling. We designed and implemented a home-cage training device that couples a whisker stimulus to the mouse drinking source, suitable for freely-moving animals. Training occurred during the animal's normal active period and did not involve animal handling, a significant source of stress that may impair learning (Francis and Kanold, 2017). Sensory association training using a gentle airpuff stimulus drove progressive changes in behavior that occurred quickly enough to enable detailed electrophysiological investigation, but were slow enough to capture sequential changes in synaptic function as they occurred across the cortical column (Poddar et al., 2013).

The training setup we developed was easily adapted to alter the contingency between water reward and conditioned stimulus for pseudotraining, and could be further modified to alter other task parameters such as reward valence, frequency, or sensory stimuli delivered. We anticipate that home-cage training paradigms will be particularly useful for integrating cutting-edge recording, imaging, and stimulating technologies in freely-moving animals. The application of automated and home-cage training will be critical for connecting experience-induced patterns of neuronal activity in cortical circuits with defined behaviors across many subjects.

Conclusion

Our analysis of synaptic changes reveals the footprints of plasticity that are induced during an associative learning task that might be difficult to isolate during dynamic recording of neural activity. Importantly, our study did not address how SAT

activates thalamic and neocortical neurons *in vivo*, nor how it alters their response properties after training. Future experiments with fine-scale cell-type and temporal resolution will illuminate how activity in VPM, POm, and specific layers of the neocortex are engaged by and changed during learning.

The progressive emergence of POm- plasticity at infragranular synapses, followed by POm input potentiation at L2 Pyr neurons and an increase in intralaminar L2-L2 excitatory synaptic strength suggests that supragranular layers may have a higher threshold but a large capacity for experience-dependent plasticity. These findings will be essential to develop and test data-constrained models of synaptic change and neural spiking.

3.4 Materials and Methods

Animals

All experimental procedures were conducted in accordance with the NIH guidelines and were approved by the Institutional Animal Care and Use Committee at Carnegie Mellon University.

Experiments targeting excitatory neurons were performed on C57Bl6 mice (Harlan). In a small subset of experiments, ChR2 expression was driven transgenically by crossing Nelf1Cre (Gong et al., 2007)(MMRC Stock No: 037424-UCD) animals or ETV1creER (Gong et al., 2007; Taniguchi et al., 2011) (Jackson Laboratory Stock No: 013048) animals with Ai32 (Jackson Laboratory Stock No. 024109, ChR2(H134R)EYFP) animals to generate offspring that express ChR2 specifically in VPM and L5Pyr neurons

respectively. ETV1Cre expression was initiated by injection of 2mg tamoxifen (100uL of 20mg/ml, Tocris Cat No 6342, https://www.jax.org/research-and-faculty/tools/cre-repository/tamoxifen) 8-12 days before behavioral training. Experiments were performed on animals of both sexes. Animals were stereotaxically injected between postnatal day 12-18 (P12-18), began training at P19-28, and were sacrificed for recording at P20-P30.

Viral Injections

ChR2 tagged with m-cherry or YFP (300-500 nl; AAV1.CAG.hChR2(H134R)-mCherry.WPRE.SV40, Catalog No. 100054-AAV1, Addgene, Cambridge, MA; AAV2-hSyn-hChR2(H134R)-EYFP, Deisseroth Lab, UNC Vector Core, Chapel Hill, NC) was stereotaxically injected into the VPM or POm thalamic nucleus following a small craniotomy (VPM: bregma -1.3, lateral 1.8, depth 3.4, POm: bregma -1.7, lateral 1.00, depth 3.25 mm) of isoflurane-anaesthetized mice using a Hamilton syringe (Hamilton; Reno, NV), Stoelting infusion pump (Stoelting; Wood Dale, IL, Model #53210), and custom injection cannulas (Plastics One; Phoenix, AZ). Mice were treated once with ketoprofen after injection (5 mg/kg, Sigma-Aldrich; St. Louis, MO) and additional doses were administered as necessary. Mice recovered in their home cage for 7-13 days prior to sensory association training (SAT).

Automated home-cage sensory association training

Animals were singly housed in a 7x12 cm standard mouse cage outfitted with a custom-designed chamber with an infrared beam-break in front of a recessed lickport with a capacitor to detect individual lick events. Animals were maintained on a 12 hour light-dark schedule, with lights on at 7 am. The lickport was the sole source of water in the

cage, and animals were not otherwise water restricted. Food was provided ad libitum. Animals were typically introduced to the training cage at noon and allowed one day to acclimate to the cage. They readily learned to drink at the lickport without intervention or shaping, where ~1-3 mls of water were dispensed each day. Water was provided on 80% of the beambreak-initiated trials, without any predictive cue on the acclimation day. At noon on the second day, a small nozzle for air delivery (inner diameter 1/16 in) was inserted into the ceiling of the chamber ~ 4 cm above the average location of the right vibrissa during drinking. Mouse position for the airpuff was not stereotyped, and the number and amplitude of whisker movements evoked were not monitored.

We elected to use a gentle airpuff as the stimulus in our sensory association task for several reasons. First, airpuff stimuli can target multiple whiskers without whisker contact, well-suited for automated home-cage-training. Second, animals can be directly introduced to the training cage without whisker trimming or whisker prostheses that can be difficult to maintain over long training periods. Third, because multiple whiskers can be stimulated in a single trial, the cortical region for analysis encompasses a wide area of S1, facilitating fine-scale analysis in acute brain slices (in comparison to single-whisker stimulation paradigms).

For all trials, including during acclimation, IR beam break triggered a variable delay (200-800ms) before trial initiation, after which the nozzle delivered a short (500 ms) pulse of compressed air at 6 psi (measured by a gas regulator). Water was delivered 500 ms after the airpuff offset (1s after trial start), and approximately 50 ul of water was dispensed for each trial. Airpuffs and water were delivered as described for

80% of the beambreak-initiated trials (a random number between 0 and 100 was generated and if it was less than 80, water was delivered). The remaining 20% of trials had no airpuff and no water delivery but otherwise had identical trial structure and incidental auditory cues, including variable pre-trial delay. After trial initiation, a new trial could not be triggered until 1s after water delivery, and additional IR beam breaks during the trial were ignored. In a subset of experiments, mice received a pseudo-training paradigm which was identical to the previously described trial structure except that water was delivered on 50% of trials randomly determined irrespective of stimulus delivery. All animals performed either ≤ 25 or ≥ 150 trials, so a small minority of animals that failed to perform 25 trials was excluded from analysis.

Data was analyzed in Matlab and excel using custom scripts that align measured licks to individual trials and measure the delay from trial start for each lick. PSTHs of lick behavior were generated relative to trial start (following the initial delay) so that changes in licking behavior could be aligned to CS and US delivery. To quantitate learning-related behavioral changes, lick rates were compared between water or stimulus trials to lick rates for no-water “blank” trials (100ms bins) on Day 0 and in the last 8 hrs of training day 1 or 2. We differentiated between consummatory licking (required for water consumption) and anticipatory licking prior to water delivery (evidence that an association between the sensory stimulus and the prediction of a future water “reward”) (Cohen et al., 2012). Anticipatory lick events (300ms preceding water delivery, 700-1000ms after t=0) were measured throughout training in 4 hour bins for water delivery trials and for blank trials. Performance was defined as the difference between lick rate for stimulus and blank trials, which was measured and plotted in 4 hour time bins.

Regression of electrophysiology and behavior utilized each animal's performance quantified for the last 20% of trials performed. All measurements of behavior were calculated for individual animals and then combined to generate aggregate values.

Slice Preparation and Injection Site Confirmation

Injected mice were sacrificed by brief isoflurane anesthesia and decapitation between 11am and 3pm. 350 um thick off-coronal slices (One cut, 45° rostro-lateral and 25° rostro-dorsal) designed to preserve columnar connections in the somatosensory cortex were prepared in ice-cold artificial cerebrospinal fluid (ACSF) composed of (in mM): 119 NaCl, 3.5 KCl, 1 NaH2PO4, 26.2 NaHCO3, 11 glucose, 1.3 MgSO4, and 2.5 CaCl2 equilibrated with 95%/5% O2/CO2. Slices were allowed to recover at room temperature for 45 minutes in the dark before recording. The injection site was confirmed anatomically using the mCherry-tagged ChR2 fluorescence in cell bodies at the injection site and the characteristic pattern of fluorescent axonal labeling in the barrel cortex, concentrated in L4 and L6 for VPM and L1 and L5a for POm (Meyer et al., 2010b). Slices that had fluorescently labeled axons outside of the target layers were discarded. Retrogradely-labeled, ChR2+ neurons were not observed in the somatosensory cortex.

Although ChR2 expression levels could differ between animals, experiments were repeated across many animals, mice were assigned to experimental groups without expression information, and all controllable experimental variables were kept consistent. Additionally, fluorescent ChR2 labeling in the cortex was monitored. A consistent minimum expression threshold for inclusion was applied, and no difference was observed in the mean or range of fluorescent intensity between control and trained animals.

General Electrophysiology

Cortical excitatory neurons were targeted for whole-cell recording in the posteromedial barrel subfield using an Olympus light microscope (BX51WI) using borosilicate glass electrodes resistance 4-8 MΩ. Electrode internal solution for evoked activity experiments, was composed of (in mM): 125 potassium gluconate, 10 HEPES, 2 KCl, 0.5 EGTA, 4 Mg-ATP, and 0.3 Na-GTP, pH 7.25-7.30, 280 mOsm. Internal solution for quantal EPSC experiments was composed of (in mM) 130 cesium gluconate, 10 HEPES, 0.5 EGTA, 8 NaCl, 10 Tetraethylammonium chloride (TEA-Cl), 4 Mg-ATP and 0.4 Na-GTP, pH 7.25-7.30, 280-290 mOsm and typically contained QX-314 (5mM, lidocaine N-ethyl bromide, Tocris). For some cells trace amounts of AlexaFluor 594 were added to the internal solution to confirm cell targeting.

Electrophysiological data were acquired using a Multiclamp 700A amplifier (Axon Instruments, Foster City, CA) and a National Instruments acquisition interface (National Instruments; Austin, TX). Data were filtered at 3 kHz, digitized at 10 kHz and collected by Igor Pro 6.0 (Wavemetrics, Lake Oswego, Oregon). Cells were allowed to recover from break-in for 5 minutes before data collection. Presumptive excitatory neurons were targeted for whole-cell or juxtacellular recording based on Pyr soma morphology (or stellate nature morphology in L4), intermediate Ri, (354 ± 23 MΩ), and regular-spiking phenotypes in response to current injections. Rs and Ri were monitored for the duration of experiments and cells with Ri below 100 MΩ, Rs greater than 40 MΩ, or where Rs changed by more than 30% over the course of data collection were excluded from further analysis.

Following recording, cells were imaged to determine their laminar location based on depth from pial surface and relevant cytoarchitectural features. L2 neurons were defined as neurons up to 100 um below the cell-sparse area of L1, typically 50-150 um below the pial surface. L4 neurons are defined as inside the upper and lower limit of the L4 barrel, but were selected from both “barrel” and “septal” regions, since segregated barrel and septal circuits in mouse L4 are unclear (Feldmeyer et al., 2013). L5a neurons, referred to as “L5” for brevity, were recorded from the area up to 150um below L4 barrels.

Evoked cortical activity

ChR2-expressing thalamic axons were stimulated by delivering trains of light pulses (5 pulses, 80ms ISI, 0.05Hz inter-trial interval) through a 40x water-immersion objective (Olympus) at the recording site using a white LED (Prizmatix, Israel) in combination with an excitation filter (40nm bandwith centered at 480nm; Chroma; Bellows Falls, VT). Max light intensity at 470 nm was measured at 2.13 mW distributed over a beam area ~1 mm diameter, and the timing of optogenetic stimulation was controlled by a Master-8 (A.M.P.I; Jerusalem, Israel). Responses in excitatory cortical neurons were measured in either the whole cell or juxtacellular configuration in a modified ACSF solution identical to cutting solution but with (in Mm) 2.5cvKCl, 0.5 MgSO4, and 1 CaCl2 (Audette et al., 2017).

Spike data from at least 10 consecutive trials for each cell was binned at 10ms intervals and averaged across all cells of a given population to generate an average PSTH. The average firing rate was calculated for 500ms pre-stim, during stim, and post-stim. A cell was included in the fraction of spiking cells if any action potential(s) was

observed in the stimulus or post-stimulus window. Evoked activity experiments were performed for control animals, which had undergone at least one day of cage acclimation but received no sensory stimuli, and for animals that had undergone 24 hrs of sensory association training.

In a subset of experiments, POm- evoked activity in L2 pyramidal neurons was recorded from SAT 24 animals before and after making an incision through L4. Incisions of 1-2mm were manually performed with a custom knife. For each post-incision L2 cell to be included in analysis, an adjacent pre-cut cell was recorded to insure that the slice had sufficient ChR2 expression to drive cortical activity. Evoked activity was measured as previously describe. To insure that our incision did not fundamentally alter the direct POm input onto L2 Pyr neurons, the onset latency and slope of the earliest identifiable POm-evoked EPSP were measured. The slope of the initial rise was defined as the maximum slope before a second inflection point.

Input-specific quantal EPSC measurements

Quantal amplitude measurements were performed in the standard ACSF solution used during cutting but containing $SrCl_2$ instead of $CaCl_2$ and in the presence of the NMDA receptor antagonist AP5 (50uM, Tocris Catalog No. 0106, Minneapolis, MN). Well-isolated individual quantal EPSCs were recorded at -70mV following input-specific optical stimulation (1 pulse, 5ms, variable intensity) of ChR2-expressing axons (Biane et al., 2016; Wen and Barth, 2011). Quantal events were manually selected but blind to cell identity based on their short rise time, isolated baselines, and absence of multiple inflection points indicative of a compound event. Events occurring between 50 and 500ms following stimulation (minimum of 25 per cell) were analyzed using Minianalysis

software (Synaptosoft, Decatur, GA) aligned to rise, and averaged to generate an average qEPSC trace for each cell. The average qEPSC trace for each cell in an experimental group was then aligned to rise to generate a global qEPSC amplitude. The amplitude of each event was averaged to determine a cell's average qEPSC amplitude and cumulative distribution histograms were generated from a pool of qEPSCs containing 25 randomly selected events from each cell in an experimental group. Since the amplitude of quantal events can be influenced by Rs, only cells below 25 MΩ were included. Experiments in ETV1Cre mice were performed in the presence of the GABAa receptor antagonist Picrotoxon (50uM, Tocris, Cat. No. 1128) due to a small number of inhibitory neurons in the ETV1-Cre expressing population (Lu et al., 2017). L2-L2 and L5-L5 connections were stimulated using a concentric bipolar stimulating electrode (FHC Catalog No. CBCRC75, Bowdoin, ME) placed in L2 or L5 100-400 uM away from the recorded neuron. For qEPSC experiments, light or electrical stimulus intensity was low and calibrated individually for each cell to evoke an initial multiquantal EPSC between 50 and 150pA.

Quantification and Statistical Analysis

Unless specifically noted in figure legend, calculations and statistics were performed on cells and all statistical tests are non-parametric Mann-Whitney (unpaired) or Wilcoxon (paired) rank sum tests, and significance values are reported in figure or when references in results. All average values are mean ± SEM unless indicated. Cell (n) and animal values (N) are reported in each figure. Animals were randomly assigned to experimental group, and quantal amplitude experiments were analyzed blind to cell identity.

4 Final Discussion

4.1 Summary

Our results identify a translaminar cortical circuit in the mouse somatosensory system that is driven by direct input from the higher order thalamic nucleus POm and undergoes rapid synaptic plasticity in a learning-dependent manner. We used ChR2-medited optogenetic activation to stimulate pathway-specific thalamic inputs to the cortex in acute brain slices of naïve animals and animals that had undergone whisker-mediated association learning. Cortical responses were measured in a layer- and cell type-specific manner using targeted whole-cell patch clamp recording in a variety of recording conditions to measure specific properties of POm-mediated cortical activity. We found that POm thalamic inputs make monosynaptic connections to cortical neurons in layer-specific manner, generating different modes of processing in deep and superficial layers. In L5, POm provided direct monosynaptic input to Pyr neurons, which could drive precisely-timed short latency-action potentials in some neurons even in the absence of other inputs. These action potentials were aligned by fast, feedforward inhibition mediated by PV-expressing inhibitory neurons, a similar mode of processing that occurs for primary thalamic inputs to L4. In superficial layers, Pyr neurons did not receive fast feedforward inhibition and smaller direct EPSPs driven by POm could summate over multiple stimulations. In both layers, tonic firing of SST inhibitory neurons was silenced by POm activation, presumably by 5HT-expressing inhibitory neurons, a subset of which were driven by POm. POm also drove prolonged recurrent network activity, which required connections between L5 and L2, revealing a previously unappreciated functional connection between these layers. These results established

that activity levels in the translaminar circuit between L2 and L5 can be driven by the higher order thalamic nucleus POm.

A critical feature of these neurons is their propensity for rapid changes in activity level during salient sensory experience. Our initial findings suggest a potential role for plasticity in the POm thalamocortical circuit in driving these altered responses. To test this hypothesis, we tested thalamically evoked activity patterns and connection strengths in the POm and VPM input pathway following whisker-mediated association training. Surprisingly, we observed increased thalamically evoked activity in both L2 and L5 that was revealed by POm, but not VPM stimulation. This increased activity was present after just 24 hours of training, a time point coinciding with the appearance of behavioral evidence for a learned association. By testing the quantal strength of these inputs, we determined that increased activity was caused by synaptic strengthening at direct POm to L5 synapses, but not any other synaptic change. Increased activity in superficial layers was inherited from L5 via transmission of L5 spike output through ascending intracortical connections. These synaptic changes were specific for learning, as an equal or larger number of stimulus presentations was not sufficient to drive plasticity. Finally, we identified this deep-layer POm to cortex plasticity as the first in a sequence of cortical changes, as longer time periods of training drove further synaptic changes at thalamic (POm →) and intracortical (L2 →) inputs onto superficial excitatory neurons. Together, these results reveal that POm directly drives activity in a translaminar cortical circuit and is the site of rapid sequential experience-dependent synaptic plasticity during learning. POm therefore may confer many of the functional

properties of L2 and L5 neurons during sensory processing and learning which have often been attributed to intracortical connectivity patterns.

4.2 Implications for other higher order thalamocortical pathways

Our investigation of the higher order thalamic nucleus POm shows that multiple thalamic streams can play an important role in driving cortical activity and in initiating experience-dependent plasticity in a single cortical region. This finding has widespread implications for other thalamocortical systems throughout the brain. Most directly, the pattern of higher-order thalamocortical input to primary sensory areas is a common motif across sensory systems and across organisms (Arcaro et al., 2015; Lee and Sherman, 2012; Purushothaman et al., 2012; Roth et al., 2016; Weinberger, 2004). The lateral pulvinar (LP) in the visual system and the medial and dorsal subdivisions of the medial geniculate body (d/mMGB) in the auditory system are analogous to POm structurally and functionally. Both nuclei are reciprocally connected to the corresponding primary sensory cortex, receiving driving inputs from deep layers and project back to nongranular layers (Marion et al., 2013; Viaene et al., 2011b). Further, both nuclei provide strong driving input to granular layers of second order sensory cortex, similar to POm (Lee and Sherman, 2012; Marion et al., 2013; Viaene et al., 2011a). The cell-type specific pattern of primary thalamocortical inputs is also similar across somatosensory, visual, and auditory modalities (Cruikshank et al., 2010; Kloc and Maffei, 2014; Schiff and Reyes, 2012), suggesting that basic principles of thalamocortical circuit organization are consistent in all three sensory systems. While there is some evidence that second order thalamic nuclei in other sensory systems can affect spike rates in the cortex (Purushothaman et al., 2012; Viaene et al., 2011b), the cell-type specific wiring of

these nuclei and impact on cortical function is unknown. Given the high degree of similarity of other wiring features between the three systems, it is reasonable to predict that the wiring rules that govern higher order thalamocortical inputs will follow the principles identified for POm in the somatosensory cortex.

Similarly, mutual insights can be gained into the functional properties of higher order thalamocortical circuits in the somatosensory, visual and auditory system. Results in the human and non-human primate visual system have determined that lesions of the pulvinar result in deficits in visual representations and special attention (Chalupa et al., 1976; Snow et al., 2009). They also show that pulvinar activity plays an important role in generating activity in the cortex, as silencing the pulvinar during visual sensation disrupts activity in superficial cortical neurons (Purushothaman et al., 2012). Experiments in the mouse correlate of the pulvinar reveal activity that represents information distributed throughout the visual scene and a particular sensitivity to mismatch between expected and perceived visual stimuli (Roth et al., 2016). In the auditory system, evidence from multiple rodent species shows that the activity levels of thalamic mMGB neurons rapidly change their activity levels in a stimulus-specific manner in classic associative conditioning (Edeline, 1990; O'Connor et al., 1997; Weinberger, 2004). Together, these findings support the hypothesis that POm activity is modulated by attention and is linked to behavioral context, rather than simply representing whisker stimuli. The effect of pulvinar manipulation on cortical firing rates supports the idea that POm activity can play a prominent role in controlling activity levels in superficial neurons. Finally, the observation of rapid plasticity in mMGB during association learning supports our conclusion that the POm pathway is involved in

behavioral learning. Similarly, our results provide the first evidence that higher order thalamic inputs are the first cortical connection to undergo synaptic plasticity during learning. While the finding will need to be confirmed across different systems, our findings predict that cortical plasticity may be initiated by second order thalamocortical pathways regardless of modality.

While analogous thalamic nuclei in other sensory systems are the most obvious comparison, our findings may have implications for thalamocortical systems throughout the brain. Wiring of primary thalamocortical inputs, defined as the thalamic input that provides VGLUT2-positive boutons to L4 of a given cortical area, seem to follow similar wiring rules as primary sensory thalamic nuclei even for thalamocortical circuits in prefrontal areas (Delevich et al., 2015). Despite the considerable variability in thalamocortical structures throughout the brain (Hunnicutt et al., 2014), it is possible that thalamic inputs to nongranular cortical layers are specially positioned to undergo rapid plasticity during learning regardless of cortical region. Indeed, there is evidence that thalamocortical plasticity can occur in L5 neurons of the M1 (Biane et al., 2016). The motor cortex is unusual in that it lacks a granular L4, so it is unclear exactly how this thalamocortical system compares to other more typical systems. However, it does provide evidence that thalamocortical inputs in other brain regions can undergo synaptic plasticity. An easy starting-point for these investigations would be in S2. While POm is a higher order nucleus with respect to S1, it could be considered a primary thalamic pathway with respect to S2 as it provides strong driving input to L4 (Viaene et al., 2011a). Assessing whether these synaptic connections undergo rapid plasticity during learning would provide insight into whether presynaptic nucleus identity or the cortical

target-layer controls the plasticity of a thalamocortical connection. Our results provide a new paradigm for thalamocortical function, and broad investigations of wiring and plasticity will be necessary to determine if our findings extend to non-sensory thalamocortical systems throughout the brain.

4.3 Cell-type specificity in the POm thalamocortical circuit

A main strength of the described work is that it surveys the activity of individual neurons from many different laminar and genetic populations in identical conditions. This allows for the calculation of the average behavior of a neurons within a single group and comparison between different neuronal groups, allowing us to make predictions about how the units may interact with one another. One of the notable differences between the first and second chapter of the study is the active decision to change the level of specificity and range of sampled cell-types. Understanding the diversity of neurons and placing them into meaningful groupings is a field unto itself, and determining the right level of specificity is a fundamental challenge in neuroscience. Assuming that a given technique or approach has a set throughput, increasing the breadth of groups allows for greater coverage of the entire neuronal population and for more thorough sampling within groups. On the other hand, it ensures that groups of neurons will be mixed. This heterogeneity can often lead to negative conclusions because true effects are washed out by neurons that do not undergo a change or have opposing properties but are incorrectly grouped. Too much specificity, however, can lead to the opposite problem where the properties of a very specific group of neurons can be characterized, but a smaller portion of the whole pool of neurons will be sampled. Both types of studies can be extremely useful, provided that the level of

specificity used is commensurate with the goals of the study. Additionally, the level of specificity must match the precision of all other experimental techniques.

In our cell-type specific characterization of POm inputs, we elected to use a systematic approach where excitatory neurons were assessed across all excitatory layers, including a laminar separation between L5a and L5b. We found that the strength of input onto excitatory neurons was largely based on depth, and closely matched the pattern of axon-dendrite overlap predicted in other studies (Meyer et al., 2010b). While we did not find multimodal peaks within given laminar pools of excitatory neurons, we likely did not sample densely enough to accurately characterize this level of heterogeneity. Viral expression of ChR2 also has inherent variability in expression level which makes it challenging to identify fine-scale differences. Despite this, preliminary data has identified some specificity for excitatory neurons within the same layer. When separating neurons based on expression of the activity-dependent immediate early gene cfos, we found that fos+ neurons on average received larger inputs than nearby simultaneously-recorded fos- cells (Appendix 1). In order to reliably assess the potential for preferential POm innervation of excitatory neuron subgroups, a more precise way of stimulating thalamic axons, such as transgenic expression of ChR2, would be ideal. Then, experiments focused on excitatory neuron subclasses specified by their projection target or genetic markers could be reasonably expected to yield reliable results.

When assessing inhibitory neurons, we elected to use three commonly used genetic markers that separate the neuron pool into virtually comprehensive and non-overlapping groups. To offset the increased density of neural subtypes, we focused our

analysis on L2 and L5. This approach was rewarding by finding distinct classes of responses in the three neuron subpopulations. PV neurons fired reliable short-latency action potentials, SST neurons typically fired tonic action potentials that were suppressed by POm, while 5HT neurons were generally quiet at rest and showed longer-latency slower EPSPs and action potentials. Highlighting the complexity of neuron type decisions, this level of precision, which was outstanding comparing to thalamocortical characterizations performed in this region and others, did not capture explain the full variability within the data. While PV neurons were typically uniform in their POm responses, SST neurons within the same layer were inhibited to very different degrees by POm activation. The 5HT population, however, was by far the most variable. 5HT neurons are a genetically heterogeneous group and the firing phenotype of many 5HT cells are a continuum (Jiang et al., 2013b, 2015; Lee et al., 2010; Prönneke et al., 2015). In our hands, POm responses were diverse, ranging from reliable action potentials – though longer latency than PV neurons – to a complete lack of input altogether.

As a first pass at addressing this variability, we recorded from the VIP-expressing sub-population that is known to make up roughly 40% of 5HT neurons and have a distinct pattern of connections (Rudy et al., 2011). However, we viewed almost as much response variability even within the exclusively VIP-expressing population. This joins an abundance of other data that suggest that even these neurons contain multiple meaningful subgroups (Lee et al., 2010; Prönneke et al., 2015). Due to experimental limitations at the time, it was not practical to explicitly investigate the population of neurons that express 5HT but not VIP. However, even among neurons that had a firing

phenotype prototypical of non-VIP neurogliaform cells, we viewed large diversity in response magnitude. This variability, while not the principle point of the paper, is extremely interesting and raises the possibility that distinct subgroups of 5HT neurons could mediate very specific patterns of inhibition between individual long-range inputs and local cortical targets. If input and output patterns adhere to this level of specificity, relatively small numbers of highly specified 5HT neurons could hold a great deal of control over the pattern of information flow through the cortical circuit, allowing for highly specific and variable cortical processing modes. Digging into this variability will require studies that focus on highly specific populations using combinations of cutting edge genetic techniques, morphological tracing, and functional connectomics.

In the second phase of research, the requirements and limitations of our experiment refocused our level of cell-type specificity. Unlike the initial investigation, our goal was not to perform a characterization in parallel across a comprehensive collection of cell types. While such an approach might be reasonable, the addition of a behavioral component decreased the throughput of the experiment, making it more challenging to address highly specific cell-types. Even more importantly, the goal of this investigation was not just to characterize a potential change in thalamically evoked activity, but also to understand at a synaptic level what generated these altered activity patterns. After performing an initial screen revealing an apparent change in POm-evoked activity level, we were faced with a decision about how to proceed. The prominent change in short-latency action potential generation in L5a, which receives the strongest input from POm, suggested a mechanism that involved excitatory synaptic transmission, and we thus elected to investigate altered synaptic strength within the POm excitatory circuit at

different time points in learning. In order to complete the large matrix of experiments required for this study, we focused entirely on L5a rather than recording from neurons distributed throughout L5. While fewer neurons in L5b receive input from POm, and POm input is weaker even in recipient cells, we do not discount the possibility of synaptic changes in L5b. Morphologically, neurons in L5a (thin-tufted) have smaller apical dendritic arbors and smaller somas, while neurons in L5b (thick-tufted) have more expansive apical dendritic branching and have larger somas. Thick-tufted L5b neurons also typically exhibit an intrinsic-bursting firing phenotype (Agmon and Connors, 1992; Jacob et al., 2012; Schubert et al., 2001). These properties generally map onto two developmentally distinct populations of neurons, defined as intratelencephalic neurons (IT) and pyramidal tract (PT) neurons. PT neurons are located primarily in L5b, have large soma with intrinsically bursting firing phenotypes, and project to subcortical structures including the spinal cord, thalamus, brain-stem, and colliculus (Gao and Zheng, 2004; Harris and Shepherd, 2015; Hattox and Nelson, 2007; Killackey and Sherman, 2003; Tsiola et al., 2003). IT neurons are located in both L5a and L5b, display small and medium sized cell-bodies with a regular-spiking firing phenotype, and project to cortical targets in the ipsilateral and contralateral hemisphere as well as the striatum (Le Bé et al., 2007; Gao and Zheng, 2004; Harris and Shepherd, 2015).

While long-range projection target is tightly linked to IT or PT identity, morphological, electrophysiological, and laminar properties may exist more along a spectrum. We chose to use a simple laminar cutoff to define L5a neurons which should predominantly sample IT neurons that receive abundant input from POm and project to

superficial cortical layers (Chagnac-Amitai et al., 1990; Harris and Shepherd, 2015). Due to the somewhat imprecise laminar organization of IT and PT cells, our recorded population likely includes at least a few PT neurons especially for cells collected closer to the border of L5a and L5b. Indeed, experiments measuring evoked activity allowed for electrophysiological characterization of L5 neurons, and at least one neuron recorded from L5a in both control and trained conditions exhibited an intrinsically bursting firing phenotype. Despite this, the large majority of our cellular population should comprise L5a, thin-tufted, regular-spiking cells that project to the cortex, striatum, and superficial cortical layers. Attempts to study the potential for plasticity in L5b or in more precise cellular targets should be performed with the assistance of developmental or projection target identity using retrograde tracing or genetic population markers to aid in cell characterization.

The decision to investigate excitatory synaptic strength proved fruitful but does not preclude the possibility of changes in inhibitory neuronal circuitry following learning. Increased thalamically-evoked activity in excitatory circuits could be assisted by increases or decreases in levels of inhibitory input. Preliminary data that was not included suggests that the evoked activity of PV neurons does not change (Appendix 2), but this is insufficient to claim that there is no change in PV-mediated inhibition. First, as PV neurons are already highly active following optogenetic stimulation of POm, an increase in synaptic strength would be difficult to see. An increase in PV activity would be counterintuitive given the increase in excitatory spiking, but we cannot rule out the possibility. More importantly, changes in PV-mediated inhibition could also occur at their inhibitory connections onto other cortical neurons, which we have not assessed. We

also have not checked for any changes in the SST or 5HT pathway, both of which could conceivably undergo alterations during learning. While we chose to focus this recent study on excitatory transmission, the potential contributions of inhibitory neuron plasticity during learning is an important avenue that should be pursued. Even if inhibitory neuron circuitry is not altered in a way that is prolonged, the precise activity of these neurons almost certainly play a role in the mechanism that generates cortical plasticity in the behaving animal.

4.4 The mechanisms of plasticity in the POm thalamocortical circuit

Our results identify the cell-type specific pattern of connections in the POm thalamocortical circuit and show that the state of the circuit has changed dramatically in a way that is measurable in brain slices after learning. What is lacking, however, is evidence about the activity patterns that occur in an intact animal to generate these changes. While the data necessary to define a comprehensive mechanism of thalamocortical plasticity does not currently exist, there are many lines of evidence that support the feasibility of POm thalamocortical plasticity. As discussed in the introduction, a major concern with the intracortical model of plasticity is the low firing rate of excitatory neurons and high firing rates of inhibitory neurons that are observed in cortical neurons (Barth and Poulet, 2012; Gentet et al., 2012; de Kock et al., 2007). Since most conceptualizations of cortical plasticity incorporate activity-dependent strengthening, low firing rates are problematic. Rate-dependent and spike-time dependent plasticity rules rely on either the number or precise timing of action potentials (Malenka and Bear, 2004). While there is a growing understanding that postsynaptic action potentials are not required for plasticity, a substantial amount of presynaptic

activity is still required to generate NMDA-dependent plateau potentials that facilitate plasticity in dendrites independent from the cell body. Our results provide some insight into this conundrum.

First, while the exact details of firing patterns or information content in POm are not known, firing rates in POm even in the absence of a whisker stimulation are higher than intracortical rates. Sensory stimuli further activate POm neurons, (Masri et al., 2008; Sosnik et al., 2001; Urbain et al., 2015) leading to far more activity in pre-synaptic thalamic terminals than in terminals originating from other excitatory neurons. This could allow POm thalamic inputs to generate more post-synaptic action potentials or plateau potentials during which synaptic strengthening can happen at these inputs. Which of the many proposed synaptic learning rules applies to these synapses is unclear, but the sequential laminar pattern of synaptic plasticity does suggest an initial mechanism that depends on post-synaptic action potentials. After 24 hours of training, we found evidence for synaptic strengthening only at POm to L5 synapses. Our experiments show that POm activity is capable of driving short latency action potentials in L5 in vitro. While the impact of POm action potentials on L5 neurons in vivo has not been determined, the strength of these inputs rivaled those recorded in L4 for VPM, suggesting that they can contribute meaningfully to action potential generation in their post-synaptic targets. In the basal condition, POm-evoked spiking in L2 was almost never observed, and cumulative POm input strength was much lower. Accordingly, the quantal strength of POm to L2 synapses was undistinguishable between control animals and animals trained for 24 hours. Given this double dissociation, it is reasonable to

hypothesize that synaptic strengthening in L5 was enabled by greater post-synaptic evoked activity levels (Figure 23).

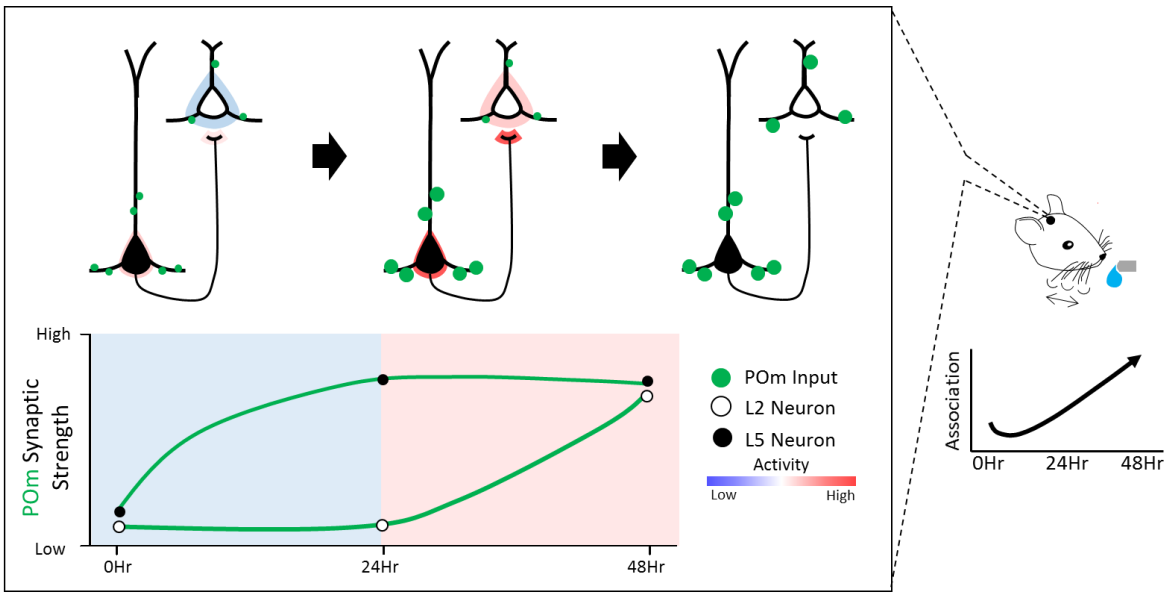

Figure 23. Early synaptic plasticity at POm to L5 synapses facilitates thalamocortical synaptic plasticity in superficial layers by increasing POm-evoked activity level.

After 48 hours, however, POm inputs onto L2 neurons, as well as recurrent local connections in L2, do display larger quantal amplitudes compared to both control and 24-hour trained animals. What allows for synaptic plasticity at this later time point but not after 24 hours? We found that POm stimulation evoked categorically greater levels of activity in superficial neurons at the 24 hour time point prior to any strengthening of synapses in that layer. This was caused by increased activity of L5 neurons that provide input to L2 via ascending intracortical connections. While our knowledge of POm and intracortical firing rates in vivo is limited, it is easily conceivable that when POm is active in the behaving animal, increased synaptic strength in L5 leads to a greater number of action potentials, and thus stronger input to L2 neurons. This increased input might result in greater action potential rates in L2 neurons, providing more opportunities for spike-dependent mechanisms of plasticity. Plasticity mechanisms that do not involve post-synaptic action potentials, which have been reported for POm inputs to L2 neurons (Gambino et al., 2014), might also be enhanced, as increased L5 input could help generate post-synaptic NMDA potentials that allow strengthening of nearby coincident inputs from POm or other L2 neurons. If this is true, it suggests a specific step-wise dependency that would allow L5 Pyr neuron activity to gate, or even instruct plasticity in superficial layers (Figure 23). This hypothesis could be tested by specifically silencing L5 neurons during training and then surveying the strength of inputs onto superficial neurons. Specific silencing of L5 Pyr neurons can be accomplished by expressing DREADDs or other chemogenetic inhibitors in neurons expressing ETV1cre or another L5-specific population marker. Synaptic strength could then be tested through quantal

amplitude of POm or local inputs. The precision of the finding could be further enhanced by inhibiting L5 Pyr neurons through CNO application at restricted time points, to determine when L5 Pyr neuron activity is required.

While activity level differences between pre- and post-synaptic neurons support this simple activity-dependent mechanism of POm thalamocortical plasticity, there are many other components to keep in mind. First, is the learning-dependent nature of the observed synaptic strengthening. Equal or greater presentations of the multiwhisker sensory stimulus when not predictively paired with water reward were not sufficient to drive plasticity at POm to L5 synapses. The interpretation of this result with respect to mechanism is not straightforward, since the activity of POm is so poorly understood. In the simple hypothetical scenario where the sensory stimulation in the two paradigms drives equal levels of cortical activity, learning signals in the form of neuromodulators could gate cortical plasticity (Bao et al., 2001; Froemke et al., 2007). Indeed, it has been shown in multiple systems that Ach signaling from the basal forebrain is important for synaptic plasticity. Activation of the basal forebrain during stimulus presentation is sufficient to drive expansion of the cortical representation of that stimulus (Bakin and Weinberger, 1996; Froemke et al., 2007; Shulz et al., 2003). Perhaps, in the case of our experiment, water reward generates a strong cholinergic signal, which coincides with the basal level of activity in the POm thalamocortical circuit, enabling plasticity to occur. This, of course, requires that cortical activity persists throughout the 500ms trace between stimulus presentation and water reward. Interestingly, our results and others have shown that POm activation can drive prolonged cortical activity that persists on the time scale of hundreds of milliseconds to seconds, both in vivo and in vitro (Jouhanneau

et al., 2014; Mease et al., 2016). This, combined with the cortical feedback that drives POm, could generate a recurrent loop that maintains sensory responses over the delay and that meaningful plasticity occurs at the time of water reward, facilitated by cholinergic feedback.

This model makes some intuitive sense, though there are other factors to consider. First, basal forebrain activity is not just modulated by task feedback, and acetylcholine alters the activity of cortical circuits during attention (Chen et al., 2015b; Kuchibhotla et al., 2017). It is therefore possible that attention at the time of stimulus delivery gates plasticity through a cholinergic mechanism. Second, since POm activity levels and information content are largely unknown, it is unclear that POm neurons have similar activity levels in the predictive and non-predictive training paradigms. In fact, activity in POm appears to be modulated by both arousal, basal forebrain activity, and acetylcholine, possibly as part of the same system (Masri et al., 2006b; Sobolewski et al., 2015; Trageser, 2006). Because of this, basal forebrain activation and cholinergic activity will also affect the firing rate of POm itself, raising the possibility that acetylcholine does not have a proximal affect on cortical synaptic plasticity but rather generates synaptic plasticity by increasing the rate of cortical activity. Third, the predominant mechanism through which acetylcholine is believed to enable synaptic plasticity occurs through disinhibition of cortical interneuron populations. A seminal paper by Letskuz and Luthi found that activation of L1 inhibitory neurons likely belonging to the 5HT population was activated by Ach and drove inhibition of cortical interneurons during learning (Letzkus et al., 2011). Similar patterns of disinhibition through 5HT-mediated disinhibition have been observed in other cortical regions and in

other tasks (Fu et al., 2015; Karnani et al., 2016; Lee et al., 2013; Li et al., 2014; Pi et al., 2013). What is particularly interesting about this plasticity mechanism is that our cell-type specific characterization of POm thalamocortical input found substantial drive to 5HT inhibitory neurons and robust inhibition of SST neurons even in acute brain slices. Therefore, it is also possible that Ach does not play a role in driving the observed synaptic plasticity either directly or indirectly. Certain patterns of prolonged POm activity during stimulation or a subsequent brain state could be responsible for driving cortical plasticity in the absence of neuromodulators.

4.5 Time course of cortical synaptic plasticity during learning

We identified a previously unknown sequence of cortical synaptic changes that occurs during learning, raising many questions about the timing and duration of this process. We found that evidence for synaptic plasticity was present in POm to L5 synapses after 24 hours of training, but when does this synaptic plasticity first emerge? In a preliminary study, we surveyed POm-evoked activity levels at midnight, after 12 hours of training. At this time point, evoked activity (Appendix 3) was comparable to control animals, but there are some issues with this measurement. First, more animals will be required to measure the accurate level of evoked activity with any confidence, especially given the inherent variability in a ChR2-based evoked firing rate. Since the exact location of synaptic plasticity at this time point is known, future experiments of plasticity initiation should be conducted using the quantal amplitude assay which is less dependent on ChR2 expression levels. An additional issue, however, is that the appropriate control group of untrained animals recorded at midnight is lacking. There may be circadian dynamics that lead to changes in general cortical circuit excitability or

synaptic strength that could mask a change in synaptic strength or activity level when comparing to controls.

If synaptic plasticity at POm to L5 synapses is not initiated in the first 12 hours of training, during which animals receive at least a hundred reward-paired whisker stimuli, when does is it occur? The emergence of evidence for behavioral learning does not occur until after 12 hours of training, and is typically present by 18-24 hours of training, corresponding to 6:00am - 12:00pm. As these experiments were performed using a standard (non-reversed) light-cycle, 18 hours is a critical point since it is at or near the dark to light shift. On average, both learning and the number of trials performed typically followed a diurnal rhythm, with the greatest increase in performance occurring around this dark-to-light transition. While the behavioral patterns of individual animals will vary, these average trajectories raise two likely possibilities. First, the emergence of synaptic plasticity could correspond directly to behavioral learning, which occurs over the course of the active time period between 12 and 18 hours. Second, the emergence of synaptic plasticity actually occurs during rest, and would on average occur between 18 and 24 hours of training. An initial and straightforward experiment to separate these two scenarios would be to record after 18 hours of training to determine whether synaptic plasticity, on average has occurred. This synaptic measurement could also be compared to behavioral metrics of learning to help dissociate between the theories, especially at the 18 hour time point. Within our current data set, we attempted to determine if trial number or performance correlated with synaptic strength, but with limited success (Appendix 4). Many of our experiments, especially those at 24 hours, were carried out before performance data was recorded, preventing comparison

between individual animal physiology and behavior. Further data is therefore required to determine if performance corresponds with the extent of synaptic plasticity. Similar questions about the emergence of synaptic strengthening in superficial layers exist at later time points. Additionally, there are many local cortical connections in which we did not observe synaptic strengthening after 48 hours of training. It is known that many of these local connections have the capacity to undergo synaptic plasticity, and it will be important to check later time points to determine if these changes actually do occur during sensory association training.

Understanding the duration of synaptic changes will also be important for placing our results in the context of behavioral learning. The increased synaptic strength onto L2 and L5 neurons observed during learning dramatically increased POm-evoked cortical activity levels. It is possible that spike rates in the behaving animal might be similarly altered. It is unlikely that a learning-dependent change of this magnitude would be permanent, as cortical activity levels would continue to increase throughout an organism's life. It is more likely that, over time, homeostatic mechanisms will be engaged to keep cortical activity levels within an appropriate range. This might include the loss or weakening of excitatory synapses, the gain or strengthening of inhibitory synapses, or intrinsic cellular changes. Eventually the measurable increase in aggregate circuit activity and quantal amplitude of individual connections is likely to decline towards baseline. It will be interesting to see if this process occurs, and when it might occur relative to learning-related metrics like the eventual plateau in task performance. If mean electrophysiological changes do return to baseline, changes in long-term cortical circuitry will likely exist only in the identity of synapses and not the

aggregate total or average strength. Learning-related synaptic connections might be specifically preserved during the homeostatic process and maintained for long periods of time in either L2, L5, or both. If possible, tracking these synaptic connections longitudinally during learning would provide important information about the nature of synaptic changes that occur in primary sensory cortex during learning.

4.6 Experimental approaches for investigating timing and mechanism of thalamocortical plasticity

In order to thoroughly understand the mechanism and time course that governs learning-dependent cortical plasticity, precise and sophisticated experiments will be required. Clearly, our understanding of in vivo activity patterns of both POm and cortical neurons during learning needs to improve in order to discern between the numerous mechanistic possibilities outlined above. While many types of in vivo experiments would provide useful insight, I believe experiments that record from multiple brain regions and cell-types simultaneously during freely moving behavior will be worth their challenge and high cost. As evidenced by our study, freely-moving mouse-initiated behavior allows for high-throughput, reliable, and unbiased training that generates continual quantitative behavioral data. The ability to record neural activity longitudinally from even a single cortical or thalamic neuronal population will pay great dividends, as it will allow for registration of activity levels with behavioral metrics. This does not just apply to an overall sliding rate of performance over time, but can be expanded to include individual behavior patterns such as the inter-trial interval, the pattern of trial identity, and performance on a single-trial basis. This type of experiment, where longitudinal neuronal recordings were performed in concert with behavioral metrics, recently yielded

very interesting and interpretable findings related to monocular deprivation in the visual system (Hengen et al., 2016). This experiment did not even register data related to cell type.

I believe that each dimension of additional registered data will exponentially increase the impact of these experiments, and may even be required to gain a mechanistic understanding of how synaptic changes are initiated in vivo. The interactions that govern synaptic plasticity likely occur on the time order of 10ms or less and between many different neurons simultaneously. They might be so precise that pooled averaged neuronal behavior in the form of PSTHs which have cell-type specificity but are performed for one cell-group per animal may not have the necessary resolution. However, an experiment that recorded cortical neurons from a depth electrode while simultaneously recording from POm and VPM neurons (registered by opto-tagging a VPM or POm-specific marker) would provide spiking data for hundred or maybe thousands of neurons in three related populations with precise timing in relation to one another and to behavioral events. Similar experiments could be done to record basal forebrain in concert with one or more other involved populations. This type of registered experiment is highly challenging, but our technological capabilities are at or approaching the threshold where they will become feasible. I believe that experiments in this vein, though technologically challenging, will be transformative in our ability to make powerful connections between the interactions of precise circuit elements, synaptic plasticity, and learning.

5 Appendices

Appendix 1: Activity-dependent gene expression predicts POm input amplitude in L2 neurons

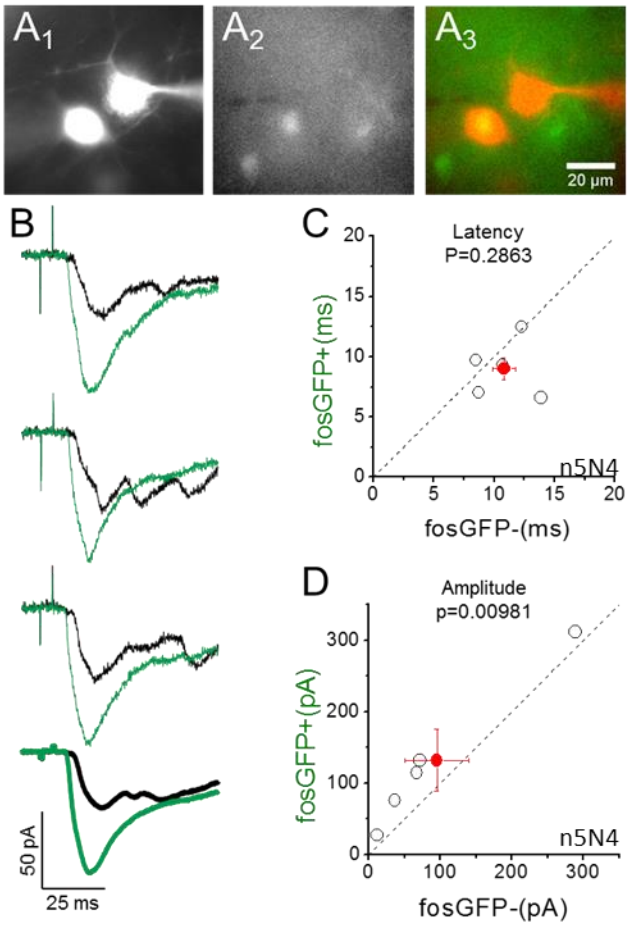

(A) Images of a simultaneously recorded L2 pyramidal neuron pair filled with Alexa dye (A1), fosGFP fluorescence (A2), and merged (A3). (B) Individual responses of a fosGFP+/fosGFP- neuron pair to 5 ms light stimulation of ChR2 expressing PoM axons and average response over multiple sweeps for the pair (bold). (C) Average onset latency of 5 neuron pairs in response to 5ms light stimulation. Red circle shows mean value. (D) Average amplitude of 5 neuron pairs (4 animals) in response to 5ms light stimulation. Red circle shows mean value +/- standard error.

Methods details fosGFP-expressing and non-expressing neurons were identified by GFP fluorescence in fosGFP transgenic mouse line and targeted for simultaneous whole-cell patch clamp recording. Responses to 5ms optical activation of ChR2-expressing POm axons in the barrel cortex were measured in voltage clamp holding at -70mV in the presence of TTX and 4AP.

Appendix 2: POm activation of PV neurons during learning

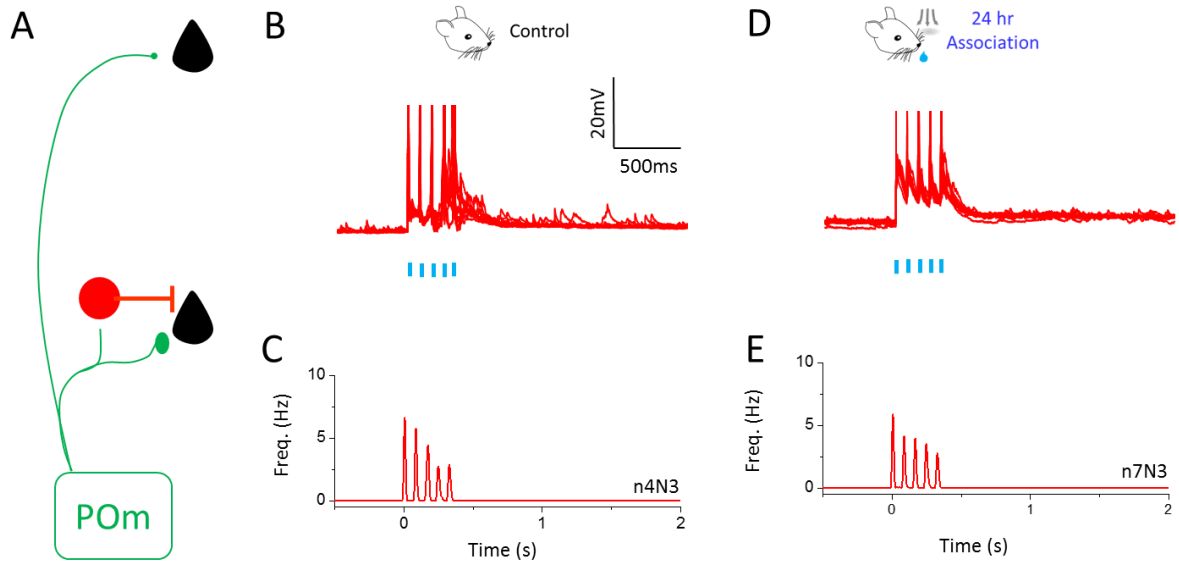

(A) Schematic of experimental protocol. (B) 10 consecutive trials with 5 light pulses (5ms, 80ms ISI) from a single example L5 PV neurons in a control animal. (C) Aggregate PSTH of POm-evoked activity in PV neurons in control animals, 10ms bins. (D,E) Same as (B,C) but for animals that had undergone 24 hours of sensory association training.

Methods details PV-expressing inhibitory neurons in L5a were targeted for whole-cell patch clamp recording using fluorescent imaging in a mouse line expressing Cre recombinase under the control of the PV promoter crossed to a fluorescent reporter line (see page 78). Responses to POm stimulation was measured as for cortical Pyr neurons (see page 129) in control animals and animals that had undergone 24 hours of sensory association training. PSTHs were computed for 10m bins.

Appendix 3: POm-evoked cortical activity after 12 hours of sensory association training

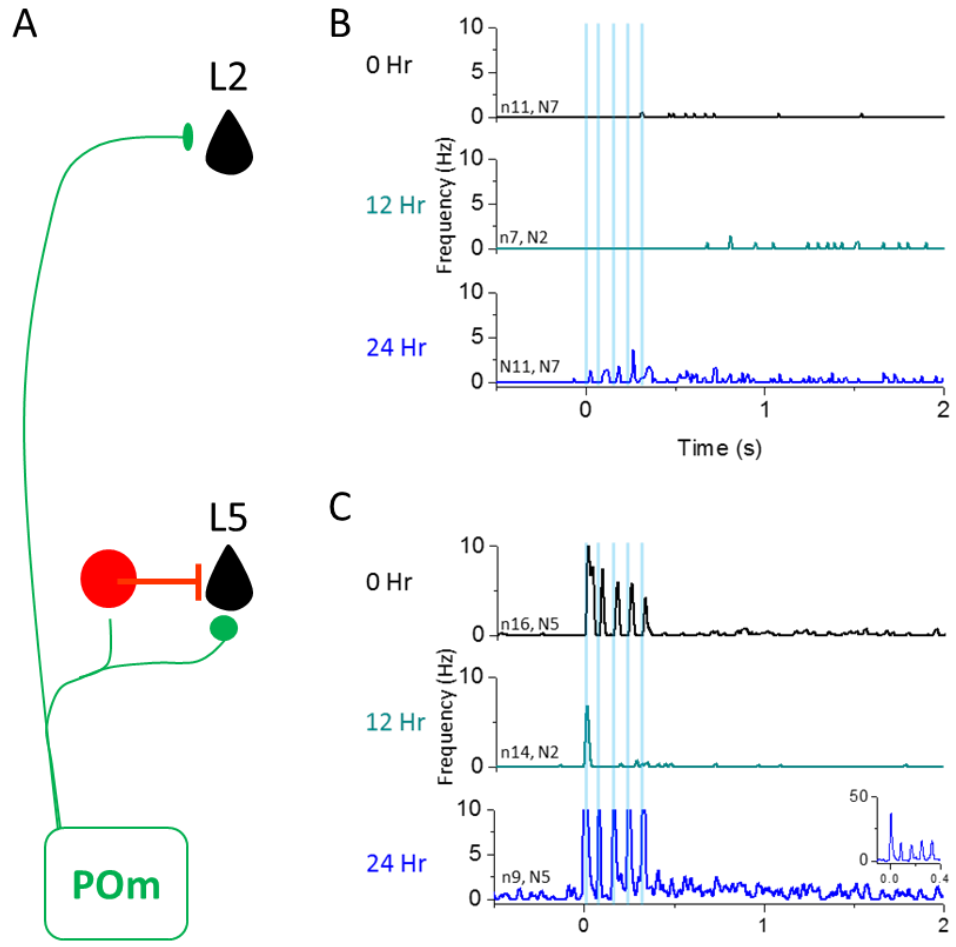

(A) Schematic of experimental setup with ChR2 expressed in POm axons and recordings from either L2 or L5 Pyr neurons. (B) Aggregate POm-evoked PSTH (10ms bins) following POm stimulation (5pulses, 5ms, 80ms ISI) in L2 Pyr neurons after different lengths of sensory association training. (C) Same as (B) but for L5 Pyr neurons.

Methods details Pyr neurons in L2 and L5a were targeted for whole-cell patch clamp recording in C57 mice that had undergone 0, 12, or 24 hours of sensory association training following 24 hours of acclimation. Responses to POm stimulation was measured as for cortical Pyr neurons in animals that had ChR2 virally expressed in POm neurons (see page 129). PSTHs were computed for 10m bins.

Appendix 4: Relationship between thalamocortical synaptic strength and behavioral parameters

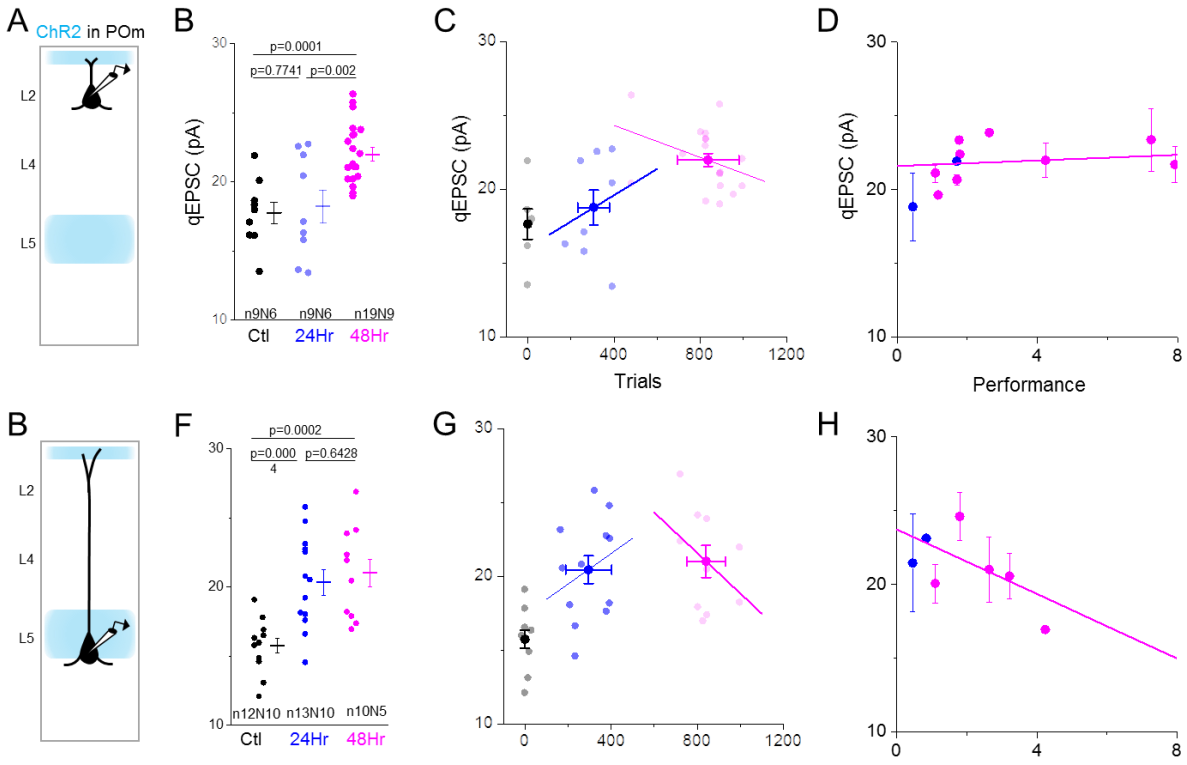

(A) Schematic of experimental setup. (B) Quantal amplitude of POm synaptic inputs recorded in L2 Pyr neurons. Each point denotes that average qEPSC amplitude recorded in a single cell in control animals and after 24 or 48 hours of sensory association training. (C) qEPSC amplitude for every cell plotted against the number of animals performed by the animal the cell came from for control (black), 24hr (blue), and 48hr (pink) SAT animals. Lines show linear regression of all cells from a condition. (D) qEPSC amplitude of each cell plotted against the performance metric measured as the difference between lick rate (Hz) on stimulus trials and blank trials for the last 20% of trials performed for SAT24 (blue) and SAT48 (pink) animals. (E-H) Same as (A-D) but for L5 Pyr neurons. All error bars represent SEM.

6 References

Ackman, J.B., Burbridge, T.J., and Crair, M.C. (2012). Retinal waves coordinate patterned activity throughout the developing visual system. Nature *490*, 219–225.

Acsády, L. (2017). The thalamic paradox. Nat. Neurosci. *20*, 901–902.

Adaikkan, C., and Rosenblum, K. (2015). A molecular mechanism underlying gustatory memory trace for an association in the insular cortex. Elife *4*, 1–15.

Agmon, a, and Connors, B.W. (1992). Correlation between intrinsic firing patterns and thalamocortical synaptic responses of neurons in mouse barrel cortex. J. Neurosci. *12*, 319–329.

Agmon, a, Yang, L.T., O'Dowd, D.K., and Jones, E.G. (1993). Organized growth of thalamocortical axons from the deep tier of terminations into layer IV of developing mouse barrel cortex. J. Neurosci. *13*, 5365–5382.

Ahissar, E., Sosnik, R., and Haldarilu, S. (2000). Transformation from temporal to rate coding in a somatosensory thalamocortical pathway. Nature *406*, 302–306.

Ahissar, E., Sosnik, R., Bagdasarian, K., and Haidarliu, S. (2001). Temporal frequency of whisker movement. II. Laminar organization of cortical representations. J. Neurophysiol. *86*, 354–367.

Albieri, G., Barnes, S.J., De Celis Alonso, B., Cheetham, C.E.J., Edwards, C.E., Lowe, A.S., Karunaratne, H., Dear, J.P., Lee, K.C., and Finnerty, G.T. (2015). Rapid bidirectional reorganization of cortical microcircuits. Cereb. Cortex *25*, 3025–3035.

Allen, C.B., Celikel, T., and Feldman, D.E. (2003). Long-term depression induced by sensory deprivation during cortical map plasticity in vivo. Nat. Neurosci. *6*, 291–299.

Alloway, K.D., Hoffer, Z.S., and Hoover, J.E. (2003). Quantitative comparisons of corticothalamic topography within the ventrobasal complex and the posterior nucleus of the rodent thalamus. Brain Res. *968*, 54–68.

Arcaro, M.J., Pinsk, M.A., and Kastner, S. (2015). The Anatomical and Functional Organization of the Human Visual Pulvinar. J. Neurosci. *35*, 9848–9871.

Armstrong-James, M., Fox, K., and Das-Gupta, A. (1992a). Flow of excitation within rat barrel cortex on striking a single vibrissa. J. Neurophysiol. *68*, 1345–1358.

Armstrong-James, M., Fox, K., and Das-Gupta, A. (1992b). Flow of excitation within rat barrel cortex on striking a single vibrissa. J. Neurophysiol.

Atallah, B. V., Bruns, W., Carandini, M., and Scanziani, M. (2012). Parvalbumin-Expressing Interneurons Linearly Transform Cortical Responses to Visual Stimuli. Neuron *73*, 159–170.

Audette, N.J., Urban-Ciecko, J., Matsushita, M., and Barth, A.L. (2017). POm

Thalamocortical Input Drives Layer-Specific Microcircuits in Somatosensory Cortex. Cereb. Cortex 1–17.

Avermann, M., Tomm, C., Mateo, C., Gerstner, W., and Petersen, C.C.H. (2012). Microcircuits of excitatory and inhibitory neurons in layer 2/3 of mouse barrel cortex. J. Neurophysiol. *107*, 3116–3134.

Bakin, J.S., and Weinberger, N.M. (1996). Induction of a physiological memory in the cerebral cortex by stimulation of the nucleus basalis. Proc. Natl. Acad. Sci. U. S. A.

Banerjee, A., Meredith, R.M., Rodríguez-Moreno, A., Mierau, S.B., Auberson, Y.P., and Paulsen, O. (2009). Double dissociation of spike timing-dependent potentiation and depression by subunit-preferring NMDA receptor antagonists in mouse barrel cortex. Cereb. Cortex *19*, 2959–2969.

Bao, S., Chan, V.T., and Merzenich, M.M. (2001). Cortical remodeling induced by activity of ventral tegmental dopamine neurons. Nature *412*, 79–83.

Barth, A.L., and Poulet, J.F.A. (2012). Experimental evidence for sparse firing in the neocortex. Trends Neurosci. *35*, 345–355.

Le Bé, J.V., Silberberg, G., Wang, Y., and Markram, H. (2007). Morphological, electrophysiological, and synaptic properties of corticocallosal pyramidal cells in the neonatal rat neocortex. Cereb. Cortex *17*, 2204–2213.

Beltramo, R., D'Urso, G., Maschio, M.D., Farisello, P., Bovetti, S., Clovis, Y., Lassi, G., Tucci, V., De Pietri Tonelli, D., and Fellin, T. (2013). Layer-specific excitatory circuits differentially control recurrent network dynamics in the neocortex. Nat. Med. *16*, 1–10.

Benedetti, B.L., Glazewski, S., and Barth, A.L. (2009). Reliable and precise neuronal firing during sensory plasticity in superficial layers of primary somatosensory cortex. J. Neurosci. *29*, 11817–11827.

Berardi, N., Pizzorusso, T., and Maffei, L. (2000). Critical periods during sensory development. Curr. Opin. Neurobiol. *10*, 138–145.

Berger, T.K., Silberberg, G., Perin, R., and Markram, H. (2010). Brief bursts self-inhibit and correlate the pyramidal network. PLoS Biol. *8*.

Biane, J.S., Takashima, Y., Scanziani, M., Conner, J.M., and Tuszynski, M.H. (2016). Thalamocortical Projections onto Behaviorally Relevant Neurons Exhibit Plasticity during Adult Motor Learning. Neuron *89*, 1173–1179.

Bock, D.D., Lee, W.-C.A., Kerlin, A.M., Andermann, M.L., Hood, G., Wetzel, A.W., Yurgenson, S., Soucy, E.R., Kim, H.S., and Reid, R.C. (2011). Network anatomy and in vivo physiology of visual cortical neurons. Nature *471*, 177–182.

Brasier, D.J., and Feldman, D.E. (2008). Synapse-Specific Expression of Functional Presynaptic NMDA Receptors in Rat Somatosensory Cortex. J. Neurosci. *28*, 2199–2211.

Brecht, M., Roth, A., and Sakmann, B. (2003). Dynamic Receptive Fields of

Reconstructed Pyramidal Cells in Layers 3 and 2 of Rat Somatosensory Barrel Cortex. J. Physiol. *553*, 243–265.

Brown, S.P., and Hestrin, S. (2009). Intracortical circuits of pyramidal neurons reflect their long-range axonal targets. Nature *457*, 1133–1136.

Bureau, I., Von Paul, F. Saint, and Svoboda, K. (2006). Interdigitated paralemniscal and lemniscal pathways in the mouse barrel cortex. PLoS Biol. *4*, 2361–2371.

Buxhoeveden, D.P., and Casanova, M.F. (2002). The minicolumn hypothesis in neuroscience. Brain *125*, 935–951.

Cao, V.Y., Ye, Y., Mastwal, S., Ren, M., Coon, M., Liu, Q., Costa, R.M., and Wang, K.H. (2015). Motor Learning Consolidates Arc-Expressing Neuronal Ensembles in Secondary Motor Cortex. Neuron *86*, 1385–1392.

Caras, M.L., and Sanes, D.H. (2017). Top-down modulation of sensory cortex gates perceptual learning. Proc. Natl. Acad. Sci. *114*, 201712305.

Carvell, G.E., and Simons, D.J. (1990). Biometric analyses of vibrissal tactile discrimination in the rat. J. Neurosci.

Chagnac-Amitai, Y., Luhmann, H.J., and Prince, D. (1990). Burst Generating and Regular Spiking Layer 5 Pyramidal Neurons of Rat Neocortex. J. Comp. Neurol. *2965984313*.

Chalupa, L.M., Coyle, R.S., and Lindsley, D.B. (1976). Effect of pulvinar lesions on visual pattern discrimination in monkeys. J. Neurophysiol.

Chandrasekaran, S., Navlakha, S., Audette, N.J., McCreary, D.D., Suhan, J., Bar-Joseph, Z., and Barth, A.L. (2015). Unbiased, High-Throughput Electron Microscopy Analysis of Experience-Dependent Synaptic Changes in the Neocortex. J. Neurosci. *35*, 16450–16462.

Cheetham, C.E.J., Hammond, M.S.L., Edwards, C.E.J., and Finnerty, G.T. (2007). Sensory Experience Alters Cortical Connectivity and Synaptic Function Site Specifically. J. Neurosci. *27*, 3456–3465.

Cheetham, C.E.J., Hammond, M.S.L., McFarlane, R., and Finnerty, G.T. (2008). Altered Sensory Experience Induces Targeted Rewiring of Local Excitatory Connections in Mature Neocortex. J. Neurosci. *28*, 9249–9260.

Cheetham, C.E.J., Barnes, S.J., Albieri, G., Knott, G.W., and Finnerty, G.T. (2014). Pansynaptic enlargement at adult cortical connections strengthened by experience. Cereb. Cortex *24*, 521–531.

Chen, J.L., Carta, S., Soldado-Magraner, J., Schneider, B.L., and Helmchen, F. (2013). Behaviour-dependent recruitment of long-range projection neurons in somatosensory cortex. Nature *499*, 336–340.

Chen, J.L., Margolis, D.J., Stankov, A., Sumanovski, L.T., Schneider, B.L., and Helmchen, F. (2015a). Pathway-specific reorganization of projection neurons in

somatosensory cortex during learning. Nat. Neurosci. *18*, 1101–1108.

Chen, N., Sugihara, H., and Sur, M. (2015b). An acetylcholine-activated microcircuit drives temporal dynamics of cortical activity. Nat. Neurosci. *18*, 892–902.

Chen, S.X., Kim, A.N., Peters, A.J., and Komiyama, T. (2015c). Subtype-specific plasticity of inhibitory circuits in motor cortex during motor learning. Nat. Neurosci. *18*, 1109–1115.

Chenn, A. (2011). Neural Precursors Regulation of Cerebral Cortical Size by Control of Cell Cycle Exit in Neural Precursors. *365*, 365–370.

Chiaia, N.L., Rhoades, R.W., Bennett-Clarke, C.A., Fish, S.E., and Killackey, H.P. (1991). Thalamic processing of vibrissal information in the rat. I. Afferent input to the medial ventral posterior and posterior nuclei. J. Comp. Neurol. *314*, 201–216.

Chittajallu, R., Pelkey, K. a, and McBain, C.J. (2013). Neurogliaform cells dynamically regulate somatosensory integration via synapse-specific modulation. Nat. Neurosci. *16*, 13–15.

Chmielowska, J., Carvell, G.E., and Simons, D.J. (1989). Spatial organization of thalamocortical and corticothalamic projection systems in the rat SmI barrel cortex. J. Comp. Neurol. *285*, 325–338.

Clancy, K.B., Schnepel, P., Rao, A.T., and Feldman, D.E. (2015). Structure of a single whisker representation in layer 2 of mouse somatosensory cortex. J. Neurosci. *35*, 3946–3958.

Clem, R.L. (2010). Ongoing in Vivo Experience in the Neocortex. Science (80-.). *101*, 101–105.

Clem, R.L., and Barth, A. (2006). Pathway-specific trafficking of native AMPARs by in vivo experience. Neuron *49*, 663–670.

Cohen, J.Y., Haesler, S., Vong, L., Lowell, B.B., and Uchida, N. (2012). Neuron-type-specific signals for reward and punishment in the ventral tegmental area. Nature *482*, 85–88.

Constantinople, C.M., and Bruno, R.M. (2013). Deep cortical layers are activated directly by thalamus. Science (80-.). *1591*, 1591–1594.

Crair, M.C., and Malenka, R.C. (1995). A critical period for long-term potentiation at thalamocortical synapses. Nature *375*, 325–328.

Crandall, S.R., Cruikshank, S.J., and Connors, B.W. (2015). A Corticothalamic Switch: Controlling the Thalamus with Dynamic Synapses. Neuron *86*, 768–782.

Crandall, S.R., Patrick, S.L., Cruikshank, S.J., and Connors, B.W. (2017). Infrabarrels Are Layer 6 Circuit Modules in the Barrel Cortex that Link Long-Range Inputs and Outputs. Cell Rep. *21*, 3065–3078.

Crochet, S., Poulet, J.F.A., Kremer, Y., and Petersen, C.C.H. (2011). Synaptic mechanisms underlying sparse coding of active touch. Neuron.

Cruikshank, S.J., Lewis, T.J., and Connors, B.W. (2007). Synaptic basis for intense thalamocortical activation of feedforward inhibitory cells in neocortex. Nat. Neurosci. *10*, 462–468.

Cruikshank, S.J., Urabe, H., Nurmikko, A. V., and Connors, B.W. (2010). Pathway-Specific Feedforward Circuits between Thalamus and Neocortex Revealed by Selective Optical Stimulation of Axons. Neuron *65*, 230–245.

Cruikshank, S.J., Ahmed, O.J., Stevens, T.R., Patrick, S.L., Gonzalez, A.N., Elmaleh, M., and Connors, B.W. (2012). Thalamic control of layer 1 circuits in prefrontal cortex. J. Neurosci. *32*, 17813–17823.

D'amour, J., and Froemke, R. (2015). Inhibitory and Excitatory Spike-Timing-Dependent Plasticity in the Auditory Cortex. Neuron *86*, 514–528.

Delevich, K., Tucciarone, J., Huang, Z.J., and Li, B. (2015). The Mediodorsal Thalamus Drives Feedforward Inhibition in the Anterior Cingulate Cortex via Parvalbumin Interneurons. J. Neurosci. *35*, 5743–5753.

Deschênes, M., Veinante, P., and Zhang, Z.W. (1998). The organization of corticothalamic projections: Reciprocity versus parity. Brain Res. Rev. *28*, 286–308.

Diamond, M.E., Armstrong-James, M., Budway, M.J., and Ebner, F.F. (1992). Somatic sensory responses in the rostral sector of the posterior group (POm) and in the ventral posterior medial nucleus (VPM) of the rat thalamus: Dependence on the barrel field cortex. J. Comp. Neurol. *319*, 66–84.

Diamond, M.E., Huang, W., and Ebner, F.F. (1994). Laminar Comparison of Somatosensory Cortical Plasticity Author (s): Mathew E . Diamond , Wei Huang and Ford F . Ebner Published by : American Association for the Advancement of Science Stable URL : http://www.jstor.org/stable/2884667 JSTOR is a not-for-. Science (80-.). *265*, 1885–1888.

Douglas, R.J., and Martin, K. a C. (2007). Mapping the matrix: the ways of neocortex. Neuron *56*, 226–238.

Douglas, R.J., Martin, K.A.C., and Whitteridge, D. (1989). A Canonical Microcircuit for Neocortex. Neural Comput. *1*, 480–488.

Ebara, S., Kumamoto, K., Matsuura, T., Mazurkiewicz, J.E., and Rice, F.L. (2002). Similarities and differences in the innervation of mystacial vibrissal follicle-sinus complexes in the rat and cat: A confocal microscopic study. J. Comp. Neurol. *449*, 103–119.

Edeline, J.M. (1990). Frequency-specific plasticity of single unit discharges in the rat medial geniculate body. Brain Res.

Fanselow, E.E., and Connors, B.W. (2010). The roles of somatostatin-expressing (GIN) and fast-spiking inhibitory interneurons in UP-DOWN states of mouse neocortex. J. Neurophysiol. *104*, 596–606.

Fanselow, E.E., Richardson, K.A., and Connors, B.W. (2008). Selective , State-

Dependent Activation of Somatostatin-Expressing Inhibitory Interneurons in Mouse Neocortex. J. Neurophysiol. *100*, 2640–2652.

Feldman, D.E. (2000). Timing-based LTP and LTD at vertical inputs to layer II/III pyramidal cells in rat barrel cortex. Neuron *27*, 45–56.

Feldman, D.E., and Brecht, M. (2005). Map plasticity in somatosensory cortex. Science (80-.). *310*, 810–815.

Feldmeyer, D., Brecht, M., Helmchen, F., Petersen, C.C.H., Poulet, J.F.A., Staiger, J.F., Luhmann, H.J., and Schwarz, C. (2013). Barrel cortex function. Prog. Neurobiol. *103*, 3–27.

Fino, E., and Yuste, R. (2011). Dense inhibitory connectivity in neocortex. Neuron *69*, 1188–1203.

Fox, K. (1992). A critical period for experience-dependent synaptic plasticity in rat barrel cortex. J. Neurosci. *12*, 1826–1838.

Fox, K. (2002). Anatomical pathways and molecular mechanisms for plasticity in the barrel cortex. Neuroscience *111*, 799–814.

Francis, N.A., and Kanold, P.O. (2017). Automated Operant Conditioning in the Mouse Home Cage. Front. Neural Circuits *11*, 1–6.

Froemke, R.C., Merzenich, M.M., and Schreiner, C.E. (2007). A synaptic memory trace for cortical receptive field plasticity. Nature *450*, 425–429.

Fu, Y., Tucciarone, J.M., Espinosa, J.S., Sheng, N., Darcy, D.P., Nicoll, R.A., Huang, Z.J., and Stryker, M.P. (2014). A cortical circuit for gain control by behavioral state. Cell *156*, 1139–1152.

Fu, Y., Kaneko, M., Tang, Y., Alvarez-Buylla, A., and Stryker, M.P. (2015). A cortical disinhibitory circuit for enhancing adult plasticity. Elife *2015*, 1–12.

Furuta, T., Timofeeva, E., Nakamura, K., Okamoto-Furuta, K., Togo, M., Kaneko, T., and Deschenes, M. (2008). Inhibitory Gating of Vibrissal Inputs in the Brainstem. J. Neurosci.

Furuta, T., Urbain, N., Kaneko, T., and Deschenes, M. (2010). Corticofugal Control of Vibrissa-Sensitive Neurons in the Interpolaris Nucleus of the Trigeminal Complex. J. Neurosci. *30*, 1832–1838.

Gabernet, L., Jadhav, S.P., Feldman, D.E., Carandini, M., and Scanziani, M. (2005). Somatosensory integration controlled by dynamic thalamocortical feed-forward inhibition. Neuron *48*, 315–327.

Galvez, R. (2006). Vibrissa-Signaled Eyeblink Conditioning Induces Somatosensory Cortical Plasticity. J. Neurosci. *26*, 6062–6068.

Galvez, R., Weible, A.P., and Disterhoft, J.F. (2007). Cortical barrel lesions impair whisker-CS trace eyeblink conditioning. Learn. Mem. *14*, 94–100.

Gambino, F., Pagès, S., Kehayas, V., Baptista, D., Tatti, R., Carleton, A., and Holtmaat, A. (2014). Sensory-evoked LTP driven by dendritic plateau potentials in vivo. Nature *515*, 116–119.

Gao, W.J., and Zheng, Z.H. (2004). Target-specific differences in somatodendritic morphology of layer V pyramidal neurons in rat motor cortex. J. Comp. Neurol. *476*, 174–185.

Garvert, M.M., Moutoussis, M., Kurth-Nelson, Z., Behrens, T.E.J., and Dolan, R.J. (2015). Learning-Induced plasticity in medial prefrontal cortex predicts preference malleability. Neuron *85*, 418–428.

Gavornik, J.P., and Bear, M.F. (2014). Higher brain functions served by the lowly rodent primary visual cortex. Learn. Mem. *21*, 527–533.

Gentet, L.J., Kremer, Y., Taniguchi, H., Huang, Z.J., Staiger, J.F., and Petersen, C.C. (2012). Unique functional properties of somatostatin-expressing GABAergic neurons in mouse barrel cortex. Nat Neurosci *15*, 607–612.

Gilbert, C.D., and Li, W. (2012). Adult Visual Cortical Plasticity. Neuron *75*, 250–264.

Glazewski, S., and Barth, A.L. (2015). Stimulus intensity determines experience-dependent modifications in neocortical neuron firing rates. Eur. J. Neurosci. *41*, 410–419.

Glazewski, S., and Fox, K. (1996). Time course of experience-dependent synaptic potentiation and depression in barrel cortex of adolescent rats. J. Neurophysiol. *75*, 1714–1729.

Gong, S., Doughty, M., Harbaugh, C.R., Cummins, A., Hatten, M.E., Heintz, N., and Gerfen, C.R. (2007). Targeting Cre recombinase to specific neuron populations with bacterial artificial chromosome constructs. J. Neurosci. *27*, 9817–9823.

Greig, L.C., Woodworth, M.B., Galazo, M.J., Padmanabhan, H., and Macklis, J.D. (2013). Molecular logic of neocortical projection neuron specification, development and diversity. Nat. Rev. Neurosci. *14*, 755–769.

Groh, A., Bokor, H., Mease, R.A., Plattner, V.M., Hangya, B., Stroh, A., Deschenes, M., and Acsády, L. (2014a). Convergence of cortical and sensory driver inputs on single thalamocortical cells. Cereb. Cortex *24*, 3167–3179.

Groh, A., Bokor, H., Mease, R.A., Plattner, V.M., Hangya, B., Stroh, A., Deschenes, M., and Acsády, L. (2014b). Convergence of cortical and sensory driver inputs on single thalamocortical cells. Cereb. Cortex *24*, 3167–3179.

Hangya, B., Pi, H.J., Kvitsiani, D., Ranade, S.P., and Kepecs, A. (2014). From circuit motifs to computations: Mapping the behavioral repertoire of cortical interneurons. Curr. Opin. Neurobiol. *26*, 117–124.

Harris, K.D., and Mrsic-Flogel, T.D. (2013). Cortical connectivity and sensory coding. Nature *503*, 51–58.

Harris, K.D., and Shepherd, G.M.G. (2015). The neocortical circuit: themes and variations. Nat. Neurosci. *18*, 170–181.

Harris, J. a, Harris, I.M., and Diamond, M.E. (2001). The topography of tactile working memory. J. Neurosci. *21*, 8262–8269.

Hattox, A.M., and Nelson, S.B. (2007). Layer V Neurons in Mouse Cortex Projecting to Different Targets Have Distinct Physiological Properties. J. Neurophysiol. *98*, 3330–3340.

Haydar, T.F., Kuan, C.Y., Flavell, R.A., and Rakic, P. (1999). The role of cell death in regulating the size and shape of the mammalian forebrain. Cereb. Cortex.

Hengen, K.B., Torrado Pacheco, A., McGregor, J.N., Van Hooser, S.D., and Turrigiano, G.G. (2016). Neuronal Firing Rate Homeostasis Is Inhibited by Sleep and Promoted by Wake. Cell *165*, 180–191.

Herculano-Houzel, S. (2009). The human brain in numbers: a linearly scaled-up primate brain. Front. Hum. Neurosci. *3*, 31.

Herculano-Houzel, S. (2012). The remarkable, yet not extraordinary, human brain as a scaled-up primate brain and its associated cost. Proc. Natl. Acad. Sci. *109*, 10661–10668.

Herculano-Houzel, S., Collins, C.E., Wong, P., Kaas, J.H., and Lent, R. (2008). The basic nonuniformity of the cerebral cortex. Proc. Natl. Acad. Sci. *105*, 12593–12598.

Hippenmeyer, S., Vrieseling, E., Sigrist, M., Portmann, T., Laengle, C., Ladle, D.R., and Arber, S. (2005). A developmental switch in the response of DRG neurons to ETS transcription factor signaling. PLoS Biol. *3*, 0878–0890.

Hofman, M.A. (1989). On the evolution and geometry of the brain in mammals. Prog. Neurobiol.

Holtmaat, A., Wilbrecht, L., Knott, G.W., Welker, E., and Svoboda, K. (2006). Experience-dependent and cell-type-specific spine growth in the neocortex. Nature *441*, 979–983.

Hooks, B.M., Hires, S.A., Zhang, Y.X., Huber, D., Petreanu, L., Svoboda, K., and Shepherd, G.M.G. (2011). Laminar analysis of excitatory local circuits in vibrissal motor and sensory cortical areas. PLoS Biol. *9*.

Hooks, B.M., Mao, T., Gutnisky, D.A., Yamawaki, N., Svoboda, K., and Shepherd, G.M.G. (2013). Organization of Cortical and Thalamic Input to Pyramidal Neurons in Mouse Motor Cortex. J. Neurosci. *33*, 748–760.

Hu, H., and Agmon, A. (2016). Differential Excitation of Distally versus Proximally Targeting Cortical Interneurons by Unitary Thalamocortical Bursts. J. Neurosci. *36*, 6906–6916.

Hunnicutt, B.J., Long, B.R., Kusefoglu, D., Gertz, K.J., Zhong, H., and Mao, T. (2014). A comprehensive thalamocortical projection map at the mesoscopic level. Nat. Neurosci.

17, 1276–1285.

Jacob, V., Petreanu, L., Wright, N., Svoboda, K., and Fox, K. (2012). Regular Spiking and Intrinsic Bursting Pyramidal Cells Show Orthogonal Forms of Experience-Dependent Plasticity in Layer V of Barrel Cortex. Neuron *73*, 391–404.

Jacquin, M.F., Woerner, D., Szczepanik, A.M., Riecker, V., Mooney, R.D., and Rhoades, R.W. (1989). Structure-function relationships in rat brainstem subnucleus interpolaris. IV. Vibrissa primary afferents. J. Comp. Neurol. *243*, 266–279.

Jacquin, M.F., Chiaia, N.L., Haring, J.H., and Rhoades, R.W. (1990). Intersubnuclear connections within the rat trigeminal brainstem complex. Somatosens. Mot. Res.

Jensvold, M.L.A., and Gardner, R.A. (2000). Interactive use of sign language by cross-fostered chimpanzees (Pan troglodytes). J. Comp. Psychol.

Ji, X.Y., Zingg, B., Mesik, L., Xiao, Z., Zhang, L.I., and Tao, H.W. (2016). Thalamocortical Innervation Pattern in Mouse Auditory and Visual Cortex: Laminar and Cell-Type Specificity. Cereb. Cortex *26*, 2612–2625.

Jiang, X., Wang, G., Lee, A.J., Stornetta, R.L., and Zhu, J.J. (2013a). The organization of two new cortical interneuronal circuits. Nat. Neurosci. *16*, 210–218.

Jiang, X., Wang, G., Lee, A.J., Stornetta, R.L., and Zhu, J.J. (2013b). The organization of two new cortical interneuronal circuits Supplementary Information for The organization of two new cortical interneuronal circuits. *218*.

Jiang, X., Shen, S., Cadwell, C.R., Berens, P., Sinz, F., Ecker, A.S., Patel, S., and Tolias, A.S. (2015). Principles of connectivity among morphologically defined cell types in adult neocortex. Science (80-.). *350*, aac9462-aac9462.

Joachimsthaler, B., Brugger, D., Skodras, A., and Schwarz, C. (2015). Spine Loss in Primary Somatosensory Cortex during Trace Eyeblink Conditioning. J. Neurosci. *35*, 3772–3781.

Johnson, C.M., Peckler, H., Tai, L.H., and Wilbrecht, L. (2016). Rule learning enhances structural plasticity of long-range axons in frontal cortex. Nat. Commun. *7*, 1–14.

Johnson, M.B., Kawasawa, Y.I., Mason, C.E., Krsnik, Ž., Coppola, G., Bogdanović, D., Geschwind, D.H., Mane, S.M., State, M.W., and Šestan, N. (2009). Functional and Evolutionary Insights into Human Brain Development through Global Transcriptome Analysis. Neuron *62*, 494–509.

Jouhanneau, J.S., Ferrarese, L., Estebanez, L., Audette, N.J., Brecht, M., Barth, A.L., and Poulet, J.F.A. (2014). Cortical fos GFP expression reveals broad receptive field excitatory neurons targeted by pom. Neuron *84*, 1065–1078.

Kaas, J.H. (2012). Evolution of columns, modules, and domains in the neocortex of primates. Proc. Natl. Acad. Sci. *109*, 10655–10660.

Kaneko, T. (2013). Local connections of excitatory neurons in motor-associated cortical areas of the rat. Front. Neural Circuits *7*, 1–17.

Kaplan, E.S., Cooke, S.F., Komorowski, R.W., Chubykin, A.A., Thomazeau, A., Khibnik, L.A., Gavornik, J.P., and Bear, M.F. (2016). Contrasting roles for parvalbumin-expressing inhibitory neurons in two forms of adult visual cortical plasticity. Elife *5*, 1–27.

Karnani, M.M., Jackson, J., Ayzenshtat, I., Hamzehei Sichani, A., Manoocheri, K., Kim, S., and Yuste, R. (2016). Opening Holes in the Blanket of Inhibition: Localized Lateral Disinhibition by VIP Interneurons. J. Neurosci. *36*, 3471–3480.

Karni, A., and Sagi, D. (1991). Where practice makes perfect in texture discrimination: evidence for primary visual cortex plasticity. Proc. Natl. Acad. Sci. U. S. A. *88*, 4966–4970.

Kätzel, D., Zemelman, B. V, Buetfering, C., Wölfel, M., and Miesenböck, G. (2011). The columnar and laminar organization of inhibitory connections to neocortical excitatory cells. Nat. Neurosci. *14*, 100–107.

Kawaguchi, Y., and Kubota, Y. (1997). GABAergic cell subtypes and their synaptic connections in rat frontal cortex. Cereb. Cortex *7*, 476–486.

Kawai, R., Markman, T., Poddar, R., Ko, R., Fantana, A.L., Dhawale, A.K., Kampff, A.R., and Ölveczky, B.P. (2015). Motor Cortex Is Required for Learning but Not for Executing a Motor Skill. Neuron *86*, 800–812.

Kilgard, M.P. (1998). Cortical Map Reorganization Enabled by Nucleus Basalis Activity. Science (80-.). *279*, 1714–1718.

Killackey, H.P., and Sherman, S.M. (2003). Corticothalamic Projections from the Rat Primary Somatosensory Cortex. J. Neurosci. *23*, 7381–7384.

Kinnischtzke, A.K., Simons, D.J., and Fanselow, E.E. (2014). Motor cortex broadly engages excitatory and inhibitory neurons in somatosensory barrel cortex. Cereb. Cortex *24*, 2237–2248.

Kiritani, T., Wickersham, I.R., Seung, H.S., and Shepherd, G.M.G. (2012). Hierarchical Connectivity and Connection-Specific Dynamics in the Corticospinal-Corticostriatal Microcircuit in Mouse Motor Cortex. J. Neurosci. *32*, 4992–5001.

Klapoetke, N.C., Murata, Y., Kim, S.S., Pulver, S.R., Birdsey-Benson, A., Cho, Y.K., Morimoto, T.K., Chuong, A.S., Carpenter, E.J., Tian, Z., et al. (2014). Independent optical excitation of distinct neural populations. Nat. Methods *11*, 338–346.

Kloc, M., and Maffei, A. (2014). Target-Specific Properties of Thalamocortical Synapses onto Layer 4 of Mouse Primary Visual Cortex. J. Neurosci. *34*, 15455–15465.

Knott, G.W., Quairiaux, C., Genoud, C., and Welker, E. (2002). Formation of dendritic spines with GABAergic synapses induced by whisker stimulation in adult mice. Neuron *34*, 265–273.

Ko, H., Hofer, S.B., Pichler, B., Buchanan, K.A., Sjöström, P.J., and Mrsic-Flogel, T.D. (2011). Functional specificity of local synaptic connections in neocortical networks. Nature *473*, 87–91.

de Kock, C.P.J. De, Bruno, R.M., Spors, H., and Sakmann, B. (2007). Layer- and cell-type-speci c suprathreshold stimulus representation in rat primary somatosensory cortex. Society *1*, 139–154.

Koralek, K.A., Jensen, K.F., and Killackey, H.P. (1988). Evidence for two complementary patterns of thalamic input to the rat somatosensory cortex. Brain Res. *463*, 346–351.

Kuchibhotla, K. V., Gill, J. V., Lindsay, G.W., Papadoyannis, E.S., Field, R.E., Sten, T.A.H., Miller, K.D., and Froemke, R.C. (2017). Parallel processing by cortical inhibition enables context-dependent behavior. Nat. Neurosci.

Kuhlman, S.J., O'Connor, D.H., Fox, K., and Svoboda, K. (2014). Structural Plasticity within the Barrel Cortex during Initial Phases of Whisker-Dependent Learning. J. Neurosci. *34*, 6078–6083.

Kwan, K.Y., Lam, M.M.S., Krsnik, Z., Kawasawa, Y.I., Lefebvre, V., and Sestan, N. (2008). SOX5 postmitotically regulates migration, postmigratory differentiation, and projections of subplate and deep-layer neocortical neurons. Proc. Natl. Acad. Sci. *105*, 16021–16026.

Lambo, M.E., and Turrigiano, G.G. (2013). Synaptic and Intrinsic Homeostatic Mechanisms Cooperate to Increase L2/3 Pyramidal Neuron Excitability during a Late Phase of Critical Period Plasticity. J. Neurosci. *33*, 8810–8819.

Landers, M.S., Knott, G.W., Lipp, H.P., Poletaeva, I., and Welker, E. (2011). Synapse formation in adult barrel cortex following naturalistic environmental enrichment. Neuroscience *199*, 143–152.

Landisman, C.E., and Connors, B.W. (2007). VPM and PoM nuclei of the rat somatosensory thalamus: Intrinsic neuronal properties and corticothalamic feedback. Cereb. Cortex *17*, 2853–2865.

Lavallee, P. (2005). Feedforward Inhibitory Control of Sensory Information in Higher-Order Thalamic Nuclei. J. Neurosci. *25*, 7489–7498.

Lee, C.C., and Sherman, S.M. (2012). On the classification of pathways in the auditory midbrain, thalamus, and cortex. Hear Res. *276*, 79–87.

Lee, S., Hjerling-Leffler, J., Zagha, E., Fishell, G., and Rudy, B. (2010). The Largest Group of Superficial Neocortical GABAergic Interneurons Expresses Ionotropic Serotonin Receptors. J. Neurosci. *30*, 16796–16808.

Lee, S., Kruglikov, I., Huang, Z.J., Fishell, G., and Rudy, B. (2013). A disinhibitory circuit mediates motor integration in the somatosensory cortex. Nat. Neurosci. *16*, 1662–1670.

Lee, W.A., Bonin, V., Reed, M., Graham, B.J., Hood, G., Glattfelder, K., and Reid, R.C. (2016). Anatomy and function of an excitatory network in the visual cortex. Nature *532*, 1–18.

Lefort, S., Tomm, C., Floyd Sarria, J.C., and Petersen, C.C.H. (2009). The Excitatory Neuronal Network of the C2 Barrel Column in Mouse Primary Somatosensory Cortex.

Neuron *61*, 301–316.

Lesburguères, E., Gobbo, O.L., Alaux-cantin, S., Hambucken, A., Trifilieff, P., and Bontempi, B. (2011). Early Tagging of Cortical Networks of Enduring Associative Memory. Science (80-.). 924–928.

Letzkus, J.J., Wolff, S.B.E., Meyer, E.M.M., Tovote, P., Courtin, J., Herry, C., and Lüthi, A. (2011). A disinhibitory microcircuit for associative fear learning in the auditory cortex. Nature *480*, 331–335.

Li, L., Gainey, M. a, Goldbeck, J.E., Feldman, D.E., L, L., MA, G., JE, G., and DE, F. (2014). Rapid homeostasis by disinhibition during whisker map plasticity. Proc. Natl. Acad. Sci. U. S. A. *111*, 1616–1621.

Liao, C.C., Chen, R.F., Lai, W.S., Lin, R.C.S., and Yen, C.T. (2010). Distribution of large terminal inputs from the primary and secondary somatosensory cortices to the dorsal thalamus in the rodent. J. Comp. Neurol. *518*, 2592–2611.

Lu, J., Tucciarone, J., Padilla-Coreano, N., He, M., Gordon, J.A., and Josh Huang, Z. (2017). Selective inhibitory control of pyramidal neuron ensembles and cortical subnetworks by chandelier cells. Nat. Neurosci. *20*, 1377–1383.

MacLean, E.L. (2016). Unraveling the evolution of uniquely human cognition. Proc. Natl. Acad. Sci. *113*, 6348–6354.

Makino, H., Hwang, E.J., Hedrick, N.G., and Komiyama, T. (2016). Circuit Mechanisms of Sensorimotor Learning. Neuron *92*, 705–721.

Malenka, R.C., and Bear, M.F. (2004). LTP and LTD: An embarrassment of riches. Neuron *44*, 5–21.

Margolis, D.J., Lütcke, H., and Helmchen, F. (2014). Microcircuit dynamics of map plasticity in barrel cortex. Curr. Opin. Neurobiol. *24*, 76–81.

Marion, R., Li, K., Purushothaman, G., Jiang, Y., and Casagrande, V.A. (2013). Morphological and neurochemical comparisons between pulvinar and V1 projections to V2. J. Comp. Neurol. *521*, 813–832.

Masri, R., Trageser, J.C., Bezdudnaya, T., Li, Y., Keller, A., Trageser, J.C., Bezdudnaya, T., and Li, Y. (2006a). Cholinergic Regulation of the Posterior Medial Thalamic Nucleus. 2265–2273.

Masri, R., Trageser, J.C., Bezdudnaya, T., Li, Y., and Keller, A. (2006b). Cholinergic Regulation of the Posterior Medial Thalamic Nucleus. J. Neurophysiol. *96*, 2265–2273.

Masri, R., Bezdudnaya, T., Trageser, J.C., and Keller, A. (2008). Encoding of stimulus frequency and sensor motion in the posterior medial thalamic nucleus. J. Neurophysiol. *100*, 681–689.

Mcgann, J.P. (2015). Associative learning and sensory neuroplasticity : how does it happen and what is it good for ? 567–576.

McGarry, L.M., Packer, A.M., Fino, E., Nikolenko, V., Sippy, T., and Yuste, R. (2010).

Quantitative classification of somatostatin-positive neocortical interneurons identifies three interneuron subtypes. Front. Neural Circuits *4*, 12.

Mease, R.A., Metz, M., and Groh, A. (2016). Cortical Sensory Responses Are Enhanced by the Higher-Order Thalamus. Cell Rep. *14*, 208–215.

Le Merre, P., Esmaeili, V., Charrière, E., Galan, K., Salin, P.A., Petersen, C.C.H., and Crochet, S. (2018). Reward-Based Learning Drives Rapid Sensory Signals in Medial Prefrontal Cortex and Dorsal Hippocampus Necessary for Goal-Directed Behavior. Neuron *97*, 83–91.e5.

Mesik, L., Ma, W.-P., Li, L.-Y., Ibrahim, L.A., Huang, Z.J., Zhang, L.I., and Tao, H.W. (2015). Functional response properties of VIP-expressing inhibitory neurons in mouse visual and auditory cortex. Front. Neural Circuits *9*, 22.

Meyer, H.S., Wimmer, V.C., Oberlaender, M., De Kock, C.P.J., Sakmann, B., and Helmstaedter, M. (2010a). Number and laminar distribution of neurons in a thalamocortical projection column of rat vibrissal cortex. Cereb. Cortex *20*, 2277–2286.

Meyer, H.S., Wimmer, V.C., Hemberger, M., Bruno, R.M., De Kock, C.P.J., Frick, A., Sakmann, B., and Helmstaedter, M. (2010b). Cell type-specific thalamic innervation in a column of rat vibrissal cortex. Cereb. Cortex *20*, 2287–2303.

Miller, K.D. (2016). Canonical computations of cerebral cortex. Curr. Opin. Neurobiol. *37*, 75–84.

Minnery, B.S. (2003). Response Transformation and Receptive-Field Synthesis in the Lemniscal Trigeminothalamic Circuit. J. Neurophysiol. *90*, 1556–1570.

Miyoshi, G., Hjerling-leffler, J., Karayannis, T., Sousa, V.H., Butt, J.B., Battiste, J., Johnson, J.E., Machold, R.P., and Fishell, G. (2010). Genetic fate mapping reveals that the caudal ganglionic eminence produces a large and diverse population of superficial cortical interneurons. J. Neurosci. *30*, 1582–1594.

Moore, J.D., Mercer Lindsay, N., Deschênes, M., and Kleinfeld, D. (2015). Vibrissa Self-Motion and Touch Are Reliably Encoded along the Same Somatosensory Pathway from Brainstem through Thalamus. PLoS Biol. *13*, 1–28.

Morishima, M. (2006). Recurrent Connection Patterns of Corticostriatal Pyramidal Cells in Frontal Cortex. J. Neurosci. *26*, 4394–4405.

Mrsic-Flogel, T.D., Hofer, S.B., Ohki, K., Reid, R.C., Bonhoeffer, T., and Hübener, M. (2007). Homeostatic Regulation of Eye-Specific Responses in Visual Cortex during Ocular Dominance Plasticity. Neuron *54*, 961–972.

Neske, G.T., Patrick, S.L., and Connors, B.W. (2015). Contributions of Diverse Excitatory and Inhibitory Neurons to Recurrent Network Activity in Cerebral Cortex. J. Neurosci. *35*, 1089–1105.

O'Connor, D.H., Peron, S.P., Huber, D., and Svoboda, K. (2010). Neural activity in barrel cortex underlying vibrissa-based object localization in mice. Neuron *67*, 1048–1061.

O'Connor, K.N., Allison, T.L., Rosenfield, M.E., and Moore, J.W. (1997). Neural activity in the medial geniculate nucleus during auditory trace conditioning. Exp. Brain Res.

Oberlaender, M., De Kock, C.P.J., Bruno, R.M., Ramirez, A., Meyer, H.S., Dercksen, V.J., Helmstaedter, M., and Sakmann, B. (2012a). Cell type-specific three-dimensional structure of thalamocortical circuits in a column of rat vibrissal cortex. Cereb. Cortex *22*, 2375–2391.

Oberlaender, M., Ramirez, A., and Bruno, R.M. (2012b). Sensory Experience Restructures Thalamocortical Axons during Adulthood. Neuron *74*, 648–655.

Ohno, S., Kuramoto, E., Furuta, T., Hioki, H., Tanaka, Y.R., Fujiyama, F., Sonomura, T., Uemura, M., Sugiyama, K., and Kaneko, T. (2012). A morphological analysis of thalamocortical axon fibers of rat posterior thalamic nuclei: A single neuron tracing study with viral vectors. Cereb. Cortex *22*, 2840–2857.

Olàh, S., Komlòsi, G., Szabadics, J., Varga, C., Tòth, E., Barzò, P., Tamas, G., and Barzò, P. (2007). Output of neurogliaform cells to various neuron types in the human and rat cerebral cortex. Front. Neural Circ *1*, 1–7.

Packer, A.M., and Yuste, R. (2011). Dense, Unspecific Connectivity of Neocortical Parvalbumin-Positive Interneurons: A Canonical Microcircuit for Inhibition? J. Neurosci. *31*, 13260–13271.

Pala, A., and Petersen, C.C.H. (2015). InVivo Measurement of Cell-Type-Specific Synaptic Connectivity and Synaptic Transmission in Layer 2/3 Mouse Barrel Cortex. Neuron *85*, 68–76.

Petersen, C.C.H. (2007). The Functional Organization of the Barrel Cortex. Neuron *56*, 339–355.

Petreanu, L., Huber, D., Sobczyk, A., and Svoboda, K. (2007). Channelrhodopsin-2-assisted circuit mapping of long-range callosal projections. Nat. Neurosci. *10*, 663–668.

Petreanu, L., Mao, T., Sternson, S.M., and Svoboda, K. (2009). The subcellular organization of neocortical excitatory connections. Nature *457*, 1142–1145.

Pfeffer, C.K., Xue, M., He, M., Huang, Z.J., and Scanziani, M. (2013). Inhibition of inhibition in visual cortex: the logic of connections between molecularly distinct interneurons. Nat. Neurosci. *16*, 1068–1076.

Pi, H.-J., Hangya, B., Kvitsiani, D., Sanders, J.I., Huang, Z.J., and Kepecs, A. (2013). Cortical interneurons that specialize in disinhibitory control. Nature *503*, 521–524.

Pierret, T., Lavallée, P., and Deschênes, M. (2000). Parallel streams for the relay of vibrissal information through thalamic barreloids. J. Neurosci. *20*, 7455–7462.

Poddar, R., Kawai, R., and Ölveczky, B.P. (2013). A fully automated high-throughput training system for rodents. PLoS One *8*, 1–10.

Polley, D.B., Kvašňák, E., and Frostig, R.D. (2004). Naturalistic experience transforms sensory maps in the adult cortex of caged animals. Nature *429*, 67–71.

Porter, J.T., Johnson, C.K., and Agmon, a (2001). Diverse types of interneurons generate thalamus-evoked feedforward inhibition in the mouse barrel cortex. J. Neurosci. *21*, 2699–2710.

Prabhakar, S., Visel, A., Akiyama, J.A., Shoukry, M., Lewis, K.D., Holt, A., Plajzer-Frick, I., Morrison, H., FitzPatrick, D.R., Afzal, V., et al. (2008). Human-specific gain of function in a developmental enhancer. Science (80-.). *321*, 1346–1350.

Prönneke, A., Scheuer, B., Wagener, R.J., Möck, M., Witte, M., and Staiger, J.F. (2015). Characterizing VIP neurons in the barrel cortex of VIPcre/tdTomato mice reveals layer-specific differences. Cereb. Cortex *25*, 4854–4868.

Purushothaman, G., Marion, R., Li, K., and Casagrande, V. a (2012). Gating and control of primary visual cortex by pulvinar. Nat. Neurosci. *15*, 905–912.

Rakic, P. (1995). A small step for the cell, a giant leap for mankind: a hypothesis of neocortical expansion during evolution. Trends Neurosci. *18*, 383–388.

Rakic, P. (2008). Confusing cortical columns. Proc. Natl. Acad. Sci.

Rakic, P. (2009). Evolution of the neocortex: a perspective from developmental biology. Nat. Rev. Neurosci. *10*, 724–735.

Rioult-Pedotti, M.S., Friedman, D., and Donoghue, J.P. (2000). Learning-induced LTP in neocortex. Science (80-.). *290*, 533–536.

Rodríguez-Moreno, A., and Paulsen, O. (2008). Spike timing-dependent long-term depression requires presynaptic NMDA receptors. Nat. Neurosci. *11*, 744–745.

Roe, A.W., Pallas, S.L., Hahm, J.O., and Sur, M. (1990). A map of visual space induced in primary auditory cortex. Science (80-.).

Roth, M.M., Dahmen, J.C., Muir, D.R., Imhof, F., Martini, F.J., and Hofer, S.B. (2016). Thalamic nuclei convey diverse contextual information to layer 1 of visual cortex. Nat. Neurosci. *19*, 299–307.

Rudy, B., Fishell, G., Lee, S., and Hjerling-Leffler, J. (2011). Three groups of interneurons account for nearly 100% of neocortical GABAergic neurons. Dev. Neurobiol. *71*, 45–61.

Sacco, T., and Sacchetti, B. (2010). Role of Secondary Sensory Cortices. Science (80-.). *649*, 649–656.

Sakurai, K., Akiyama, M., Cai, B., Scott, A., Han, B.X., Takatoh, J., Sigrist, M., Arber, S., and Wang, F. (2013). The Organization of Submodality-Specific Touch Afferent Inputs in the Vibrissa Column. Cell Rep. *5*, 87–98.

Sanchez-Vives, M. V, and McCormick, D.A. (2000). Cellular and network mechanisms of rhythmic recurrent activity in neocortex. Nat. Neurosci. *3*, 1027–1034.

Schiff, M.L., and Reyes, a. D. (2012). Characterization of thalamocortical responses of regular-spiking and fast-spiking neurons of the mouse auditory cortex in vitro and in silico. J. Neurophysiol. *107*, 1476–1488.

Schubert, D., Staiger, J.F., Cho, N., Kötter, R., Zilles, K., and Luhmann, H.J. (2001). Layer-specific intracolumnar and transcolumnar functional connectivity of layer V pyramidal cells in rat barrel cortex. J. Neurosci. *21*, 3580–3592.

Schwartz, S., Maquet, P., and Frith, C. (2002). Neural correlates of perceptual learning : A functional MRI study of visual texture discrimination. *100*, 1–6.

Sharma, J., Angelucci, A., and Sur, M. (2000). Induction of visual orientation modules in auditory cortex. Nature.

Sherman, S.M. (2016). Thalamus plays a central role in ongoing cortical functioning. Nat. Neurosci. *16*, 533–541.

Shibata, K., Sasaki, Y., Kawato, M., and Watanabe, T. (2016). Neuroimaging evidence for 2 types of plasticity in association with visual perceptual learning. Cereb. Cortex *26*, 3681–3689.

Shruti, S., Clem, R.L., and Barth, A.L. (2008). A seizure-induced gain-of-function in BK channels is associated with elevated firing activity in neocortical pyramidal neurons. Neurobiol. Dis. *30*, 323–330.

Shulz, D.E., Ego-Stengel, V., and Ahissar, E. (2003). Acetylcholine-dependent potentiation of temporal frequency representation in the barrel cortex does not depend on response magnitude during conditioning. J. Physiol. Paris *97*, 431–439.

Silberberg, G., and Markram, H. (2007). Disynaptic Inhibition between Neocortical Pyramidal Cells Mediated by Martinotti Cells. Neuron *53*, 735–746.

Simons, D.J. (1978). Response properties of vibrissa units in rat SI somatosensory neocortex. J. Neurophysiol. *41*, 798–820.

Simons, D.J., and Carvell, G.E. (1989). Thalamocortical response transformation in the rat vibrissa/barrel system. J. Neurophysiol. *61*, 311–330.

Siucinska, E., and Kossut, M. (1996). Short-lasting classical conditioning induces reversible changes of representational maps of vibrissae in mouse SI cortex-A 2DG study. Cereb. Cortex.

Siucinska, E., and Kossut, M. (2004). Experience-dependent changes in cortical whisker representation in the adult mouse: A 2-deoxyglucose study. Neuroscience *127*, 961–971.

Sjöström, P.J., and Häusser, M. (2006). A Cooperative Switch Determines the Sign of Synaptic Plasticity in Distal Dendrites of Neocortical Pyramidal Neurons. Neuron *51*, 227–238.

Sjöström, P.J., Turrigiano, G.G., and Nelson, S.B. (2001). Rate, timing, and cooperativity jointly determine cortical synaptic plasticity. Neuron *32*, 1149–1164.

Snow, J.C., Allen, H.A., Rafal, R.D., and Humphreys, G.W. (2009). Impaired attentional selection following lesions to human pulvinar: Evidence for homology between human and monkey. Proc. Natl. Acad. Sci. *106*, 4054–4059.

Sobolewski, A., Kublik, E., Swiejkowski, D.A., Kamiński, J., and Wróbel, A. (2015). Alertness opens the effective flow of sensory information through rat thalamic posterior nucleus. Eur. J. Neurosci. *41*, 1321–1331.

Sosnik, R., Haidarliu, S., and Ahissar, E. (2001). Temporal frequency of whisker movement. I. Representations in brain stem and thalamus. J. Neurophysiol. *86*, 339–353.

Staiger, J.F., Zilles, K., and Freund, T.F. (1996). Innervation of VIP-immunoreactive neurons by the ventroposteromedial thalamic nucleus in the barrel cortex of the rat. J. Comp. Neurol. *367*, 194–204.

Stepanyants, A., Martinez, L.M., Ferecsko, A.S., and Kisvarday, Z.F. (2009). The fractions of short- and long-range connections. PNAS *106*.

Stern, E.A., Maravall, M., and Svoboda, K. (2001). Rapid development and plasticity of layer 2/3 maps in rat barrel cortex in vivo. Neuron *31*, 305–315.

Summerfield, C., Greene, M., Wager, T., Egner, T., Hirsch, J., and Mangels, J. (2006). Neocortical connectivity during episodic memory formation. PLoS Biol. *4*, 855–864.

Sumser, A., Mease, R.A., Sakmann, B., and Groh, A. (2017). Organization and somatotopy of corticothalamic projections from L5B in mouse barrel cortex. Proc. Natl. Acad. Sci. *114*, 201704302.

Swadlow, H. a, and Gusev, a G. (2002). Receptive-field construction in cortical inhibitory interneurons. Nat. Neurosci. *5*, 403–404.

Takahashi, T. (2010). Transmission by Driving AMPA. Science (80-.). *1585*, 1585–1589.

Tan, Z., Hu, H., Huang, Z.J., and Agmon, A. (2008). Robust but delayed thalamocortical activation of dendritic-targeting inhibitory interneurons. Proc. Natl. Acad. Sci. U. S. A. *105*, 2187–2192.

Taniguchi, H., He, M., Wu, P., Kim, S., Paik, R., Sugino, K., Kvitsani, D., Fu, Y., Lu, J., Lin, Y., et al. (2011). A Resource of Cre Driver Lines for Genetic Targeting of GABAergic Neurons in Cerebral Cortex. Neuron *71*, 995–1013.

Thomson, A.M., and Lamy, C. (2007). Functional maps of neocortical local circuitry. Front. Neurosci. *1*, 19–42.

Tomasello, M., and Rakoczy, H. (2003). What makes human cognition unique? From individual to shared to collective intentionality. Mind Lang. *18*, 121–147.

Trageser, J.C. (2006). State-Dependent Gating of Sensory Inputs by Zona Incerta. J. Neurophysiol. *96*, 1456–1463.

Tsiola, A., Hamzei-Sichani, F., Peterlin, Z., and Yuste, R. (2003). Quantitative morphologic classification of layer 5 neurons from mouse primary visual cortex. J. Comp. Neurol. *461*, 415–428.

Urbain, N., and Deschenes, M. (2007). A New Thalamic Pathway of Vibrissal

Information Modulated by the Motor Cortex. J. Neurosci. *27*, 12407–12412.

Urbain, N., Salin, P.A., Libourel, P.A., Comte, J.C., Gentet, L.J., and Petersen, C.C.H. (2015). Whisking-Related Changes in Neuronal Firing and Membrane Potential Dynamics in the Somatosensory Thalamus of Awake Mice. Cell Rep. *13*, 647–656.

Urban-Ciecko, J., Fanselow, E.E., and Barth, A.L. (2015). Neocortical somatostatin neurons reversibly silence excitatory transmission via GABAb receptors. Curr. Biol. *25*, 722–731.

Veinante, P., and Deschênes, M. (1999). Single- and multi-whisker channels in the ascending projections from the principal trigeminal nucleus in the rat. J. Neurosci. *19*, 5085–5095.

Veinante, P., Jacquin, M.F., and Desch Nes, M. (2000a). Thalamic Projections From the Whisker- Sensitive Regions of the Spinal Trigeminal Complex in the Rat. J. Comp. Neurol *420*, 233–243.

Veinante, P., Jacquin, M.F., and Deschênes, M. (2000b). Thalamic projections from the whisker-sensitive regions of the spinal trigeminal complex in the rat. J. Comp. Neurol. *420*, 233–243.

Vélez-Fort, M., Rousseau, C. V., Niedworok, C.J., Wickersham, I.R., Rancz, E.A., Brown, A.P.Y., Strom, M., and Margrie, T.W. (2014). The stimulus selectivity and connectivity of layer six principal cells reveals cortical microcircuits underlying visual processing. Neuron *83*, 1431–1443.

Viaene, A.N., Petrof, I., and Sherman, S.M. (2011a). Properties of the thalamic projection from the posterior medial nucleus to primary and secondary somatosensory cortices in the mouse. Proc. Natl. Acad. Sci. *108*, 18156–18161.

Viaene, A.N., Petrof, I., and Sherman, S.M. (2011b). Synaptic properties of thalamic input to layers 2/3 and 4 of primary somatosensory and auditory cortices. J. Neurophysiol. *105*, 279–292.

Wall, N.R., De La Parra, M., Sorokin, J.M., Taniguchi, H., Huang, Z.J., and Callaway, E.M. (2016). Brain-Wide Maps of Synaptic Input to Cortical Interneurons. J. Neurosci. *36*, 4000–4009.

Ward, R.L., Flores, L.C., and Disterhoft, J.F. (2012). Infragranular barrel cortex activity is enhanced with learning. J. Neurophysiol. *108*, 1278–1287.

Weinberger, N.M. (2004). Specific long-term memory traces in primary auditory cortex. Nat. Rev. Neurosci. *5*, 279–290.

Welker, C. (1976). Receptive fields of barrels in the somatosensory neocortex of the rat. J. Comp. Neurol. *166*, 173–189.

Welker, E., Armstrong-James, M., Van der Loos, H., and Kraftsik, R. (1993). The mode of activation of a barrel column: response properties of single units in the somatosensory cortex of the mouse upon whisker deflection [published erratum appears in Eur J Neurosci 1993 Oct 1;5(10):1421]. Eur J Neurosci *5*, 691–712.

Wen, J.A., and Barth, A.L. (2011). Input-Specific Critical Periods for Experience-Dependent Plasticity in Layer 2/3 Pyramidal Neurons. J. Neurosci. *31*, 4456–4465.

Wiesel, T.N., and Hubel, D.H. (1963). SINGLE-CELL RESPONSES IN STRIATE CORTEX OF KITTENS DEPRIVED OF VISION IN ONE EYE. J. Neurophysiol.

Wimmer, V.C., Bruno, R.M., De Kock, C.P.J., Kuner, T., and Sakmann, B. (2010a). Dimensions of a projection column and architecture of VPM and POm axons in rat vibrissal cortex. Cereb. Cortex *20*, 2265–2276.

Wimmer, V.C., Broser, P.J., Kuner, T., and Bruno, R.M. (2010b). Experience-induced plasticity of thalamocortical axons in both juveniles and adults. J. Comp. Neurol. *518*, 4629–4648.

Woolsey, T.A., and Van der Loos, H. (1970). The structural organization of layer IV in the somatosensory region (S I) of mouse cerebral cortex. The description of a cortical field composed of discrete cytoarchitectonic units. Brain Res. *17*, 205–242.

Xu, H., Jeong, H.Y., Tremblay, R., and Rudy, B. (2013). Neocortical Somatostatin-Expressing GABAergic Interneurons Disinhibit the Thalamorecipient Layer 4. Neuron *77*, 155–167.

Xue, M., Atallah, B. V, and Scanziani, M. (2014). Equalizing excitation-inhibition ratios across visual cortical neurons. Nature *511*, 596–600.

Yamashita, T., Pala, A., Pedrido, L., Kremer, Y., Welker, E., and Petersen, C.C.H. (2013). Membrane potential dynamics of neocortical projection neurons driving target-specific signals. Neuron *80*, 1477–1490.

Yassin, L., Benedetti, B.L., Jouhanneau, J.S., Wen, J.A., Poulet, J.F.A., and Barth, A.L. (2010). An Embedded Subnetwork of Highly Active Neurons in the Neocortex. Neuron *68*, 1043–1050.

Yu, C., Derdikman, D., Haidarliu, S., and Ahissar, E. (2006). Parallel Thalamic Pathways for Whisking and Touch Signals in the Rat. PLoS Biol. *4*.

Yu, C., Horev, G., Rubin, N., Derdikman, D., Haidarliu, S., and Ahissar, E. (2015). Coding of object location in the vibrissal thalamocortical system. Cereb. Cortex *25*, 563–577.

Yu, Y.C., Bultje, R.S., Wang, X., and Shi, S.H. (2009). Specific synapses develop preferentially among sister excitatory neurons in the neocortex. Nature *458*, 501–504.

Yuste, R. (2015). From the neuron doctrine to neural networks. Nat. Rev. Neurosci. *16*, 487–497.

Zhang, S., Xu, M., Kamigaki, T., Phong Hoang Do, J., Chang, W.-C., Jenvay, S., Miyamichi, K., Luo, L., and Dan, Y. (2014). Long-range and local circuits for top-down modulation of visual cortex processing. Science (80-.). *345*, 660–665.

Zhou, M., Liang, F., Xiong, X.R., Li, L., Li, H., Xiao, Z., Tao, H.W., and Zhang, L.I. (2014). Scaling down of balanced excitation and inhibition by active behavioral states in

auditory cortex. Nat. Neurosci. *17*, 841–850.

Zilberter, M., Holmgren, C., Shemer, I., Silberberg, G., Grillner, S., Harkany, T., and Zilberter, Y. (2009). Input specificity and dependence of spike timing-dependent plasticity on preceding postsynaptic activity at unitary connections between neocortical layer 2/3 pyramidal cells. Cereb. Cortex *19*, 2308–2320.